Report of the Sea Ice Thickness Workshop

19–21 November 1991
New Carrollton, Maryland

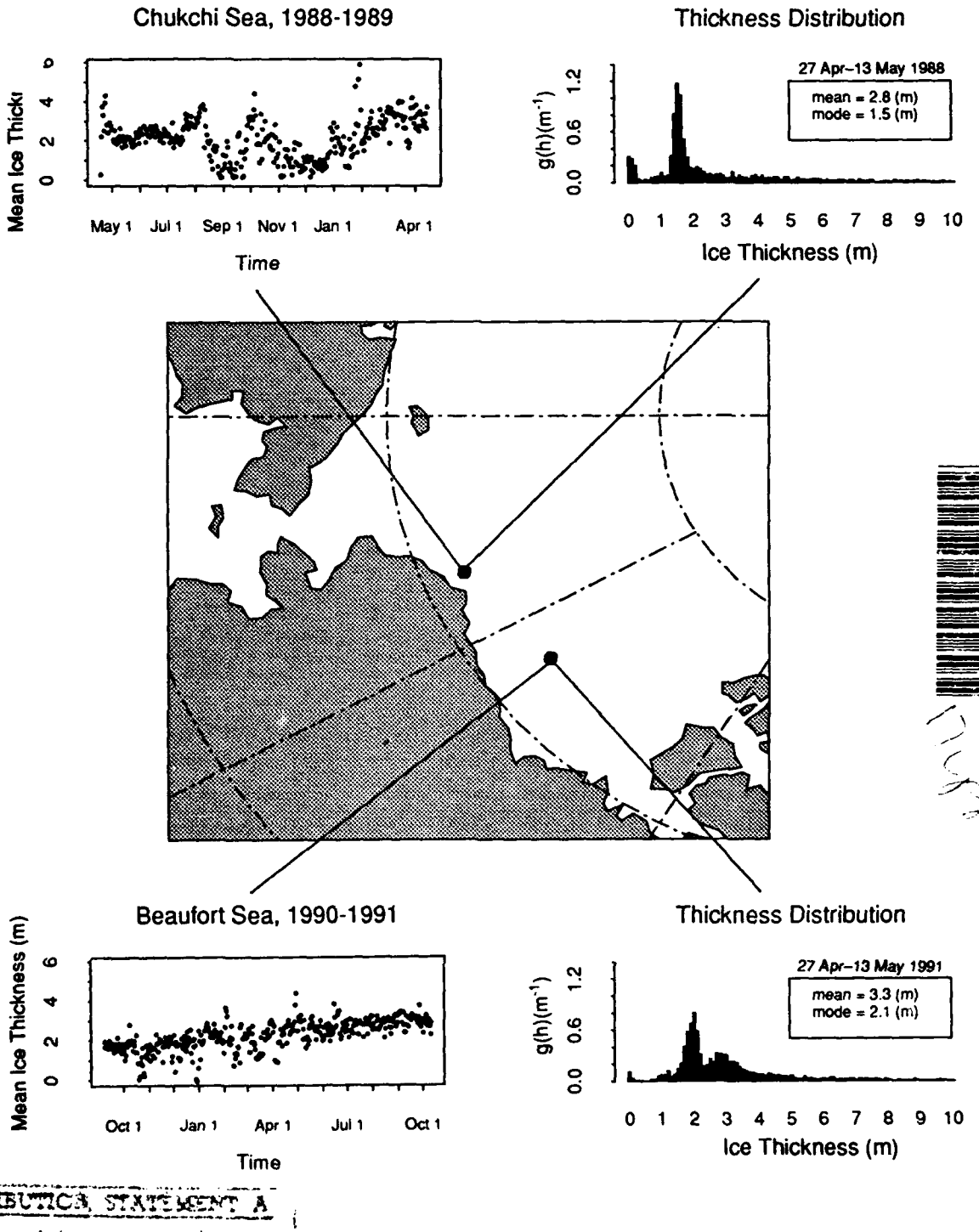

Cover figure: Sea ice thickness distributions measured by upward looking sonar in the Chukchi and Beaufort seas. (Data provided by R. Moritz.)

Report of the Sea Ice Thickness Workshop

19-21 November 1991
New Carrollton, Maryland

Sponsored by
National Aeronautics and Space Administration

Edited by
A.S. Thorndike, C. Parkinson, and D.A. Rothrock

October 1992

Additional copies can be obtained from

Polar Science Center • Applied Physics Laboratory
University of Washington
1013 NE 40th Street • Seattle, Washington 98105-6698
(206) 543-1300

TABLE OF CONTENTS

Appendix C: Models

Appendix D: Bibliography

LIST OF FIGURES

I. Executive Summary and Recommendations

A workshop devoted to sea ice thickness was held in New Carrollton, Maryland, from 19 to 21 November 1991. The purpose was to bring together interested scientists to review the current understanding of the field and to develop ideas for future research. The abstracts of the presentations made at the workshop are collected in the appendices. In the body of the report we discuss the current state of knowledge and recommend actions and research directions that would improve our understanding of sea ice thickness.

Many questions in sea ice physics, air sea interaction, climate dynamics, and ice engineering depend on knowledge about the state of the ice pack, in particular the distribution of ice thicknesses in any region. The workshop did not focus on these applications. Instead, the emphasis was on the three questions

- what is the current distribution of sea ice thickness?
- what mechanical and thermal processes determine the thickness distribution?

  and

- what are the techniques for measuring ice thickness?

As understanding of these fundamental issues improves, so will our ability to address the many related topics.

Understanding the thickness distribution of sea ice is essential for understanding its mass balance. We must know how much ice there is, how it varies in time and space, where the ice is produced and where it melts, and how rapidly it is transported from place to place. Because of the variability of ice thickness on all scales from meters to thousands of kilometers, it is difficult to construct useful averages from limited data. We do not yet know the mean thickness of sea ice in the Arctic Basin even to one significant figure. We do not know anything about its interannual variability. We do not know which regions around the perimeter of the basin are net ice sources and which are sinks. Lacking such basic knowledge, we might not recognize changes that occur in the sea ice system over the next few decades. And if we cannot document the changes in the sea ice itself, we will not be able to assess the role of sea ice in climate change or answer such basic questions as: Is sea ice a sensitive indicator of climate change? Is ice–albedo feedback as important as models predict? Do changes in the ice export through Fram Strait regulate deep convection in the Greenland Sea? Improved observations of the ice pack are needed to document the current conditions and to monitor possible changes.

Increased emphasis on studies related to ice thickness are timely for several reasons, primarily the increased data availability. For instance, ice thickness data from submarine missions under the ice may soon be widely available to the scientific community; moored upward looking sonar devices now monitor ice thickness in selected locations; aircraft laser profiles of the relief of sea ice provide useful thickness estimates; and satellite synthetic aperture radar affords a new level of detail on ice motion. Furthermore, a theoretical context already exists for interpreting ice thickness data and for including in sea ice models the processes that control its thickness. It cannot be tested or refined without more extensive data.

The recommendations that follow are an attempt to collect our thoughts in one place and to draw attention to an area of research that offers opportunities for new progress. Recommendations appear in several sections, particularly V and VI. They have been boiled down for presentation in this summary. Particular roles for NASA are highlighted within the strategies in Section VI.

1. *Existing data.* There is a need to use data from existing sources to estimate the current state of the ice pack. This includes identifying sources of data, agreeing on standard definitions and procedures for interpreting the data, and placing all data in public archives. We recommend adoption of the definitions in Appendix A-III.

2. *Measurement techniques.* Efforts should be made to coordinate submarine missions with the objectives of the research community. In particular, an unclassified record of ice draft should be made routinely, either in real time or immediately following a submarine cruise, to circumvent the issue of classification, declassification, and release of data.

   Intercomparisons of thickness measurements by different techniques should be continued. High importance is attached to further development and assessment of the two youngest methods: aircraft laser profiling and moored upward looking sonar.

   Development of Doppler ice velocity capabilities for the moored sonars should be pursued for use in determining the ice volume flux.

3. *Fram Strait monitoring.* A program to monitor the flux of ice volume through Fram Strait should be maintained for at least 15 years. The community should recognize and endorse the current program of the World Climate Research

Programme, outlined in Section VI, and coordinate other field studies and data analyses to support this effort.

4. *Lagrangian drift.* A field program to measure changes in the ice thickness distribution following a Lagrangian element should be conducted during this decade. The program must include repeated surveys of ice thickness, monitoring of ice growth, and monitoring of ice motion. It should endure through two full annual cycles. The objective is to assess the ice thickness distribution theory by measuring each term in the evolution equation.

5. *Modeling.* An effort is needed to assemble data sets for input to sea ice models. Of special importance are cloud cover and radiative properties, sea ice albedo, and surface temperature.

   Efforts to couple sea ice and ocean models should be accelerated.

   Special field studies should be designed to examine model results. For example, regions that appear to be ice producers in model runs might be ideal locations for moored sonars or for special acquisition of SAR images. These studies should document the processes that shape the thickness distribution, so we can determine whether models are getting the right result for the right reason.

To NASA, we recommend the following:

1. *Interpretation of satellite data.* Continued research to develop techniques for inferring properties of the sea ice and atmosphere deserves the highest priority. In particular, improved techniques are needed for estimating the distribution of liquid, solid, and gaseous water in the atmosphere, the surface temperature of the ice, the ice albedo, and the radiative fluxes at the surface and as functions of height in the atmosphere. There are well known difficulties in such an endeavor, mainly the inability to distinguish clouds from sea ice in some circumstances. It is time to assess what can and cannot be achieved with AVHRR and ERBE data, and what prospects there are for improvements over the next couple of decades resulting from the atmospheric radiation program (ARM) and the earth observing system (EOS).

2. *Data sets.* The modeling community requires suitable data sets for forcing and verifying models. NASA could play a useful role in defining these data sets and assembling them. With a public database, comparisons between models and interpretation of model results would be enhanced.

3. *Development of measurement techniques.* Continued support for development of an aircraft laser profilometer system is recommended. Such a system could play an important role in the Lagrangian drift experiment advocated in this report.

4. *Ice kinematics from SAR.* The current SAR system and followup systems resolve ice motion with enough detail to study local kinematic processes such as the formation of leads and pressure ridges. The models for these processes in the thickness distribution theory have no basis in observation. In particular, the assumed relationship between large scale and local deformations is a guess that could be supported or refuted using the SAR data.

   The SAR data can also be used to estimate ice advection, and this would be a strong contribution to the program to monitor the flux of ice through Fram Strait.

II. Introduction

The Sea Ice Thickness Workshop was convened to review our theoretical understanding about the thermal and mechanical processes that determine ice thickness, our observational knowledge of ice thickness, and our growing capabilities to measure it. Before the workshop, participants wrote abstracts of the material they would present; these are collected here in the appendices. Ideas for research that would have substantial payoff in the near future were discussed and are presented in this report, with the hope that

- research efforts can be focused on two or three clearly defined questions about the dynamics and thermodynamics of sea ice thickness
- experiments can be designed to clarify the accuracies and intercomparability of various observational methods
- some standardization of observations, definitions, and analysis might render our database of ice thickness more useful both as a geophysical record and as a tool for refining theory and models.

The thickness of sea ice is the distance from its lower interface with the ocean to its upper interface with either a snow cover or the atmosphere. Because of the irregular and transitional nature of these two interfaces, there is an ambiguity of a few centimeters in the notion of ice thickness. In fact, the several mechanical, acoustical, and electromagnetic techniques for estimating the position of these interfaces differ in what they "see" as the interface. Since most of these observational techniques see only one of the interfaces, the position of the sea surface is also usually measured, and sea ice thickness must be estimated from either ice draft or ice freeboard by some form of isostatic relation. These issues are reviewed in Section III.

The notion of a uniform sheet of sea ice is central to most treatments of ice growth and melt, to large-scale ice models, and to climate models focused on the stability of the sea ice cover. Theory describes a thermodynamic equilibrium in which the ice grows thick enough that heat conducted up through the ice balances the net radiative loss to the atmosphere from the upper surface. In global warming experiments with climate models containing level, equilibrium sea ice submodels, a doubling of carbon dioxide causes a strongly amplified warming in polar regions, with larger ice-free areas in the summer Arctic and a thinner ice cover. Models predict that the climate is stable not only in its present state, but also in a warmer state in which the Arctic Ocean is ice free and much warmer because of greatly enhanced summer radiative absorption. Sea ice thickness also plays an important role in the freshwater balance of the Arctic Ocean

and the Greenland Sea, making the largest single contribution to freshwater flux through Fram Strait.

Natural sea ice, however, is not a uniform level slab in equilibrium. Its surfaces are rough and irregular, and it is densely fractured by open leads. This irregularity of ice thickness is due largely to ice motion that breaks floes apart, causing new ice to form throughout the winter. Much of this ice is broken and piled into thick ridges. Although we do not yet know how much of this detail is relevant for global scale processes, it is clear that models omitting all of this complexity cannot satisfactorily describe air–ice–ocean interaction.

Regions of modest size contain ice of many different thicknesses. This distribution of ice thickness is important for describing many aspects of the interaction among ocean, sea ice, and atmosphere. It is defined by considering an area R, which might be a circle of radius 200 km, centered at $\boldsymbol{x}$. Let $dA(h, h + dh)$ represent the area within R covered by ice having thickness in the range $(h, h + dh)$. The ice thickness distribution $g(h)$ defined by

$$g(h)\, dh = dA(h, h + dh)/R$$

has the properties of a probability density function with dimensions of (length)$^{-1}$. Some observed distributions are shown in Figure 1. It is important to note that when a finite

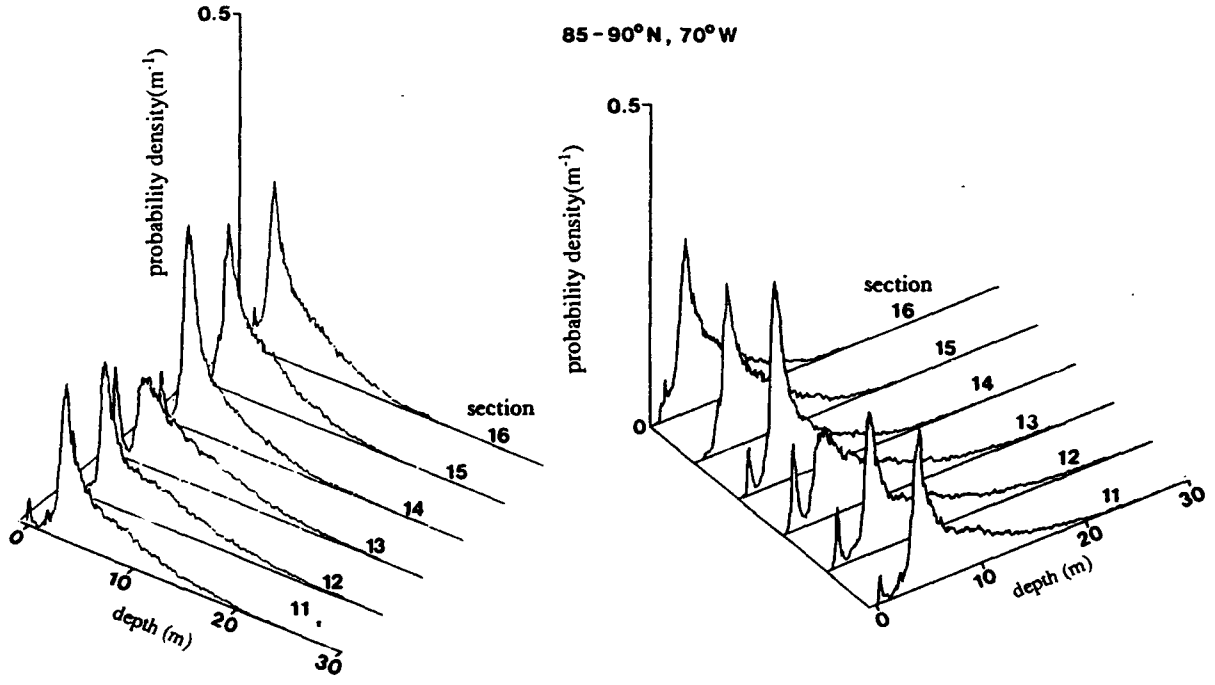

Figure 1. Typical measured ice thickness distributions for the region between Greenland and the North Pole (Wadhams, 1981).

fraction of R is ice free, g will have a delta function at $h = 0$, so g includes information about ice concentration as well as thickness. The mean ice thickness in R is

$$\bar{h} = \int_0^\infty hg(h)dh$$

and does *not* exclude areas of open water. The distribution is a function of h, but also varies with $\boldsymbol{x}$ and time: $g(h, \boldsymbol{x}, t)$; what we know about these variations is reviewed in Section IV. There is no solid evidence that a natural scale, say, smaller than synoptic atmospheric structure and yet averaging over many floes, exists for R.

In any reference to the ice thickness distribution, we should be careful to state the region R, which might be the entire Arctic Ocean, or a much smaller area. In studies of how the thickness distribution changes, the region R might be held fixed, or allowed to move with the ice. The thickness distribution is governed by the equation

$$\partial g/\partial t = \mathrm{div}(\boldsymbol{v}g) - \partial(fg)/\partial h + \psi$$

where $f(h, \boldsymbol{x}, t) = dh/dt$ is the thermodynamic growth rate of ice of thickness h, $\boldsymbol{v}$ is the horizontal velocity vector, and ψ is a function that mechanically redistributes ice from one thickness to another, modeling the formation of leads and pressure ridges (see Figure 2). Knowledge of these processes controlling the ice thickness and its distribution is reviewed in Section V. The fact that ice is present in a variety of thicknesses, particularly newly formed thin ice, strongly affects some processes. In winter, for instance, the intense upward turbulent heat exchange from thin ice to the atmosphere tends to balance the downward flux over the much larger area of thicker ice. Ice growth is rapid in thin ice areas, resulting in strong salt fluxes to the ocean surface. A good estimate of this surface salinity forcing is important for understanding the thermohaline circulation of the polar oceans and their interaction with the world ocean.

The spatial structure that arises from these thermal and mechanical processes can be usefully described by statistics of identifiable features such as level ice, leads, floes, and ridges. These are discussed in Section IV. For instance, trafficability to surface vehicles, internal wave generation, and atmospheric drag coefficients have all been examined in terms of ridge statistics. Similarly, the summer albedo and heat budget can be related to lead areas. Marine mammal habitat is affected by floe size and ice

concentration. Submarine operations require information on the thickness, size, and spacing of leads. Spatial structure can also be described by more abstract statistics of top and bottom surfaces such as the spatial autocorrelation function or spectrum, the roughness, and the fractal dimension. These are the natural tools, for instance, for describing the acoustic and electromagnetic scattering properties of the surface. Very little connection has been made between these two descriptive approaches.

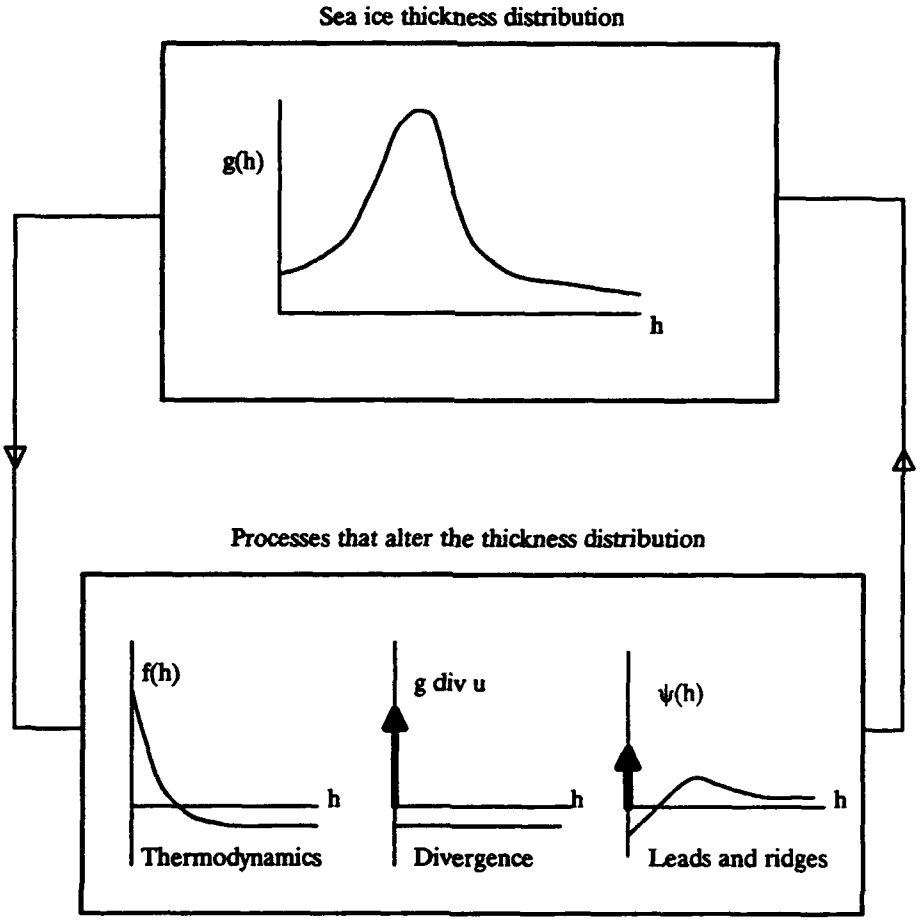

Figure 2. The ice thickness distribution is maintained by thermal and mechanical processes. Over an annual average, thermal processes cause thin ice to grow thicker, and thick ice to grow thinner. Divergence of the ice pack is a source of open water and a sink of ice-covered area. Ice deformation simultaneously produces open leads and squeezes thin ice together to form pressure ridges. Thus it is a source of open water, a sink of thin ice, and a source of thick ice. Finally advection, not illustrated, carries the entire distribution with the mean ice velocity. Because the time scales for these processes are comparable to the residence time for ice in the Arctic Basin, equilibrium distributions may never be realized.

These concepts—the ice thickness distribution, the abundance of certain ice features, and the spatial statistics of the ice surface—are well enough developed that the community should be able to agree on definitions and to reach a consensus regarding the accuracy of various techniques for measurement and interpretation. At the same time, theoretical ideas for why the ice pack has the structure it has have been stymied for lack of adequate data. This situation is changing as more relevant observations appear, in particular from moored, upward-looking sonars, submarine traverses, synthetic aperture radar, and other remote sensing tools. These are reasons to be optimistic that new understanding of the ice cover and the processes that maintain it is within reach. The recommendations of this workshop outline several specific activities that would contribute to this greater understanding.

III. Techniques for Measuring Sea Ice Thickness

Drilling a hole is the most reliable way to determine the thickness of sea ice, and the least practical. It is the preferred technique for local surveys, to check the thickness of a runway, to decide where to cut a large hole for access to the ocean, or to verify some other measurement technique. But it has no value for large-scale surveying or long-term monitoring.

Useful techniques for these purposes are described in Appendix B and include upward looking sonar from submarines and from fixed moorings, and laser profiling from airplanes (Appendix B-IX). These methods each measure only the profile of the bottom surface of the ice or of the top surface of the snow. Interpretation in terms of thickness relies on the overall isostatic equilibrium of the floating ice and on an independent estimate of the snow depth and density.

Other electromagnetic techniques, still under development, are described by Kovacs (Appendix B-XI). They are unlikely to have any value for large-scale observations in the near future.

Finally, there are several remote sensing techniques that can provide information about thin ice, open water, and perhaps other ice types. Estimates of these quantities help to constrain the important thin end of the ice thickness distribution. The abstracts in Appendix B contain more information about drill holes (B-I and B-II) and about using satellite imagery (B-XIII). No method is known for determining from space ice thickness greater than 1 m.

Upward looking sonar devices measure the time it takes an acoustic pulse to travel from a transmitter–receiver, located perhaps 50 m below the ice, to the ice bottom and back (see Figure 3). The hydrostatic pressure at the sensor is also measured. The travel time is related to distance based on some assumptions about the average sound velocity in the water column above the sensor, leading to an estimate of the depth of the sensor below the ice. The depth of the sensor below the sea surface is deduced from the measured pressure and an assumption about the average density of the water column. The ice draft is the difference between these two depths. Ice thickness is estimated by multiplying by a constant related to the densities of sea ice and sea water and applying a correction for the snow layer. Despite the assumptions that have to be made regarding the sound velocity, the snow, and the densities of water and ice, the method succeeds in determining ice thickness to within 0.5 m or better. This is adequate to

resolve the thickness distribution in the central Arctic and to resolve its seasonal and major geographical variations.

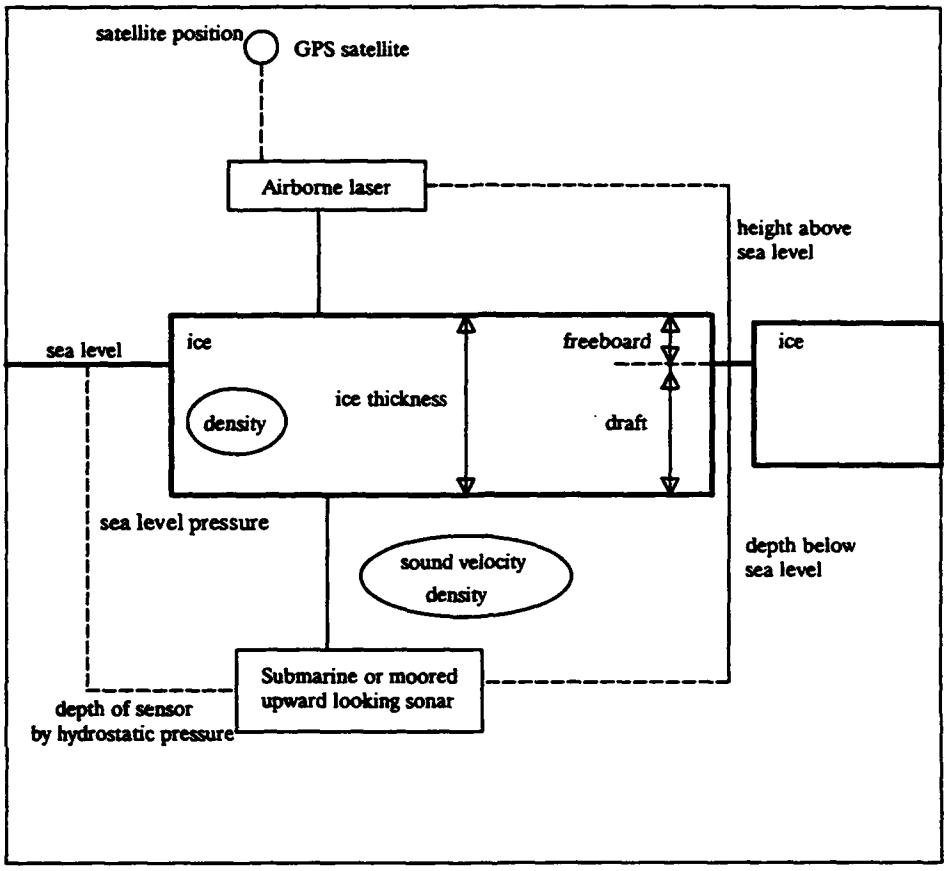

Figure 3. Ice thickness estimates based on upward looking sonar or on airborne altimetry rely on measurements of the distance from the sensor to the surface and on a separate determination of the distance from the sensor to sea level. Occasional open leads can be used to confirm the distance to sea level. The circled quantities emphasize assumptions or independent measurements that need to be made to convert the raw measurements into ice thicknesses.

There are a number of difficulties in the interpretation of sonar data. Because of the finite angular beam pattern, the ray responsible for the first return to the sensor may not have traveled vertically (see Figure 4). In effect, the first return comes from the ice nearest the sensor, and small areas of thin ice may be missed. This biases the data toward thicker ice, a bias that cannot be ignored when the bottom surface is very rough. An approximate correction can be made for this based on simulations of the measurement process over fictitious surfaces where drafts are known at all points.

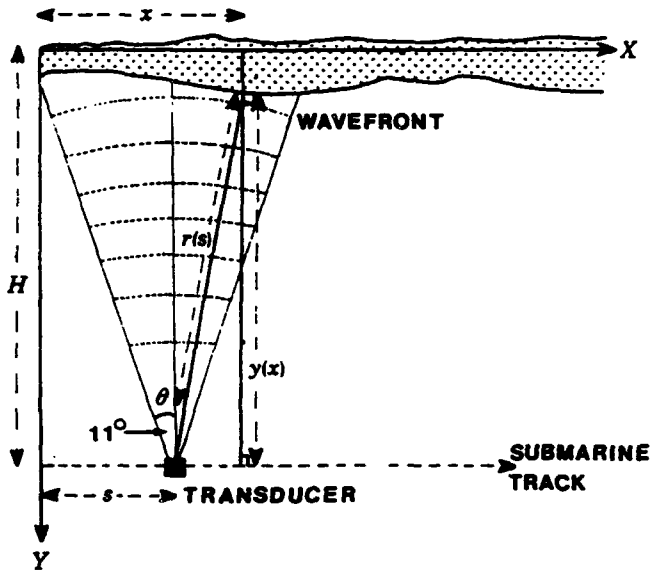

Figure 4. The sonar measures the distance to the closest point on the ice surface within the beam pattern of the sensor. It will not in general equal the vertical distance to the ice (from Wadhams, 1981).

Another problem concerns the orientation of the sensor: any departure from vertical makes the acoustic path longer and the ice apparently thinner than it really is.

Submarines have been prowling around beneath the ice for about 30 years. A summary of U.S. and British missions is given in Table 1. Although upward looking sonar observations of the ice canopy were made on all missions, the data are not of uniform quality. Early missions had wide beam sonars and analog recording. It is doubtful that those data are of sufficient quality to justify the effort to convert them into a usable format. Experts who have studied the U.S. archive believe useful data are to be had from the tracks listed in Table 2. While this is a substantial data set, the coverage in space and time is uneven. Only about half the central Arctic is sampled, and most of the data are from the fall and spring. Figures 5a and 5b show summer and winter data from the U.S. and British submarines. Data from U.S. submarine missions do not reside in a public archive.

Table 1. U.S. and British arctic submarine cruises with upward looking sonar.

Year	U.S.	British	
1957/58	2	0	
1959	1	0	
1960	2	0	
1961	0	0	
1962	2	0	
1963	0	0	
1964	0	0	By season (U.S. only)
1965	0	0	Spring – 17
1966	0	0	Summer – 15
1967	1	0	Fall – 7
1968	0	0	Winter – 2
1969	2	0	
1970	2	0	
1971	0	1	
1972	0	0	
1973	0	0	
1974	0	0	
1975	1	0	
1976	1	1	
1977	1	0	
1978	1	0	
1979	1	1	
1980	0	0	
1981	1	0	
1982	2	0	
1983	1	0	
1984	4	0	
1985	3	1	
1986	4	0	
1987	3	1	
1988	3	0	
1989	2	1	
1990	3	0	

Table 2. Submarine tracks with useful data from upward-looking sonars (from Bourke and McLaren, in press).

Submarine	Date	Track Length
Nautilus	August 1958	2580 km
Sargo	February 1960	729 km
Seadragon	August 1960	541 km
Queenfish	February 1967	669 km
Queenfish	August 1970	3559 km
Gunard	April 1976	1400 km
Sovereign	October 1976	3750 km
Flying Fish	May 1977	420 km
Pintado	September 1978	1250 km
Tautog	October 1984	300 km
Archerfish	April 1986	3200 km
Billfish	April 1987	2823 km

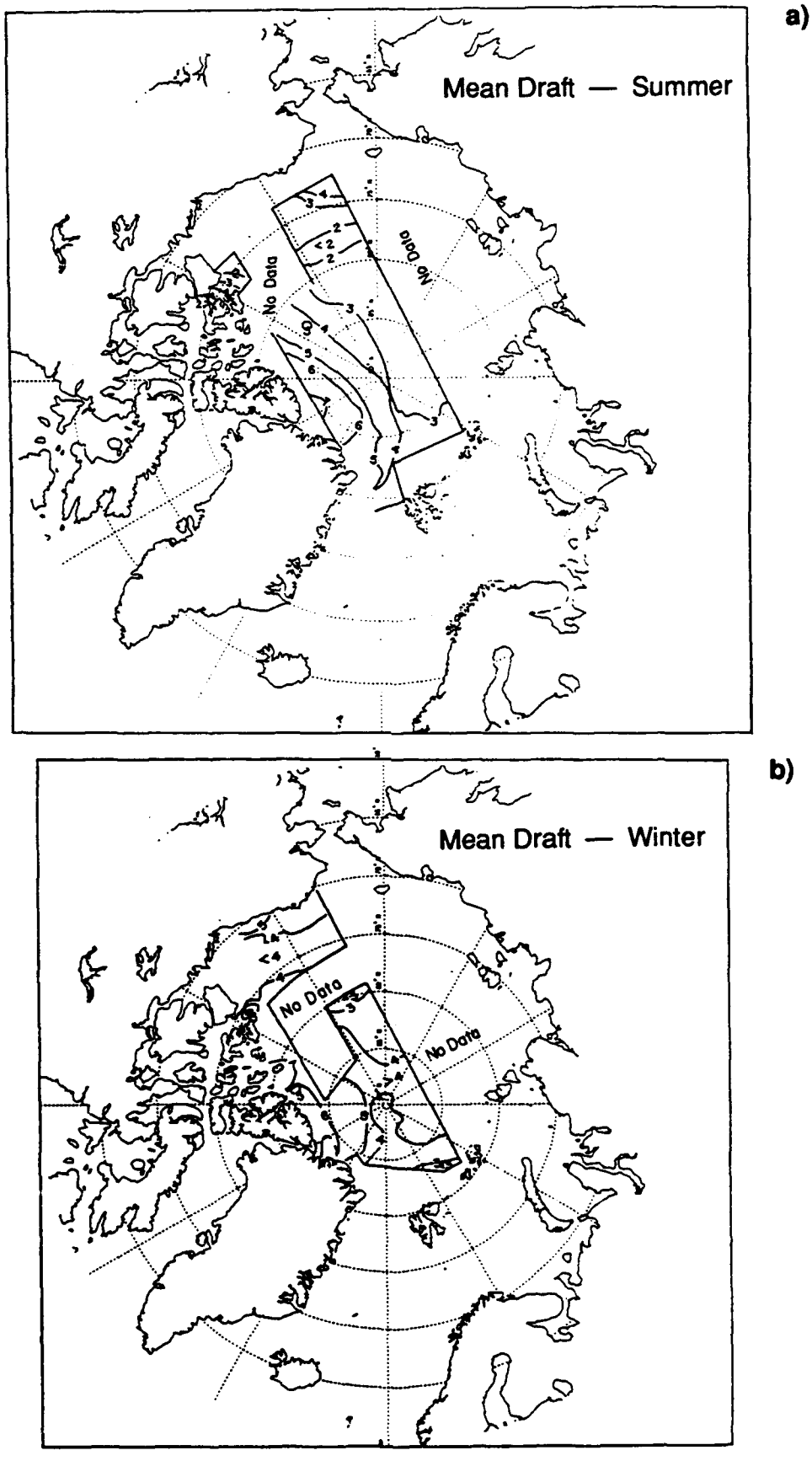

Figure 5. The mean ice draft from summer and winter submarine cruises (from Bourke and McLaren, in press).

As a measurement system for future observations, the submarine has obvious strengths and weaknesses. It is a proven system. It can observe the entire ice pack, except in depths less than about 50 m, during any season. However, at present no mechanisms exist to coordinate U.S. submarine missions with civilian scientific requirements. There is no reason why such mechanisms cannot be developed. They would have to provide some civilian scientific input to mission plans and to data processing and analysis, with prompt public access to data. In the process, it would have to be recognized that scientific work was one of the missions of the submarine fleet, and resources would have to be committed to supporting that work.

Moored upward-looking sonar instruments have been used for only a few seasons, but there is no question they are effective (see Appendices B-VII and B-VIII). Their main limitations arise from difficulty in deploying and recovering the instruments in permanently ice-covered regions. Fixed moorings are able to sample the ice thickness as the ice moves overhead. With a low data rate, successive measurements sample widely and unevenly spaced points. This is a desirable sampling strategy for estimating ice thickness distribution, but it cannot describe the shape of the ice surface, count pressure ridges, or discriminate between level and deformed ice.

Doppler techniques can be used to measure the velocity of the ice as well as its thickness. This would be important for measuring the transport of ice through Fram Strait, for instance. Experience will decide whether it is worth the added cost and complexity. Wadhams (Appendix B-V) discusses some of the strengths and weaknesses of the submarine and moored sonar measurements.

Electromagnetic sounding of ice thickness at radar and radio frequencies is the only technique that purports to observe both top and bottom ice surfaces. The propagation of VHF, UHF, and radar energy through the ice cover is strongly affected by the variable ice crystallographic structure, thermal gradients, and the geometries of brine and gas bubbles. Radar sounding has successfully observed the thickness of cold, first-year ice and of multiyear ice, but has not been able to see the bottom of warm or briny ice, or deformed first-year ice. On the other hand, ice is quite transparent to VLF energy (1–250 kHz), which shows a return only from the ice–ocean interface. Distance to the top snow surface can be measured by a laser. Like sonar sounding, the fairly wide VLF antenna pattern complicates the interpretation. Electromagnetic sounding surveys are generally carried out from helicopters and fixed-wing aircraft; if further developed and validated, they could add an important thickness measurement capability.

Finally, airborne profiles of the top surface using lasers have been shown to correlate well with the ice thickness (see Appendix B-IX, Figure 2; Comiso et al., 1991; Wadhams et al., 1991). The principles are similar to the sonar measurement. In this case the height of the airplane is determined by the Global Positioning System. The measurement has the fundamental handicap that the multiplicative factor to convert height above sea level to thickness is about 9, rather than about 1.1 for draft to thickness. Therefore small errors in determining the topside profile lead to large errors in thickness. Variable and unknown snow depths make the situation worse by altering the height to draft ratio. If further experience confirms the potential of airborne profiling methods, it could open the way to systematic ice thickness surveying.

None of the techniques discussed can determine the rate of change of ice thickness, yet this growth or melt rate is a critical element in the theory of the ice thickness distribution. The only reliable technique is the hot wire thickness gauge originally developed by Untersteiner, but it is labor intensive and has never worked well for very thick ice. There is a need for an automated growth and melt rate measurement system.

IV. Current Knowledge of Sea Ice Thickness

Observations of ice thickness have been accumulating since Nansen's time. McLaren et al. (1990) summarized some of these data. Nansen reported average thicknesses for ice floes in the Transpolar Drift Stream in the range of 3.1 to 3.8 m. Zubov gave average values of 2.3 to 3.3 m for the thickness of perennial ice, with the maximum thickness of undeformed ice being 5 m. Koerner's measurements from the late 1960s gave a mean thickness of 3.7 m along his path from Barrow to Svalbard. These measurements were made at drill holes or along cracks in the ice by people who happened to be there. Because of the large local variability of thickness, many independent measurements need to be taken to get a good average (Table 3). Furthermore, it is extremely difficult to measure the draft of deep keels this way. It is nearly impossible to avoid biasing the sample as the driller steers clear of the thinnest and the thickest ice. A conservative summary of these observations is that they give an estimate of thickness of about 3 to 4 m for 20th century ice that is in equilibrium and undeformed.

Table 3. Sampling requirements for sea ice thickness.

Quantity	Resolution	Sampling Strategy
Thickness distribution for a given region and time $g(h)$	10 bins, 10%	1000 points at least 100 m apart
Mean thickness $\bar{h}$	30 cm	100 points
	10 cm	1000 points
Secular trend $d\bar{h} / dt$	2 cm per year	100 points per survey 1 survey per year for 15 years
Ice flux at Fram Strait	10%	continuous monitoring of thickness and velocity at several locations

Submarine Data

Since the 1957/58 voyage of the *Nautilus*, the underside of the ice pack has been observed with upward looking sonar. Bourke and Garrett (1987) cite an estimate by Beal that 200,000 km of underice tracks have been made by U.S. submarines and about 15% of the data has been digitized for scientific analysis. A guess would be that the data accumulate at the rate of about 5,000 to 10,000 km of track per year.

A number of attempts have been made to use these observations to document the ice thickness distribution and its variations in space and time. The many published observations of $g(h)$ exhibit the following features (see Figure 1).

a. Most distributions from the central Arctic have a peak near $h = 3$ m.

b. The shape of the distributions for $h > 3$ m is approximately

$$g(h) \cong \exp(-h/H) \qquad h > 3 \text{ m},$$

with $H \cong 3$ m.

c. For $h < 3$ m, the distributions are highly variable. Some show a clear local maximum near 1.5 m, corresponding to first-year ice. Some have a spike at $h = 0$, indicating a finite area of open water. Most have $g(0) > 0$.

Bourke and Garrett (1987) have published maps of the average thickness $\bar{h}(\mathbf{x})$ (see Figure 6). The distribution of $\bar{h}$ is reasonably convincing. It shows that the mean thickness generally increases from the Siberian coast across the Arctic to the Canadian archipelago and Ellesmere Island. The greatest mean thicknesses of 7 m occur near the coast of Greenland and Ellesmere Island. A similar pattern was shown years ago by LeSchack et al. (1971) and by Hibler (1979), based on much smaller data sets. The great thickness of the ice in this region has been explained in terms of the convergence of the ice velocity field here, although the convergence has not been measured. This is twice the basinwide mean thickness. It confirms that mechanical processes play an important role in maintaining the thickness distribution, and this underscores the importance of modeling these processes well.

The seasonal pattern of mean thickness, shown by Bourke and Garrett, is difficult to interpret because their definition of mean thickness does not account for large regions of open water. They obtain the result that the mean thickness is greatest in summer, because of their choice of definition.

The data probably are not adequate to resolve any secular changes in thickness distribution because the sampling has not been robust enough to separate true secular change from interannual variability, seasonal variability, and geographical variability. However, the data may be adequate for estimating these sources of variance, and that would be extremely useful. McLaren and Bourke have estimated the interannual variability by comparing the mean thickness observed over a 50 km track passing through the North Pole at the same time of year for six different years between 1976 and 1990. They found a range of 3.6 to 4.3 m for this 50 km mean. For a region north of Greenland, Wadhams measured mean thickness of 6.3 m in 1976 and 4.1 m in 1987. Perhaps the best way to summarize these results is to note that we can measure variations in mean thickness but we do not have enough information to interpret them.

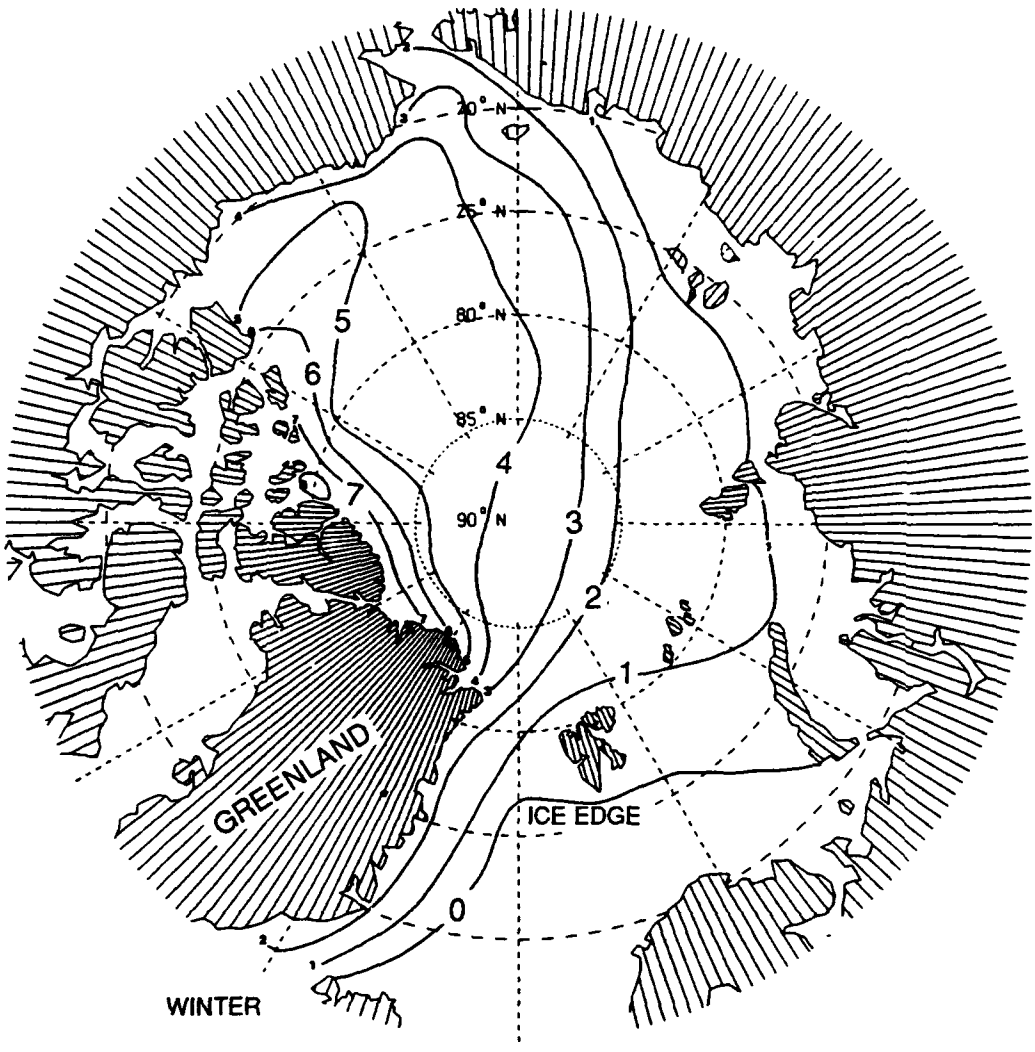

Figure 6. The mean ice draft in winter, contoured in meters (from Bourke and Garrett, 1987). The greater spatial coverage of these data compared with Figure 5 is explained by the use, in this case, of log-book entries and strip chart records from a number of cruises not used in the McLaren and Bourke study because of the difficulty in interpreting them.

Upward Looking Sonar Observations

A time series of sea ice draft, sampled every several minutes, was measured by a moored upward looking sonar (ULS) operating in the Chukchi Sea from 15 April 1988 to 15 April 1989 (Moritz, 1991). Sample ice draft distributions, estimated as histograms from individual segments of the time series, exhibit large changes in parameters including the sample mean, mode, median, and standard deviation. These changes are illustrated by four histograms drawn from distinct four-day segments of the time series (Figure 7). These figures illustrate the distributions during the end of the winter growth season, the advective incursion of polar pack ice, the open water of late summer, and the mid-winter growth season.

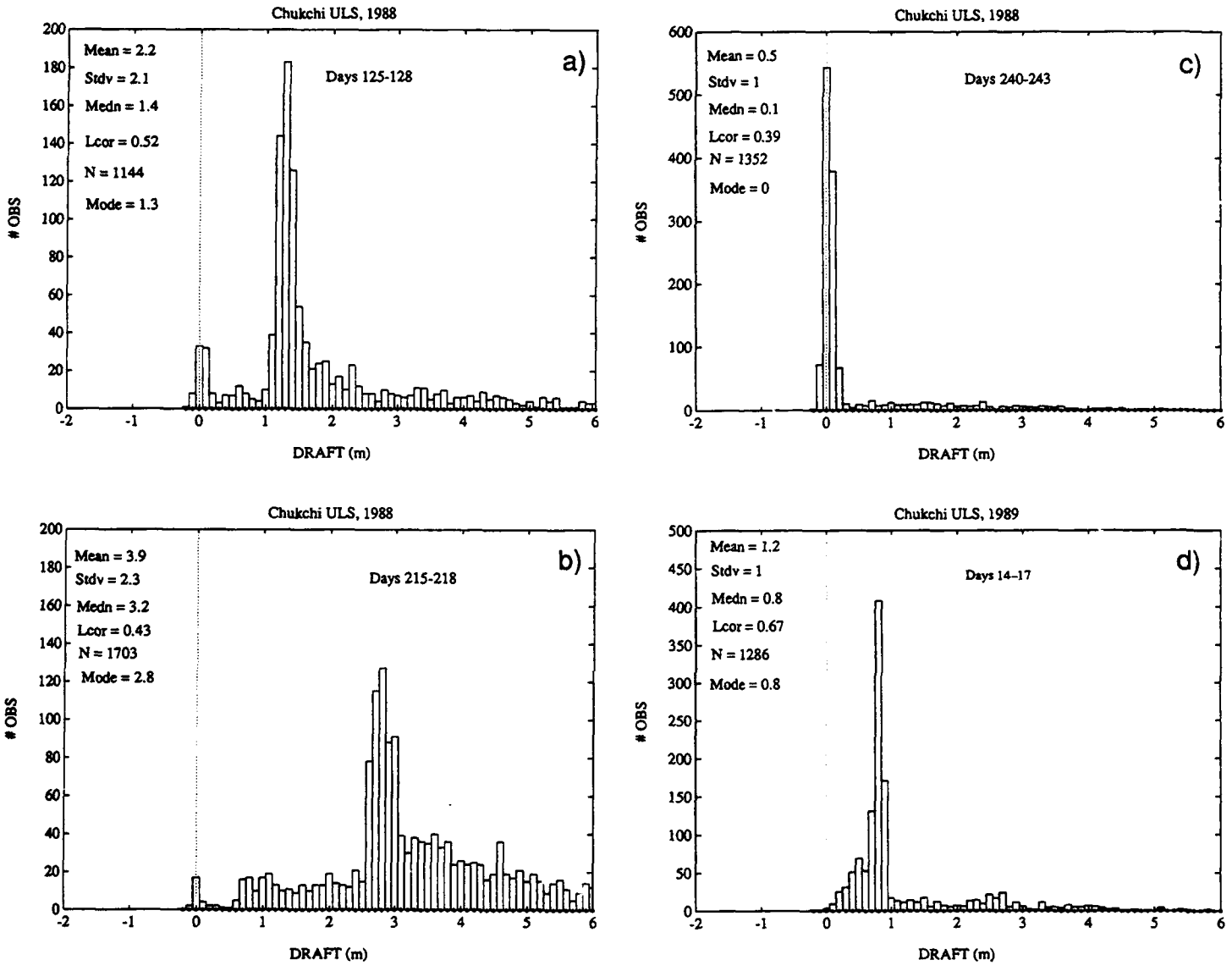

Figure 7. Histograms of sea ice draft measured by Upward Looking Sonar (ULS) in the Chukchi Sea: (a) May 1988, (b) early August 1988, (c) late August 1988, and (d) January 1989. Observations are taken at four-minute intervals. Sample statistics are shown in the upper left of each plot.

The modal ice draft can be estimated with reasonably small sampling error from segments as short as 12 hours (144 measurements). Figure 8 shows the year-long time series of modal ice drafts. A smooth version of the obvious seasonal variation is sketched on the figure, ignoring outliers and the advective event of days 200–215. This curve would be appropriate to compare with the seasonal variation of sea ice draft simulated by energy balance models forced by atmospheric heat and radiation fluxes

representing this particular year. At the points labeled "A," "B," and "C" on the curve, the estimated ice growth rates are –1.2 cm/day, –3.3 cm/day, and +0.7 cm/day, corresponding to fluxes of the latent heat of ice formation approximately as follows: –40 W m^{-2}, –110 W m^{-2}, and +25 W m^{-2}, respectively. These fluxes are calculated as $F = 1.1\ \rho\ L\ dh/dt$, where ρ is ice density, L is the latent heat of sea ice formation, h is ice draft, and t is time. Sampling of other parameters of the ice draft distribution is considered by Moritz in Appendix B-VIII.

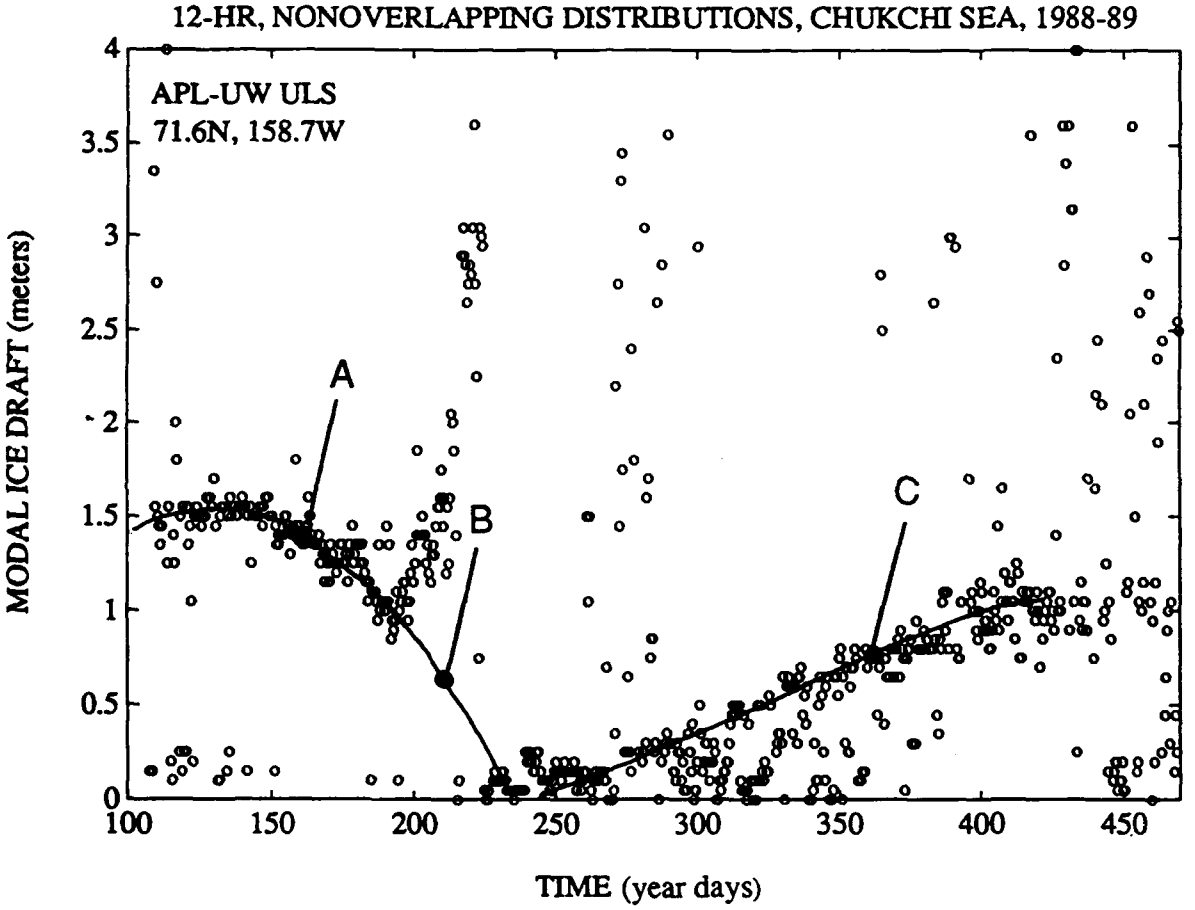

Figure 8. Time series of modal sea ice draft estimated from nonoverlapping 12-hour segments measured by a moored ULS sampling once per five minutes. Distinctive features include the decrease from days 150–195, the increase for the majority of the data points from days 250–420, and the abrupt increase from days 200–215. Analyses of concurrent time series data on winds and ice motion suggest that these features represent summer melt, winter freezeup, and advective incursion of polar pack ice, respectively. Much of the scatter in the data is attributed to sampling variability associated with estimating modal ice drafts from approximately 150 individual samples.

Ridge, Keel, and Lead Statistics

Interpretation of ice profiles in terms of ridge keels has focused on two issues: the distribution of keel drafts and the distribution of keel spacings. There have also been attempts to relate these distributions to each other. The results can be summarized as showing the following:

a. The distribution of keel drafts is about the same as the distribution of thickness itself.

b. The distribution of keel spacings for large spacings and deep keels has roughly a negative exponential shape. For example, if one restricts attention to keels deeper than h_K = 9 m and asks how likely it is to find a separation x between successive keels, the answer appears to be proportional to exp ($-\mu x$), provided x > 150 m or so.

c. The parameter μ in the distribution of keel spacings has dimension [length^{-1}]. It is related to the average number of keels per kilometer exceeding the cutoff h_K. It may be easier to think in terms of the number, K9, of deep keels per kilometer than to worry about parameters in the distribution of keel spacings. Data on K9 indicate values of about two per kilometer in the central Arctic and about four per kilometer in the thick ice region close to the Canadian archipelago and north of Ellesmere Island.

Compared with pressure ridge keels, leads are ephemeral features. They endure over time scales of days, whereas keels may endure for years. Also, it is hard to see what physics limits the widths of leads. The spacings between leads have to do with the sizes of ice floes, but even here the interpretation is not straightforward because mechanically distinct floes need not be separated by more than a narrow, unobservable crack. Still, the leads are important features, and we need to define appropriate observable properties for them. The fraction of area covered by open water and thin ice, say h < 0.1 m, is already contained in the thickness distribution. In an attempt to say how the total lead area is partitioned into distinct leads, Wadhams has defined a distribution of lead widths $n(d)$ denoting the number of leads per kilometer having widths between d and d + 1 m. For some data, he found that n was proportional to d^{-2}. The geometry of leads can vary so rapidly in time and space that it may be difficult to define lead structure that is characteristic of a given region.

Estimates of the proportion of level ice have been made using Wadhams's definition that the local thickness slope is less than 1 part in 40. For example, he reports values in the neighborhood of 50% for the central Arctic and 30–40% for the ice just north of Greenland.

Drill Hole Thickness Measurements

Direct measurement of sea ice thickness by manual drilling remains the only firm technique for accurately obtaining ice thickness. Koerner (1973) made drill hole thickness measurements on the British Transarctic Expedition and used the measurements to estimate the mass balance of the ice in the Arctic Ocean, also providing data on coverage and thicknesses of deformed and undeformed first-year and multiyear ice. Ackley et al. (1976) presented the first detailed measurements of thickness variations of multiyear floes and developed methods to relate thickness to laser profiles. Kovacs (1983) carried out many drillings of pressure ridges to establish keel to sail ratios. Wadhams et al. (1987) found that most of the undeformed ice in the eastern Weddell Sea fell into the narrow range of 40–50 cm. Eicken and Lange (Appendix B-I) found a nearly uniform distribution of ice from 0.5 to 2 m thick in the northwestern Weddell Sea, where presumably the ice is deformed (see Figure 9). In the

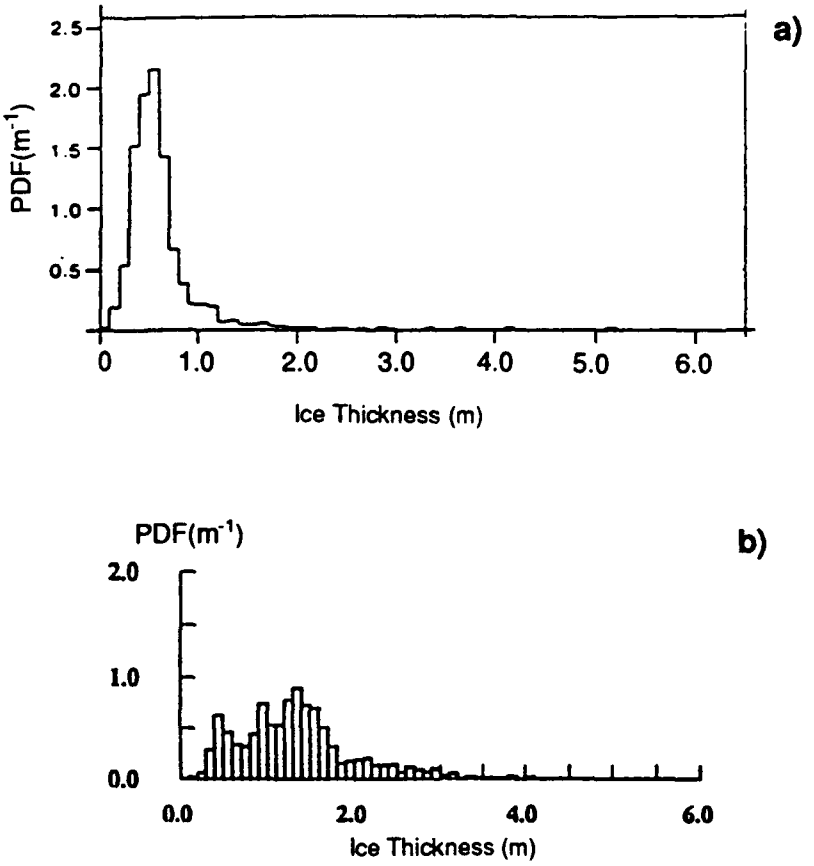

Figure 9. PDFs of ice thickness (a) in the eastern Weddell Sea and (b) the northwestern Weddell Sea.

eastern and western portions of Fram Strait, Kvambekk and Vinje (Appendix B-VII) found substantial variations in mean ice thickness, probably attributable to the ice originating from different source regions in the Arctic. Tucker (Appendix B-II) examined several sample areas on a single multiyear floe (Figure 10) and concluded that 50% of the ice sampled was derived from deformational processes. Eicken (pers. comm.) reached the same conclusion from a combination of ice structural information and drill hole measurements in the high Arctic. Drilling provides additional information such as ice freeboard, snow depth, and draft (see Eicken in Appendix B-I). New advances in hot water drilling (Govoni and Tucker, 1990) have led to far more rapid ice penetration, allowing hundreds of holes to be drilled through thick ice in a single day.

To summarize our state of knowledge, we know

1. the extent of sea ice, its seasonal and interannual variations since 1973
2. the mean thickness (±1 m) with some idea of geographical variation
3. typical thickness distributions over much of the Arctic Basin
4. typical distributions of ridging, with some geographical variation (±50%)
5. the flux of ice through Fram Strait.

We do not know

1. the ice thickness distribution over about half the Arctic Basin
2. seasonal changes in ice thickness distribution
3. total ice volume and its seasonal cycle
4. regions of net production, net loss of ice
5. the composition of the ice pack in terms of various ice types
6. the interannual variability in all the above.

These remarks refer to our observations of the ice pack. A theoretical context for interpreting these observations was mentioned in the Introduction. It consists of a differential equation for the evolution of the thickness distribution in response to thermal and mechanical forcing. Elements of the theory account for the processes of ice growth and melt, ice transport, and the formation of leads and pressure ridges. Structurally, the theory is a statement of conservation of ice volume, taking into account the sources and sinks of ice, and various ways to reconfigure existing ice volume—so, at that level, the theory is invulnerable. However, the submodels of the thermal and mechanical processes are not well founded in observations. For example,

the theory requires growth and melt rates at any location, at any time, and for any thickness. These are not well known, especially for thick ice. Another example concerns the formation of pressure ridges. The model postulates that the thinnest ice in the distribution gets squeezed together to create a ridge that is a multiple of the original thickness. This is based on the field reports that ridges are built of thin ice, but it needs quantitative support.

These modeling ideas help to organize the many issues of ice thickness by focusing on the ice thickness distribution and on the processes that maintain it rather than, say, the pressure ridge frequency. They provide the context within which to interpret new measurements.

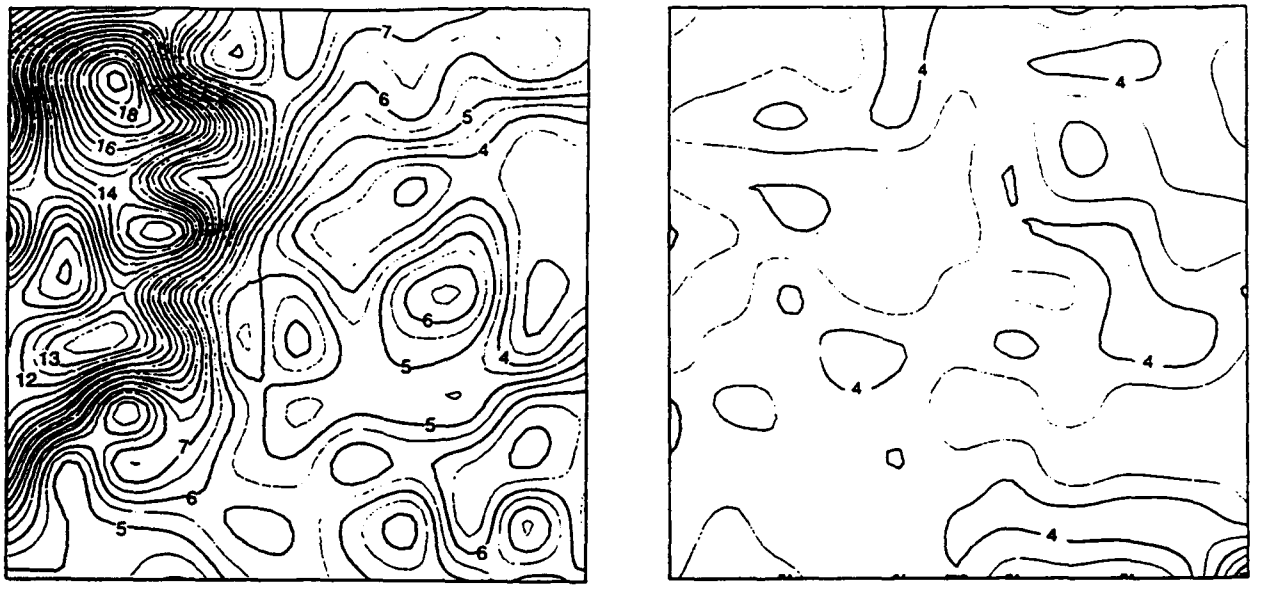

A

Mean Thickness = 7.13 m
Standard Deviation = 3.47 m

B

Mean Thickness = 3.63 m
Standard Deviation = 0.48 m

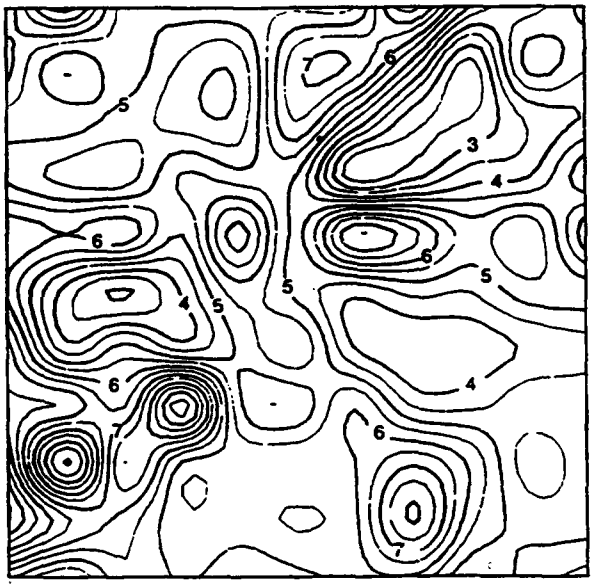

C

Mean Thickness = 5.33 m
Standard Deviation = 1.36 m

Figure 10. Contours of multiyear ice thickness (m) in 100 m by 100 m squares for an area of highly deformed ice (A), an area of undeformed ice (B), and an area containing both deformed and undeformed ice (C). Grids were located several hundred meters apart on the same multiyear floe.

V. Modeling of Sea Ice Thickness

Objective

Variations of sea ice thickness may provide an indication of whether or not significant climate change is occurring at high latitudes. Although measurements of ice thickness have increased in recent years, the routine full basin monitoring of ice thickness is unlikely to be feasible in the immediate future. One strategy for the diagnosis of variations in ice thickness is a blended approach utilizing available data in conjunction with numerical models of the sea ice cover. Data assimilation will be a key element of such a strategy, and recent work at the Naval Oceanographic and Atmospheric Research Laboratory (NOARL).* Polar Ice Prediction System (PIPS), and the University of Washington (Thomas and Rothrock, 1989) provides encouraging indications that the blending of data and ice models will indeed be useful. Model development over the next ten years, together with appropriate measurement programs, will be necessary to bring such an effort to fruition.

Background

When forced by time-varying fields of atmospheric and oceanic variables, sea ice models can provide grids of sea ice concentration, velocity, and thickness at regular time intervals. Such models clearly require calibration and verification. However, once the credibility of a model has been established through such verification procedures, the model can be a proxy source of data that supplements the temporally and spatially fragmentary measurements of sea ice. Indeed, modeling may represent the best approach to a complete space-time depiction of the distribution of sea ice thickness.

In recent years there have been experiments with sea ice models both in a stand-alone mode and in coupled ice-ocean simulations. With regard to mean ice thickness, the results of these models are consistent in many respects. Almost all models produce climatological (multiyear mean) fields in which the ice thickness increases across the Arctic from the Eurasian coastal waters to the region north of the Canadian Archipelago and Greenland. The models that have been run with interannually variable forcing also produce strong interannual variations of the spatial distribution of ice thickness. For example, model runs made at Dartmouth (Flato and Hibler, 1990), Illinois (Walsh and Zwally, 1990), and Royal Roads (Fleming and Semtner, 1991) all indicate a buildup of ice thickness along the Siberian coast during 1979–1981 to values as large as (or larger

*Now Naval Research Laboratory (NRL) Detachment.

than) those found northwest of Canada. The buildup was caused by wind forcing that differed substantially from the normal pattern.

Models also have similar sensitivities to thermodynamic forcing. For example, systematic changes of 2–5°C in the prescribed air temperatures change the equilibrium ice thickness by 0.5–1.0 m. (Note, however, that such experiments are unrealistic in the sense that other thermodynamic forcing fields are not permitted to change with the temperature.) Changes in the radiative parameterization produce major changes (e.g., factors of 2–3) in ice thickness, even when the radiative changes are within the range of parametric or observational uncertainty (Hakkinen, Appendix C-II). The parameterization of the radiative effects of clouds is one of the most delicate and uncertain steps in the estimation of radiative fluxes over the central Arctic. Finally, sea ice models are less sensitive to snowfall rates than expected (e.g., Hakkinen, Appendix C-II).

Discrepancies between ice thicknesses simulated by different models appear to stem from the treatment of the thin end of the ice thickness distribution. The so-called two-level Hibler model resolves the ice thickness distribution into only two categories. It underestimates ice thickness. This underestimate appears to be attributable to inadequate resolution of the thin ice categories. On the other hand, models with better resolution of the thickness distribution (e.g., Flato and Hibler, 1990) seem to simulate the mean thickness and its distribution with considerable success, although the simulated spatial and interannual variations of mean thickness still disagree somewhat with those deduced from sparse submarine sonar data. The effect of oceanic coupling on the Flato-Hibler thickness model remains to be seen. Although such a coupling did degrade the results of the Semtner-Fleming model, recent simulations at Dartmouth with a coupled, two-level, ice-ocean model showed improvement in the interannual variability of the ice edge, but produced ice that was thinner than observed. The NOARL coupled ice-ocean model (Piascek et al., 1991) also underestimates (by about 35%) the annual mean ice thickness in the central Arctic. Finally, we note that there has been little attempt to validate ice model simulations of several quantities that are vital elements of a climate simulation, especially the flux of sea ice through Fram Strait and its effects on the Greenland Sea stratification.

Good inputs are required for the atmospheric and oceanic forcing of sea ice models. Among these are surface wind, surface air temperature or the snow/ice surface temperature, incoming solar radiation (generally computed from the solar zenith angle and parameterized depletion—clouds, humidity, etc.), longwave radiation (generally

computed from atmospheric temperature, humidity, and cloudiness), surface albedo, snowfall rate or snow depth, oceanic heat flux, and ocean currents. The following observed quantities are required for the verification of ice model simulations: ice concentration and extent, ice thickness distribution, ice velocities and associated kinematic quantities, and surface quantities such as albedo, snow depth, and snow/ice surface temperature. Some of the above variables, such as the wind, are already available with adequate spatial and temporal resolution. Others, such as cloud cover and snow depth, are not adequate. On the basis of model experiments, the workshop participants arrived by consensus at a list of prioritized needs with regard to the improved modeling of sea ice thickness. The priorities were set not according to the relative importance of each variable's contribution to ice thickness, but according to how much improvement is likely if better data are used. The improvements would result not only from the use of more realistic forcing data, but also from the use of such data in the development of more realistic parameterizations in the model.

The prioritized variables for model forcing and model development are

A1. cloud cover (for radiative flux determinations)

A2. surface albedo

A3. oceanic heat flux and currents

A4. snow depth

A5. surface and near-surface air temperature

A6. atmospheric humidity

A7. surface temperature

A8. wind speed and direction.

The prioritized variables for model verification are

B1. ice thickness distribution

B2. ice motion

B3. surface albedo

B4. snow depth.

The low ranking of wind speed and direction in the first category is testimony to the value and adequacy of the present network of Arctic drifting buoys. Similarly, the low ranking of ice concentration and extent indicates that the satellite-derived fields of these variables meet many of the current needs of large-scale models.

Recommendations

Given the above priorities, specific recommendations for action over the next several years are listed here for the five highest-priority variables for model forcing and development and for the two highest priority variables for model verification.

Specific recommendations - observational

A1. Cloud cover and radiative impacts

1. Use existing databases to obtain spatially varying fields of cloud fraction, providing monthly climatology for model forcing.
2. Exploit the products of the International Satellite Cloud Climatology Project (ISCCP) by
    a. using ISCCP cloud parameters to improve parameterization of polar radiative fluxes
    b. improving ISCCP algorithms for retrieval of cloud information in polar regions, especially where snow/cloud discrimination has introduced some contamination into cloud statistics.

    With regard to these recommendations, the ISCCP group and others have begun work on improved polar cloud retrievals and intend to reprocess all the ISCCP data in the near future.
3. Explore uses of the atmospheric Global Climate Model output as a source of radiative forcing data for ice models.

A2. Surface albedo

1. Use satellite visible and IR data to produce gridded fields of high latitude surface albedo.
2. Consolidate and use information on the reflectivity of specific surface types such as fresh snow, melting snow, and ponded ice as functions of cloudiness, zenith angle, surface temperature, ice thickness, and snow depth.
3. Develop algorithms for parameterizing the albedo in model grid cells containing mixtures of surface types.

A3. Ocean heat flux and currents

1. Explore the use of satellite altimeter measurements to map dynamic topography of high latitude oceans, thereby permitting estimates of

geostrophic currents; temporal frequency should be sufficient to resolve seasonal and interannual variations.

2. Exploit existing fields of sea surface temperature.
3. Obtain more realistic ocean heat fluxes by coupling ice and ocean models.

A4. Snow depth

1. By direct measurement, determine spatial statistics for snow depth.
2. Using these statistics, investigate sampling strategies for estimating large-scale average snow depth and its time variations.

A5. Surface and near-surface air temperature

1. Pursue methods for retrieval of clear-sky surface temperature using thermal sensors (e.g., AVHRR, TOVS/HIRS) and possibly the retrieval of subsurface temperatures from passive microwave sensors.
2. Explore uses of atmospheric sounders (e.g., TOVS) to obtain information on near-surface air temperature.

B1. Ice thickness distribution

1. Consolidate existing data on ice thickness into a seasonal climatology.
2. Determine interannual variability of the large-scale spatial pattern of ice thickness, especially in the Siberian Arctic, where models show strong year-to-year variations in response to wind forcing.

B2. Ice motion

1. Measure the ice velocity field with sufficient detail to verify simulated strain rates.
2. Compare simulated and observed ice divergence and creation of open water. Assess the simulated ice mass budget.

General recommendation - observational

The data sets required for the forcing and verification of sea ice models are, if available, diverse and generally fragmented. We recommend that the data sets useful to ice modelers be brought together at a data center or other appropriate institution with special attention paid to data synthesis, reformatting, and quality control.

Recommendations - modeling

The following recommended activities emerged from the general session and from the discussions of the modeling subgroup at the Workshop:

C1. Accelerate the development of coupled ice-ocean models. Successful coupling will eliminate the need to specify oceanic heat fluxes and currents, as is now done in some ice models.

C2. Improve the thermodynamic component of large-scale sea ice models. Among the needed improvements are the inclusion of nonlinear temperature profiles in thick ice, effects of ice salinity on thermal properties, and the formation and drainage of surface melt ponds. An additional task is a model for the thermodynamic evolution and mechanical erosion of ridged ice.

C3. Assess the kinematic performance of dynamic sea ice models. Because the thickness distribution and mass budget of sea ice depend on kinematic quantities, there is a need to determine the adequacy of the model kinematics in both the Arctic Basin and the active subpolar seas of the North Atlantic. A combination of existing buoy data, SAR products, and additional remotely sensed data should provide input to the verification activities of modelers.

C4. Enhance the resolution of sea ice models.

VI. Science Strategies

The current ice thickness distribution is a characteristic of today's climate. Monitoring it for possible secular change is needed if we are to understand the response of sea ice to changes in other components of the climate system. Thus we have two broad objectives:

1. to know today's sea ice thickness distribution and understand the processes that cause it to vary
2. to monitor the thickness distribution for possible secular change.

At a single location, the ice thickness distribution displays a seasonal cycle that is believed to repeat approximately each year. The equilibrium cycle is maintained by thermal and mechanical processes, which alter the thickness distribution locally and move it about by advection. Our current observational and theoretical understanding of these processes is not enough to reveal which processes are most important or how the balance may vary from place to place. For some purposes, it is a fair approximation to ignore the annual cycle, thinking in terms of the annual average distribution, but even then it is not known how the balance between thermal, mechanical, and transport terms is achieved.

There is a well known circulation pattern in the Arctic Ocean that results in an annual flux of about 3×10^{12} m^3 of ice through Fram Strait. This represents about 10% of the ice stored in the basin. On average, this ice must be replenished each year within the basin. The present generation of ice models is beginning to identify regions of net ice production, but observations are not available to confirm these results.

Four strategies are described here to address these issues:

1. To document the current ice thickness distribution, including its geographical and seasonal variation, observations from submarines, moored upward looking sonars, aircraft, and satellites should be utilized more thoroughly.
2. To monitor the flux of ice through Fram Strait, a long-term program of observations of ice thickness and velocity is advocated.
3. To reach a better understanding of the processes controlling the ice thickness distribution, we recommend an intensive observing program, of limited duration, capable of resolving changes in thickness distribution, ice growth, and ice deformation.
4. To identify regions of ice production and ice loss and to assess the importance of transport terms, we support a vigorous modeling effort augmented by

specialized local observation programs to investigate regions that appear particularly interesting or anomalous in the models.

These strategies are discussed more fully below:

Strategy 1

Using data from all sources to determine geographical and seasonal structure in the ice thickness distribution.

There is a growing data set bearing on ice thickness. It includes observations from submarines, moored upward looking sonars, aerial photographs, drill holes, and satellite imagery. In time, suitable airborne laser and electromagnetic sensors may also provide useful observations in large quantities. Data from these various sources are not coordinated within any master plan to monitor ice thickness over the entire basin. Nevertheless, they are a basis for estimating the geographical and seasonal variations in ice thickness distribution. For example, there are more than ten upward looking sonars (ULSs) deployed in the Greenland Sea, including Fram Strait, Denmark Strait, and on latitude 75°N. These instruments are owned by investigators from the U.S., Germany, Norway, and Great Britain. Systematic monitoring of the ice thickness time series across Fram Strait began in 1991 and is continuing.

Data of this type will continue to be collected. At present, the best spatial distribution is provided by the submarine data, and even this appears to sample only about half the Arctic Basin. It may be possible for the civilian community to have some input into the location and season of future submarine tracks. Repeated surveys of old tracks, exploration of the marginal seas, and denser sampling in certain regions may all be possible.

In any case, the best that can be expected from the current reservoir of data, and data likely to be collected in the next decade, is a set of charts showing, for each season, the spatial structure of the ice thickness distribution, compiled from many years of data. In some places it may be possible to use data from different years to estimate the interannual variability.

In the interpretation of these data, it will be essential for the community to adopt uniform practices in data processing, and uniform definitions for quantities that are reported in the literature (see Appendix A-III). Because the data are accumulating rapidly, it is important to ensure that they are submitted in an appropriate format to a public archive, or older data will be lost as new data are acquired.

NASA's role in this strategy should be to continue to support the development of airborne laser techniques for measuring ice thickness. If this effort is successful, it may be possible to use aircraft to survey the thickness of the entire basin. Continued analysis of satellite passive microwave data, and possibly SAR data, might also serve to resolve the thin end of the ice thickness distribution.

Strategy 2

Monitoring the ice flux through Fram Strait.

The Working Group on Sea Ice and Climate of the WMO World Climate Research Programme, has plans for an Ice Thickness Monitoring Project. These plans feature extensive arrays of moored upward looking sonar instruments — 17 in the Arctic and 27 in the Antarctic. In the Arctic, the highest priority is to monitor Fram Strait. This year, several sonar instruments will be moored there. At present, the systems can measure ice thickness, but plans are in place to add the capability to measure ice velocity using the Doppler shift in frequency of signals reflected from the moving ice. Together, the thickness and velocity give the ice flux. An alternative strategy is to use sequential SAR images to measure the ice velocity. However, the rapid ice motion in Fram Strait may preclude the use of the comparatively infrequent SAR coverage for this purpose. AVHRR data can also be used for measuring ice motion and are probably adequate to resolve the variations in velocity across Fram Strait.

Particular importance is attached to observations of ice flux through Fram Strait since it integrates the net ice production over the entire basin. The situation is analogous to using the discharge of a river to summarize the hydrology of a river basin. The scientific return from these measurements will be substantial. Knowing the ice flux is essential for assessing the mass and energy balances of the Arctic and the budget of fresh water. Exchange of water and ice through Fram Strait is by far the major interaction between the Arctic Ocean and the World Ocean. The discharge of fresh water, in the form of low salinity ice, affects the stability of the Greenland Sea and may be a control on the formation of bottom water.

Ice flux through Fram Strait represents climatic conditions in the Arctic in a single variable which we may interpret directly as a measure of the ability of the Arctic to produce ice. How the Arctic will respond to climate change is not known, but it is hardly likely that the ice production will be unresponsive. It should also be emphasized that the ice flux will serve as a useful model constraint.

Although the emphasis is on ice flux, the ice thickness and velocity in Fram Strait are important in their own right as indicators of different aspects of the behavior of the ice pack. Enough is known about the time and space variability of ice thickness and velocity in Fram Strait to be able to design a safe sampling strategy. Several sensors spaced at equal intervals across the strait, with continuous time sampling, are required. When more is known, the number of sensors might be reduced. Provisions must be made to extend the observations over a period of at least 15 years. With results from the first few years, it should be possible to estimate the interannual variability, and, knowing that, to judge the uncertainty associated with any estimate of secular trend.

A rough guess is that the profiles of thickness and velocity across the strait can be estimated to within about 5%, which would give the flux to 7%. The interannual variations in flux may be this large. Whether we will see a secular change exceeding 7% in 15 years remains to be seen; the accuracy is adequate to make the result interesting whichever way it turns out.

The principal role for NASA will be to support analysis of SAR data for ice motion in the Fram Strait, and of passive microwave data for monitoring the position of the edge of the ice stream where it is eroded by the West Spitzbergen current. These are critical components of the measurement and analysis program.

Strategy 3

A program of Lagrangian measurements to correlate changes in thickness distribution with ice growth and ice deformation.

This program element will improve our understanding of the thermal and mechanical processes that determine the ice thickness distribution. The idea is to measure the quantities in the evolution equation for the thickness distribution well enough to pin down parameters in the theory, as presented by Thorndike et al. (1975), or to identify weaknesses in it. This will require measurements of the ice thickness distribution, growth and melt rates of ice of different thicknesses, and ice deformation. The most promising experimental configuration appears to be Lagrangian: the area of observation follows the motion of an ice particle. A central point would be marked by one or several buoys, after which the experiment would consist of observing the evolution of the region surrounding that central point. A tentative experimental scenario has the program beginning in 1995 and lasting for two years. The central point would be chosen on the date line at 75°N and followed as it drifts northward. Observations would be made in a circle of radius 200 km around the moving central point. Four

thickness surveys of the experimental region would be made using submarines, unmanned underice vehicles, airborne laser altimeters, or other techniques. Each survey would consist of about 2000 km of track, more or less randomly crisscrossing the test region. The measurement strategy needs to be adequate to resolve temporal changes in thickness distribution.

Growth rates should be measured at a few hundred sites, using wire thickness gauges or other techniques. For an average growth rate, the sampling rate might be as low as two observations per year per site. The emphasis would be on the thickness changes for thick ice. A system for unattended thickness measurements is urgently needed.

The ice deformation would be monitored throughout the experimental period using a number of drifting buoys and sequences of SAR images. Radarsat's wide swath would be ideal. The interpretation of the deformation would involve the classical description of deformation in terms of the strain rate tensor and direct quantification of the local opening and closing of leads.

An experiment such as this clearly involves a substantial commitment of resources. However, much of it could be done by coordinating activities that will probably be going on anyway, namely submarine missions, drifting buoys, and SAR imaging. The measurements of thickness would be new.

We would emerge from this experiment with a thickness distribution theory tested against observation and revised as needed. We would have a more solid growth rate function, $f(h,t)$, although we would still not know much about how it depends on location. We would have better observations of ice kinematics and a basis for comparing rival redistribution functions in the theory.

The appropriate role for NASA in this strategy would be to support the SAR analysis and provide aircraft laser altimetry of the test region. The experiment would also be an opportunity to learn more about all satellite remote sensing over sea ice, since so much will be known about ice conditions in the region. Particular emphasis should be given to using remote sensing data to estimate the heat fluxes near the ice surface since these control the ice growth and melt.

Strategy 4

Coordinated modeling studies and observations.

Several models now exist which include some form of ice thickness distribution. The models simulate many of the processes believed to be important in maintaining the ice cover. For example, it is possible to go to any model cell and ask how much open water is formed in response to the deformation, how much deformed ice there is and when it is formed, what the rates of production and melting of ice are, what is the spatial gradient of ice thickness distribution, and so on. On the other hand, there is little reason to believe the answers to any of these questions, since the models are based on flimsy parameterizations of the basic processes and have not been adequately tested against observations.

We believe the models will suggest observations that will quickly lead to model improvements. Two kinds of observations seem likely: special line or point sampling of ice thickness distribution, and regional process studies. An example of the first kind would be to repeat the under ice profile along the same track as followed by the *Nautilus* in 1958 and the *Queenfish* in 1970. Flato (Appendix C-I) has used these two cruises to compare against his model results, but the comparison is inconclusive. He needs more data from the same track, during a period when the wind and temperature forcing is better known, to determine whether his model has systematic bias. Records such as this are especially important because they allow measurement of the spatial structure of ice thickness and its long-term change.

Another special line survey would run from the Canadian islands to the East Siberian Sea. Model results indicate large thicknesses in the East Siberian Sea. In some winters, the mean thickness there, in these models, is as great as in the region just north of Greenland and Ellesmere. There are no observations against which to test these results.

By regional process studies, we have in mind examining the term by term contributions to the evolution of thickness distribution in regions where model results are particularly interesting or anomalous. For instance, Walsh (Appendix C-IV) has identified the regions of large ice production in his model. It would go a long way toward developing confidence in the model to know if a region really was a region of ice production, and, if so, what processes were responsible. Was the production the result of ice divergence during the growing season, or large shear (which, in the model, produces open water and thick ridges), or large growth rates?

Conclusion

Taken together, these four research strategies are certain to advance our understanding of the arctic ice pack. The strategies are not new. In most cases, we have merely identified work that is currently being done, or is in the planning stage. Many of the ideas have appeared in other planning documents. But there is here an attempt to bring together a number of activities that contribute to the overall goal of understanding sea ice thickness better. These activities are loosely related: they benefit each other, but they can proceed more or less independently.

There are no plans in place for the Lagrangian process study (strategy 3). A group of scientists and funding agencies needs to step forward to develop such plans.

VII. References

Ackley, S. F., W. D. Hibler III, F. K. Kugzruk, A. Kovacs, and W. F. Weeks, 1976. Thickness and roughness variations of Arctic multiyear sea ice, CRREL Report 76-18, U.S. Army Cold Regions Research and Engineering Laboratory, Hanover, NH, 25 pp.

Bourke, R., and C. Garrett, 1987. Sea ice thickness distribution in the Arctic Ocean, *Cold Reg. Sci. and Technol.*, **13**, 259–280.

Bourke, R. H., and A. S. McLaren, 1992. Contour mapping of Arctic Basin ice draft and roughness parameters, *J. Geophys. Res.*, in press.

Comiso, J. C., P. Wadhams, W. B. Krabill, R. N. Swift, J. P. Crawford, and W. B. Tucker III, 1991. Top/bottom multisensor remote sensing of arctic sea ice, *J. Geophys. Res.*, **96**, 2693–2709.

Flato, G. M., and W. D. Hibler III, 1990. A cavitating fluid sea ice model, in *Sea Ice Properties and Processes*, Proceedings of the W. F. Weeks Sea Ice Symposium, S. F. Ackley and W. F. Weeks, eds., CRREL Monograph 90-1, 239–242.

Fleming, G. H., and A. J. Semtner, Jr., 1991. A numerical study of interannual ocean forcing on arctic ice, *J. Geophys. Res.*, **96**, 4589–4603.

Govoni, J. W., and W. B. Tucker III, 1990. An update on portable hot-water sea ice drilling, *Cold Reg. Sci. and Technol.*, **16**, 175–178.

Hibler, W. D. III, 1979. A dynamic thermodynamic sea ice model, *J. Phys. Oceanogr.*, **9**, 815–846.

Koerner, R. M., 1973. The mass balance of the sea ice of the Arctic Ocean, *J. Glaciol.*, **12**, 173–185.

Kovacs, A., 1983. Characteristics of multiyear pressure ridges, In *Proceedings of the 7th International Conference on Port and Ocean Engineering Under Arctic Conditions* (POAC-83), Helsinki, **3**, 173–182.

LeSchack, L. A., W. D. Hibler, III, and F. H. Morse, 1971. Automatic processing of Arctic pack ice data obtained by means of submarine sonar and other remote sensing techniques, in *Propagation Limitations in Remote Sensing*, J. B. Lomax, ed., AGARD Conference Proceedings No. 90, NATO Advisory Group for Aerospace Research and Development.

McLaren, A. S., R. G. Barry, and R. H. Bourke, 1990. Could arctic ice be thinning? *Nature*, **345**, 762.

Moritz, R. E., 1991. Sampling the temporal variability of sea ice draft distribution, (abstract, Eos Supplement, Fall AGU meeting, 237–238 (ms in preparation).

Piacsek, S., R. Allard, and A. Warn-Varnas, 1991. Studies of the arctic ice cover and upper ocean with a coupled ice-ocean model, *J. Geophys. Res.*, **96**, 4631–4650.

Thomas, D. R., and D. A. Rothrock, submitted. The Arctic Ocean ice balance: A Kalman smoother estimate, *J. Geophys. Res.*

Thomas, D. R., and D. A. Rothrock, 1989. Blending sequential Scanning Multichannel Microwave Radiometer and buoy data into a sea ice model, *J. Geophys. Res.*, **94** (C8), 10,907–10,920.

Thorndike, A. S., D. A. Rothrock, G. A. Maykut, and R. Colony, 1975. The thickness distribution of sea ice, *J. Geophys. Res.*, **80**, 4501–4513.

Wadhams, P., 1981. Sea-ice topography of the Arctic Ocean in the region 70°W to 25°E, *Philos. Trans. R. Soc. London, Ser. A*, **302** (1464), 45–85.

Wadhams, P., N. R. Davis, J. C. Comiso, R. Kutz, J. Crawford, G. Jackson, W. Krabil, C. B. Sear, R. Swift, and W. B. Tucker III, 1991. Current remote sensing of arctic sea ice from submarine and aircraft, *Int. J. Remote Sensing*, **12**, 1829–1840.

Wadhams, P., M. Lange, and S. F. Ackley, 1987. The ice thickness distribution across the Atlantic sector of the Antarctic Ocean in midwinter, *J. Geophys. Res.*, 14,535–14,552.

Walsh, J. E., and H. J. Zwally, 1990. Multiyear sea ice in the Arctic: Model- and satellite-derived, *J. Geophys. Res.*, **95**, 11,613–11,628.

APPENDIX A
General

A-I

Sea Ice Thickness: An Overview

A. S. Thorndike

Department of Oceanography, OC/TO

Naval Postgraduate School

Monterey, CA 93943

Abstract: Any understanding of the behavior of sea ice, and its many interactions with other geophysical and manmade systems, must be based on a knowledge of the state of the ice pack. On small scales, the chemical composition and temperature of the ice may suffice, but for most geophysical problems other properties of the ice pack are needed to characterize its state, such as the distribution of ice thickness, the sizes of floes and leads, and so on. Many such state variables have been proposed. It is time to settle on a short list of variables that is adequate for most purposes. A straw man list consists of five numbers, each representing averages over 400 km: $G1$ = fraction of area thinner than 0.1 m, or its complement, 1-$G1$, the ice concentration, H = mean thickness, σ = standard deviation of ice thickness, $K9$ = number of ridge keels per kilometer exceeding 9 m draft, and $L100$ = number of leads per kilometer exceeding 100 m in width and less than 0.1 m ice thickness.

Two recent developments are now providing large amounts of ice thickness data. These are the declassification and release of data from submarine cruises under the ice, and the successful deployments of moored upward looking sonar instruments. With these, it seems possible to define the current state of the ice pack and to monitor the state for possible secular changes. I am not aware of any evidence in the data analyzed so far that supports secular change in the past.

The impression I have is that ice conditions in the central Arctic are remarkably uniform — at least the similarities in ice state among different regions appear to be greater than the differences. For example, the many ice thickness distributions reported all show a strong maximum near 3 m and a thick ice tail of the form $\exp(-h/H)$, where H is about 3 m. Many show a nonzero value for $g(0)$ in winter, and many have a minor but real local maximum between 1 and 2 m. Ice concentrations of about 95% are common in most areas in winter. Counts of deep ridge keels of $K9 \cong 2$/km are typical. The predominant geographical variation appears to be the increase in mean thickness and ridge count as one approaches the north coast of Greenland and Ellesmere Island. Of course, the ice pack changes dramatically as one nears the transition from an ice-covered to an ice-free ocean, as in the Bering or Greenland seas.

Theories that relate the state of the ice pack to the material properties of the ice itself and to the thermal and mechanical forces that act on it have been developed for the ice thickness distribution, but not for other state variables like the ridge and lead counts. The thickness distribution theory runs on an assumed ice growth rate, a postulated mechanism for building pressure ridges, and time series of ice deformation. There are problems with each of these, but now that we have some thickness distribution data it will be possible to put the theory to test. If we want the theory to be able to account for the geographical variations in thickness distribution, which we are beginning to be able to measure, we will need to know the geographical variations in the thermodynamics and in the ice deformation. This places additional requirements on any observational program. It may be that the first order effect is the spatial variation in long-term ice divergence and that other properties of ice deformation and thermodynamics may be regarded as spatially uniform. But I mention this only as a possibility, not even a conjecture. In any event, measurements are needed to help us understand the processes which shape the thickness distribution, as well as measurements of thickness itself. Understanding of the ridging process, the thermal response of ridges, growth and melt rates for thick ice, and geographical variations in growth rates all would be improved by appropriate observations.

One of the reasons for an interest in ice thickness is its role in global change. We have a responsibility to clarify the way sea ice participates in climate change. It would surely be an embarrassment to us if we were unable to say a few decades from now whether the ice thickness had changed. One question meriting our attention now is: what are the measurement requirements to detect a trend in mean ice thickness of, say, 0.5 m per decade? My impression is that today's observing programs are inadequate, but that they could be made adequate with modest additional effort. I don't think we are likely to monitor the ice thickness everywhere, but we may be able to monitor conditions at a few sites. In addition, priority should be given to monitoring the ice flux out of Fram Strait.

A good question is: what are the odds the Arctic Ocean will be ice free by the year 2030? Although many of us probably have an opinion, I don't pose the question for the purpose of taking a poll. Instead, I think it may be possible to give a real probabilistic answer (in the same sense that the states of a hydrogen atom have certain probabilities) — but only after our understanding of the system has improved significantly. To reach this point, we need to know whether the climate modelers' predictions of greenhouse warming have any validity, and we need a better understanding of how the sea ice state

responds to thermal forcing. Almost surely we will know in ten years whether the greenhouse warming is happening. If we do our share, we will also have documented the ice response and thermal forcing during the same decade well enough to have confidence in models that relate them. This should be enough to warrant a prediction of the 2030 ice state.

Some things that could be done immediately are

1. prepare a status report on the submarine data
2. adopt common definitions and procedures for working with ice draft data
3. determine sampling requirements for monitoring mean thickness
4. develop sampling strategy to estimate interannual variability
5. use existing data for ice thickness, ice velocity, and deformation to estimate each term in the evolution equation for ice thickness

Activities that require more thought before committing to them are

6. develop field programs to measure growth rates and radiation
7. develop field programs to observe the life cycle of pressure ridges
8. develop buoys to measure ice growth and melt.

A-II

Controls on Ice Thickness

D. A. Rothrock

Polar Science Center, Applied Physics Laboratory

University of Washington

What causes sea ice to be roughly 3 meters thick in the Arctic Ocean, and why does sea ice exhibit such a variety of thicknesses and morphological features? To the first question, the short answer is that the ability of the surface to radiate heat away must be in equilibrium with the heat conducted up through the ice and snow. To the second, the answer is that deformation of the ice cover produces new leads with open water and thin ice and causes ice to pile up into a variety of thicker forms.

In this brief review, we will respond to these two questions in more detail. To elucidate the balance between the surface heat budget and heat conduction, Thorndike (1992) has described a "toy model" that makes a helpful tradeoff: it uses a simplified description of the annual cycle of ice growth and melt but allows approximate analytic expressions to be obtained for the ice thickness as a function of various parameters such as the radiative properties of the atmosphere, surface albedo, and the conductivity of sea ice. These analytical results display the *sensitivity* of ice thickness to these quantities more cleanly and intuitively than is possible with a more detailed model.

An important feature of the toy model is that it specifies the radiative properties of the atmosphere so that the downwelling longwave radiation is determined within the model. It must satisfy a radiative balance between the ice surface and the atmosphere, but it is not specified as an external condition. About 60% of the outgoing longwave radiation is returned to the surface in winter, and about 70% in summer. About 50 W m^{-2} of downwelling longwave radiation is assumed to be supplied by warm air advected from lower latitudes. The model treats the longwave and shortwave radiation but ignores turbulent heat fluxes. It linearizes the T^4 dependence of the surface upwelling longwave radiation and approximates the ice temperature gradient as linear.

The annual cycle is idealized in four simplified seasons that bear a close resemblance to the actual cycle. In fall and winter, there is no shortwave radiation and the net surface longwave radiation is negative, increasing in proportion to surface temperature. During the autumn cooling period ice thickness is fixed and the ice is cooled until it conducts enough heat to balance the surface radiative balance. During winter, the ice grows in thickness and continues to cool. In spring and summer, there is incoming solar radiation (200 W m^{-2}). In spring, the surplus of heat at the surface

warms the ice, but no change in thickness occurs until the entire slab reaches the melting point. In summer, the ice melts at its upper surface.

The winter surface heat balance requires that the net outgoing radiation, which *increases* with temperature, be balanced by conduction through the ice which *decreases* with increasing surface temperature for a given ice thickness. This is the fundamental control on ice thickness: the efficiency with which the atmosphere lets the ice surface radiate to space compared with the efficiency with which the ice passes heat up to its surface. This net upward surface heat flux is about 10 to 30 W m^{-2} in winter. It is what distinguishes sea ice from a high-latitude continental surface, which has negligible heat flux and is therefore a few tens of degrees colder.

Solving for the temperature-thickness cycle through the four seasons, one obtains a relation between winter surface temperature and ice thickness. Temperature falls off from the freezing point with increasing thickness to an asymptotic temperature of about -45°C, equivalent to the continental situation in which no heat is supplied to the surface from below.

Requiring the growth of ice in winter to balance the melt in summer provides an analytic expression for the equilibrium ice thickness as a function of the radiative efficiency of the atmosphere, the heat supplied by atmospheric advection, shortwave radiation, albedo, oceanic heat flux to the ice bottom, and ice conductivity (Figure 1). This is an illuminating expression. The sensitivity of ice thickness to these thermal parameters is quite chilling. Each watt per square meter of surface heating reduces the ice thickness by 22 cm. Since different methods of heat delivery have different efficiencies of surface heating, they also affect ice thickness in various amounts. Each W m^{-2} of horizontal atmospheric heat advection (roughly half of which reaches the surface) reduces ice thickness by 11 cm. Each W m^{-2} of incoming shortwave radiation (about 65% of which is reflected) reduces ice thickness by 6 cm and every W m^{-2} of ocean heat flux reduces ice thickness by 33 cm. A 1% increase in albedo (say, from 0.65 to 0.66) increases ice thickness by 34 cm (see Figure 1).

If we need to observe these thermal parameters well enough to predict ice thickness to, say, ± 10%, we are in for a huge challenge!

Another interesting investigation of the winter surface heat balance is provided by Overland and Guest (1991) who, like Thorndike, describe the radiative balance between the surface and the lowest 2 km of the atmosphere, which they call the "radiative boundary layer." This RBL is an inversion caused by the efficient radiation from the surface. They surmise that about 20 W m^{-2} of downwelling radiation must be due to

ice crystals ("diamond dust"), at least in cold, clear periods. The sensible heat flux allowing for leads is about 8 W m^{-2} to the surface, a significant part of the net surface heat balance. They show that the near-surface air temperature and the sensible heat flux respond within a half day to changes in the radiative balance due to the presence or absence of clouds.

The distribution of ice thickness is maintained by the interplay between ice deformation which creates thin ice and thick, ridged ice, thus spreading the distribution, and the thermal forcing which causes thin ice to grow thicker and thick ice to melt toward an equilibrium ice thickness of about 3 meters. These effects can be described by several parameters. The kinematic parameters are the divergence rate d, and the shear rate e. The redistribution parameter describing ridging is the ridging multiplier k, which determines how much thicker the ice becomes when it ridges, and a parameter describing what ice gets ridged. Thorndike (in press) has recently suggested that this last parameter should be eliminated in an effort to make the ridging independent of the thickness distribution and thus make the theory linear. The thermal parameters are the growth rate of thin ice $f(0)$, the melt rate of thick ice $f(\infty)$, and the equilibrium ice thickness h_{eq}. These quantities along with the thickness distribution $g(h)$ need to be observed in order to test the thickness distribution theory.

The response time for the thin end of the distribution to adjust to external conditions is $h_{eq}/f(0)$, or about 3 years. The response time for thick ice is $(k-1)\ h_{eq}/-f(\infty)$, or about 50 years. Since the residence time of ice is about a decade in the Arctic Ocean and several years in the Weddell Sea, equilibrium thickness distributions are never achieved.

The thickness distribution can be thought of as an integrator: it integrates past deformation and past ice thickness growth rates, so, except for the very newest thin ice, there is no need to know the details of the deformation, only its statistics. Ice deformation is poorly observed at present, but is on the verge of being well observed by SAR satellites. Thermal data are also poorly observed, but ice growth histories could be rather well estimated from sequential thermal IR satellite data. So there is hope for better observations of the quantities that control ice thickness. Observations of the heat fluxes that govern surface temperature and growth rates are in a rather unsatisfactory state, but efforts to improve them are also under way.

Although the body of this workshop report will contain its recommendations, I offer some thoughts here about what NASA and other agencies can do to promote an

understanding of ice thickness as a climatic variable and to promote its observation. Here are some possibilities:

1. Ice or snow surface temperature is one of the most fundamental measures of the surface heat balance and is readily observable from satellites. The calibration and archiving of surface temperatures derived from satellite thermal data, properly corrected for atmospheric absorption and masked for clouds, should be given highest priority.

2. Clouds increase the downwelling longwave radiation by about 80 W m^{-2} and reduce the net surface heat loss by as much as 25 W m^{-2} in winter. Satellite cloud algorithms tend to be inapplicable for the high albedo and cold surface background of snow and ice. Satellite estimation of cloud properties and their climatologies in polar regions needs increased attention.

3. Satellite estimates of the surface radiation balance need to be calibrated with surface observations. Automated drifting stations that observe air and surface temperatures and up- and down-welling radiation have been dreamt of, and some developmental support for such stations would be a reasonable speculative investment. Without such stations, satellite observations will remain poorly calibrated; occasional field camps are not adequate.

4. Albedo is a crucial parameter and is only crudely known. Satellite data must be examined more quantitatively to obtain albedo climatologies. The Earth Radiation Budget Experiment data have not been well analyzed in polar regions.

5. Ice motion, like surface temperature, is a fundamental ice observation to which satellites are extremely well suited because radiometric accuracy is immaterial. Sufficient geometric accuracies can readily be obtained with present satellite systems. The development of automated ice tracking systems such as the Geophysical Processor System at the Alaska SAR Facility should be augmented to digest the rising tidal wave of SAR observations.

6. Snow has a strong effect on heat conduction through sea ice. The application of high microwave frequencies to the estimation of snow thickness should be reviewed and pursued if promising.

7. Ice thickness is not currently measurable from satellite, but ongoing research suggests that concentrations of one or two thin ice categories might be estimated using data from both SAR and thermal sensors, and possibly using passive

microwave data. Such a capability could complement other techniques for observing ice thickness more directly.

References

Overland, J. E., and P. S. Guest, 1991. The Arctic snow and air temperature budget over sea ice during winter, *J. Geophys. Res.*, **96**, 4651–4662.

Thorndike, A. S., 1992. A toy model linking atmospheric thermal radiation and sea ice growth, *J. Geophys. Res.*, **97**, 9401–9410.

Thorndike, A. S., in press. Estimates of sea ice thickness distribution using observations and theory, *J. Geophys. Res.*

Let:

h_{eq}	equilibrium thickness [m]
$k = 2\ W\ m^{-1}\ K^{-1}$	thermal conductivity
$\sigma = 5.8\ W\ m^{-2}\ K^{-4}$	Stefan-Boltzmann constant
$T_f = 273\ K$	freezing point temperature
$n_w, n_s = 2.5, 3.25$	winter and summer optical thickness of the atmosphere
$D = 100\ W\ m^{-2}$	poleward atmospheric heat transport
$W = -78\ W\ m^{-2}$	winter surface heat balance referenced to T_f
$S = 22\ W\ m^{-2}$	summer surface heat balance referenced to T_f
$F = 0$ to $10\ W\ m^{-2}$	heat flux from ocean to underside of ice
$F_{sw} = 200\ W\ m^{-2}$	flux of short wave radiation
$\alpha = 0.65$	surface albedo

$W = D/2 - \sigma T_f^4/n_w$

$S = (1-\alpha)F_{sw} + D/2 - \sigma T_f^4/n_s$.

Then:

$$h_{eq} = \frac{k\ n_w}{4\ \sigma\ T_f^3}\left[\frac{-W-S-2F}{S+2F}\right]$$

Parameter:	Change:	Change in equilibrium thickness:
D	100 -> 101 W m^{-2}	11 cm
F_{sw}	200 -> 201 W m^{-2}	6 cm
F	0 -> 1 W m^{-2}	33 cm
α	0.65 -> 0.66	34 cm

Figure 1. Sensitivity of equilibrium sea ice thickness to external climate.

A-III

Definitions Relating To Ice Thickness

A. S. Thorndike
University of Puget Sound, Tacoma, Washington

During the workshop, I proposed that the community adopt some uniform definitions for working with ice thickness data and for presenting results. The following are some suggestions. Obviously they involve a number of arbitrary choices. For the most part, I have tried to stick to conventional usage, as set forth in the WMO glossary of ice terms and the Navy/NOAA Ice Observation Handbook. Wadhams (1981) is the source for the definitions of ridges, leads, and level ice.

Ice thickness. Units: meters.

Sea ice thickness is measured vertically. It includes any ice in the vertical column formed predominantly from seawater. Thus it does not include snow. It does include refrozen meltwater and top surface ice which formed as a result of flooding.

Ice draft. Units: meters.

The draft is the depth of the ice/water interface below sea level. It is always positive. Possible ambiguities arise in the case of ice layers that may form at the interface between fresh summer runoff and the colder mixed layer water.

Ice thickness distribution. Units: reciprocal meters. Notation: $g(h; x, t)$.

At time t, consider a circle of radius 200 km centered at x. Let $A(h, h + dh)$ represent the area within the circle covered by ice with thickness in the range h to $h + dh$. Then $g(h)\,dh = A(h, h + dh)$ divided by the area of the circle. Confusion arises from constructing histograms with bins of different sizes, and quoting the percent of area covered by ice having thickness in each bin. For example, 10% of the area may be covered by ice with thickness between 1.5 and 2 m. One is inclined to lose track of the dependence on bin size. The thickness distribution does not have the value 10%. The correct value is 0.2 m^{-1}. (The statement in the abstract of my 1975 paper, that the thickness distribution is dimensionless, is wrong.)

Mean ice thickness, average ice thickness. Units: meters. Notation $\bar{h}$.

The mean thickness is defined in terms of the thickness distribution.

$$\bar{h} \equiv \int_0^\infty h\, g(h)\, dh.$$

Confusion arises if the mean thickness is calculated by excluding the open water. For example, consider a region containing 50% open water, 25% 1-m ice, and 25% 2-m ice. Then h = 0*0.50 + 1*0.25 + 2*0.25 = 0.75 m. The product of the mean thickness and a surface area is the total volume of ice in the area.

Variance of ice thickness. Units: meters squared. Notation: σ^2.

The variance is the second moment about the mean of the thickness distribution:

$$\sigma^2 \equiv \int_0^\infty (h - \bar{h})^2 \, g(h) \, dh.$$

Standard deviation of ice thickness. Units: meters. Notation: σ.

The standard deviation is the square root of the variance. It is the recommended measure of the width of the ice thickness distribution.

Concentration. Units: dimensionless.

The concentration has traditionally meant the fraction of area covered by ice, which could be expressed as the integral of $g(h)$ from h = 0+ to $h = \infty$. In practice, it is difficult to distinguish open water from ice a few centimeters thick. It is recommended that the lower limit of integration be set at h = 0.1 m.

$$C \equiv \int_{0.1\text{m}}^{\infty} g(h) \, dh.$$

It is the custom to identify features in the ice pack that can then be counted and measured. These include pressure ridge sails and keels, leads, floes, and deformed and undeformed ice.

Pressure ridge sails and keels.

A ridge is a feature in which the point of maximum draft or elevation is bracketed by points whose vertical distance from the datum of local undeformed ice is less than half that of the maximum. For submarine data, take the datum of local undeformed ice to be 2.5 m. For top surface data, use 0.25 m. For example, a feature with maximum draft of 9 m extends laterally on both sides of the maximum to the first local minimum having draft less than 5.75 m. The entire feature is counted as one keel. See figure.

Ridge keel index. Units: number per kilometer. Notation: K9.

K9 is the number of keels per kilometer, counting only those keels with drafts greater than 9 m.

Leads.

A lead, or open lead, refers to any place where the ocean surface is exposed. As in the definition of concentration, it is suggested that we also include areas of very thin ice, say $h < 0.1$ m.

Lead index. Units: number per kilometer. Notation: L100.

L100 is the number of leads per kilometer having widths greater than 100 m. To be counted in L100, a lead must have a continuous sequence of ice thicknesses, at least 100 m in length, not exceeding 0.1 m. The 100 m criterion is arbitrary. I wanted to be sure to avoid small features that might escape detection by some observing system, so that the index would not depend on the observing system. Also leads 100 m across are big enough to admit an icebreaker or submarine, and to stop a snowmobile or skier. This usage also corresponds to the WMO glossary of ice terms, in which an open lead must be big enough to be navigable by surface vessels.

Level ice fraction. Units: dimensionless.

The level ice fraction, or fraction of undeformed ice, is an attempt to quantify how much of the ice has not been involved in pressure ridging. It is determined by classifying each point as level or deformed. A level ice point is one whose draft differs from that of a point 10 m to either side by less than 0.25 m. The idea is to pick out points where the local slope is less than 1 in 40. The definition is not perfect, but it is easy to state and to apply. Wadhams believes it is effective in selecting the level ice.

A request for comments from a few colleagues turned up two suggestions. Tucker said it would be useful to have a sail index in addition to the proposed keel index K9. McLaren believes a 25 m criterion for leads would be more useful than the 100 m criterion proposed here.

References

Wadhams, P., 1981. Sea-ice topography of the Arctic Ocean in the region 70°W to 25°E, *Philos. Trans. R. Soc. London, Ser. A*, **302** (1464), 45–85.

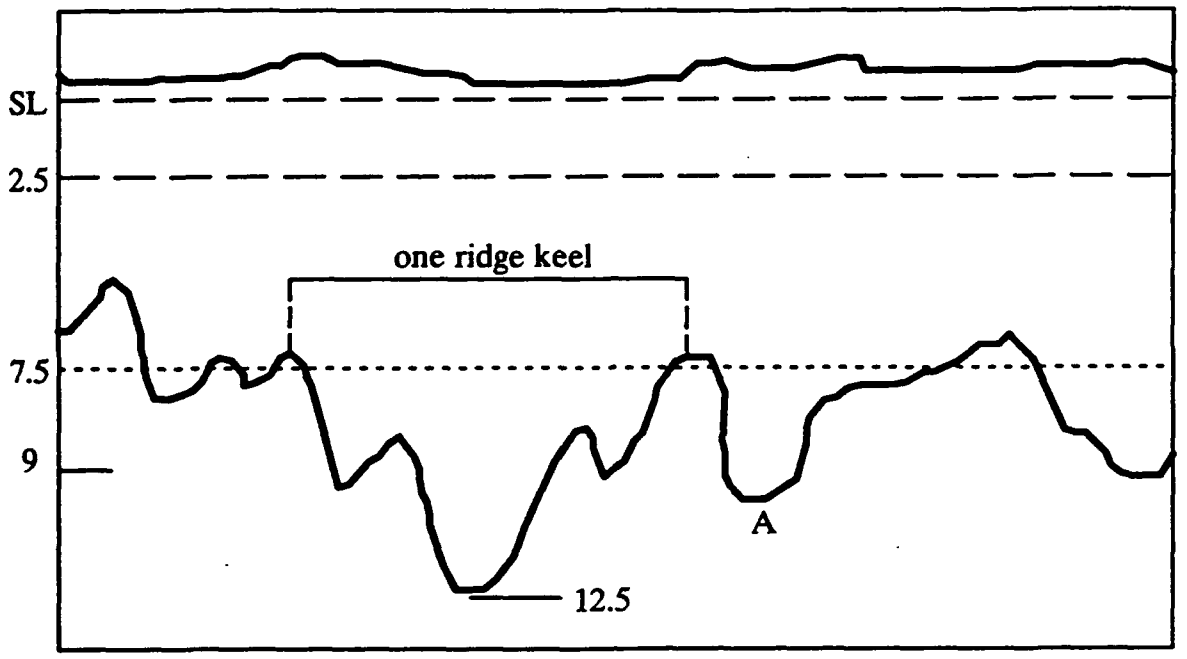

Figure 1. The feature shown adds one to the ridge count K9 because it is deeper than 9 m and is bracketed by local draft minima less than half the distance to the arbitrary datum of 2.5 m. For the 12.5 m maximum, the minima must be less than 7.5 m deep. The maximum labeled A does not count as a keel. Since it is just over 9 m deep, it would need minima 5.75 m deep, which are not present.

A-IV
Sampling Requirements

A. S. Thorndike
University of Puget Sound, Tacoma, Washington

Ice thickness has several different kinds of variation. The custom is to summarize the local variations statistically using the ice thickness distribution, $g(h)$. The large-scale spatial variation, the seasonal variation, and the secular variation are accounted for by considering the thickness distribution to be a function of location, month, and year: $g = g(h;$ location, month, year). To determine a function of this many variables using observations is a tall order. To give some idea of the task, it takes about 1000 observations of thickness to estimate $g(h)$ (see below). If we felt we needed to do this at about 100 locations, for each of 12 months, and each of 10 years, we would need 10^7 thickness measurements. If this were done by drilling, it would be 30,000 km of hole. With submarine measurements at 100 m spacing, for independence, we'd need a total of 10^6 km of track, or 10^5 km per year, which might be done with 20 missions per year. We would be wise to consider whether useful results can be deduced from fewer measurements.

The sampling demands can be reduced dramatically by

1. estimating the mean and variance of thickness, rather than the full thickness distribution
2. reducing the spatial sampling
3. reducing the temporal sampling.

Which of these ways to reduce the sampling requirements are most appropriate depends on the scientific objectives. Several examples are discussed below. There is no attempt at this point to define a particular measurement program. The examples are given to suggest the number and type of measurements required to achieve several different objectives.

1. *To estimate the thickness distribution.*

Suppose the thickness coordinate is partitioned into finite bins and the fraction of ice in a certain bin is p. Any measurement has a probability p of falling in this bin, and $1-p$ of falling elsewhere in the distribution. With N measurements, let n be the number falling in the bin, and take $s = n/N$ as an estimate of p. The estimation error $s - p$ has a standard deviation $[p\,(1 - p)/N]^{1/2}$. A reasonable objective would be to keep the standard deviation less than p/K, where K might, for example, be 10. This leads to the requirement that $N > K^2(1 - p)/p$. Since the values of p of interest to us are probably

about 0.1, and if $K = 10$, we could take $N = 1000$. For example, if typically about 10% of the ice in a region was thinner than 0.5 m, we might, with 1000 measurements, find 80 that were less than 0.5 m. Then we would estimate the proportion (s) of ice in this class to be 8% and the standard deviation (σ) of the estimation error would be 1%. A confidence interval $s - \sigma$ to $s + \sigma$, 7% to 9%, would be expected to include the true value of p about 2/3 of the time. Had we sampled only 100 points, and found 8 thinner than 0.5 m, the standard deviation of the estimation error would have been 3%, and our 2/3 confidence interval $5\% < p < 11\%$.

2. *To estimate the mean thickness in a region of homogeneous thickness distribution.*

If N independent points are drawn from a distribution having standard deviation for each point σ, the standard deviation of the sample mean is $\sigma/N^{1/2}$. Typical values are $\bar{h} = 3$ m, $\sigma = 3$ m. With $N = 100$, we could resolve the mean to within 10% of its value. It is essential for the argument that the points be independent, which means they must be separated by at least 100 m. This implies that 10 km of track will give an estimate of the mean good to about 0.3 m. However, it is doubtful whether different 10 km tracks in the same region would agree within 0.3 m because there are probably substantial inhomogeneities over these distances. This could be examined by comparing successive 10 km sections of submarine records.

3. *To estimate the mean thickness over a region for which the thickness distribution varies.*

It may be helpful to think of the ice thickness having local random variability superimposed on large-scale deterministic structure. To get a good mean thickness, the measurement points need to be sufficiently plentiful to minimize the sampling fluctuations due to the random variability and spread out evenly in space to resolve the deterministic structure. It turns out that the second consideration does not increase the number of points needed, it just requires that they be widely spread out.

4. *To estimate spatial variations in g(h).*

The above arguments (#1) imply that about 1000 points are needed in each region.

5. *To estimate seasonal changes in g(h) at a fixed point.*

Samples of 1000 points collected within a few days and repeated each season would suffice.

6. *To estimate secular trends in mean thickness.*

Suppose we imagine the mean thickness to decrease linearly with time, and that we have a sequence of M estimates of mean thickness (as in #2) spanning a period of T

years. Using these data, we can estimate the trend in mean thickness by standard linear regression. The standard deviation of the estimate of the trend is $12^{1/2}\,\sigma\,N^{-1/2}\,M^{-1/2}\,T^{-1}$. With σ = 3 m, N = 100 points per survey, M = 15 surveys, and T = 15 years, the uncertainty in the estimated trend would be 2 cm per year. Thus, the total thickness change after 15 years would have to exceed 30 cm to be detectable. This calculation does not account for interannual variability. We don't know of course, but my guess is that the interannual variability in the mean thickness of the ice coming through Fram Strait, for instance, is probably less than $\bar{h}/10$ = 0.3 m. If so, it will only slightly increase the uncertainty in the estimated trend.

7. *To estimate the ice flux across Fram Strait.*

Measurements of ice thickness and ice velocity are required to determine the flux. To determine the flux to within 10%, the thickness and velocity each need to be known to within about 5%. Until more is known, it would be a mistake to assume that the flux can be determined as the product of average thickness and average velocity, although this may turn out to be the case. Instead, it will be necessary to measure the thickness and velocity as functions of time and space and to form their product before integrating. At the very least, thickness must be measured at two or more locations to resolve the difference in thickness between the thick polar ice on the west side of the strait and the thinner ice on the east. And the velocity must be sampled every week or so to resolve the synoptic scale fluctuations. A few upward looking sonar instruments with Doppler ice velocity capability would do nicely, but it may be that some combination of the current generation of thickness-only upward looking sonars with buoy or SAR velocities would be adequate.

APPENDIX B
Measurements

B-I

Drill Hole and Ice-Core Studies of Sea-Ice Thickness Distributions in the Arctic and Antarctic

H. Eicken and M. A. Lange

Alfred Wegener Institute for Polar and Marine Research

Sea ice thickness is an important variable in the coupled ocean-ice-atmosphere system. However, there is still no reliable technique that would allow a comprehensive assessment of sea ice thicknesses in a large area through satellite based remote sensing. In the absence of such a technique, next to upward looking sonars deployed on submarines and moorings and airborne laser profilometers, field measurements remain as a crucial source of information.

In our work, we have concentrated on direct field measurements of sea ice thicknesses through mechanically drilled holes. While this may seem a somewhat outdated technique, we will demonstrate that it still offers potential for the interpretation of sea ice dynamics. We have performed extensive sea ice thickness surveys both in the Arctic and Antarctic. Important findings with regard to monitoring of the ice thickness distribution in the Arctic are summarized below.

1. Drill-hole measurements are at present the only technique that provides joint information on all three parameters relevant in the study of ice thickness distributions, i.e., snow depth, ice thickness, and freeboard or draft (measurement errors generally estimated to be <1% of the measured value). In combination, the determination of these variables for different regions and ages of ice serves well in providing estimates of mean ice and snow density needed for the extraction of ice thickness from other indirect measurements, in particular sonar and laser-profilometer data (e.g., Comiso et al., 1991). In addition, direct thickness measurements have been compared with data gathered through laser profiling to validate the information obtained from the sensor with regard to the thickness and roughness of the ice.

2. Information obtained from drill-hole thickness profiles may be important in linking ground-truth data and remote-sensing techniques. In a study conducted in the Weddell Sea, ice thickness profiles could be subdivided into four different thickness classes based on characteristics of ice thickness and snow depth probability density functions (pdf) and the actual profiles (Lange and Eicken, 1991). These classes I to IV represent deformed and undeformed first-year ice, and undeformed and deformed second or multi-year ice, respectively. The ice

surface of classes I, III, and IV is prone to flooding as a result of depression resulting either from the heavy snow load (classes III and IV) or from ridging (classes I and IV). This influences the microwave signature of the ice and may provide indirect evidence of ice thickness and its smaller-scale distribution. In addition, through the resulting formation of snow ice, it influences the mass balance of sea ice. Furthermore, the abundance and spatial distribution of these ice classes in the Weddell Sea allow the specification of dynamic processes of the sea ice cover in the area under investigation. Attempts to establish a similar classification scheme for the Arctic are currently under way.

3. The simple logistical requirements of mechanical drill-hole measurements allow for use of the method in other field programs to obtain information about the ice characteristics at a sampling site, or in connection with helicopter flights in the surrounding area. Such data are important when comparing single-floe measurements with the distribution of ice thickness over larger areas (cf. Eicken and Lange, 1989).

4. In combination with ice thickness measurements, ice core studies provide valuable information on the processes affecting the ice thickness distribution in particular areas. Studies in the Arctic and the Antarctic have shown that a combination of different investigations, i.e.,
   - ice core analysis (texture, salinity, temperature, ^{18}O)
   - surface characteristics (snow stratigraphy, snow depth)
   - ice thickness surveys

   yields a comprehensive understanding of sea ice dynamics and thermodynamics in a given area. Thus, snow-ice formation and associated processes may result in a significant contribution of meteoric ice to total ice thickness (Lange et al., 1990). For the Arctic, a recent study has shown that level, seemingly undeformed ice can in fact be composed of significant portions of ice indicative of dynamic processes other than quiet congelation of ice at the ice-water interface (Figure 1a and b). Here, parameters such as salinity (Figure 1b) or ^{18}O may yield information about ablation and transformation processes and their effect on ridged, hummocked, and level ice.

In conclusion, we feel that drill-hole measurements (in combination with studies of ice cores and surface characteristics) may aid significantly in elucidating the evolution of the ice-thickness distribution for key localities within specific regions. In combination, these techniques furnish us with information on the factors affecting the

sea-ice thickness distribution that no other method can provide as easily. At the present stage, drill-hole measurements are of equal importance in the validation of data obtained with other sensors. Evaluation, classification, and combination of such data available now and in the near future are crucial to a thorough understanding of the data obtained in monitoring sea ice thickness employing more advanced techniques.

References

Comiso, J. C., P. Wadhams, W. B. Krabill, R. N. Swift, J. P. Crawford, and W. B. Tucker III, 1991. Top/bottom multi-sensor remote sensing of Arctic sea ice, *J. Geophys. Res.*, **96**, 2693–2709.

Eicken, H., and M. A. Lange, 1989. Sea-ice thickness data: the many vs. the few, *Geophys. Res. Lett.*, **16**, 495–498.

Lange, M. A., and H. Eicken, 1991. The sea ice thickness distribution in the northwestern Weddell Sea, *J. Geophys. Res.*, **96**, 4821–4837.

Lange, M. A., P. Schlosser, S. F. Ackley, P. Wadhams, and G. S. Dieckmann, 1990. ^{18}O concentrations in the sea ice of the Weddell Sea, Antarctica, *J. Glaciol.*, **36**, 315–323.

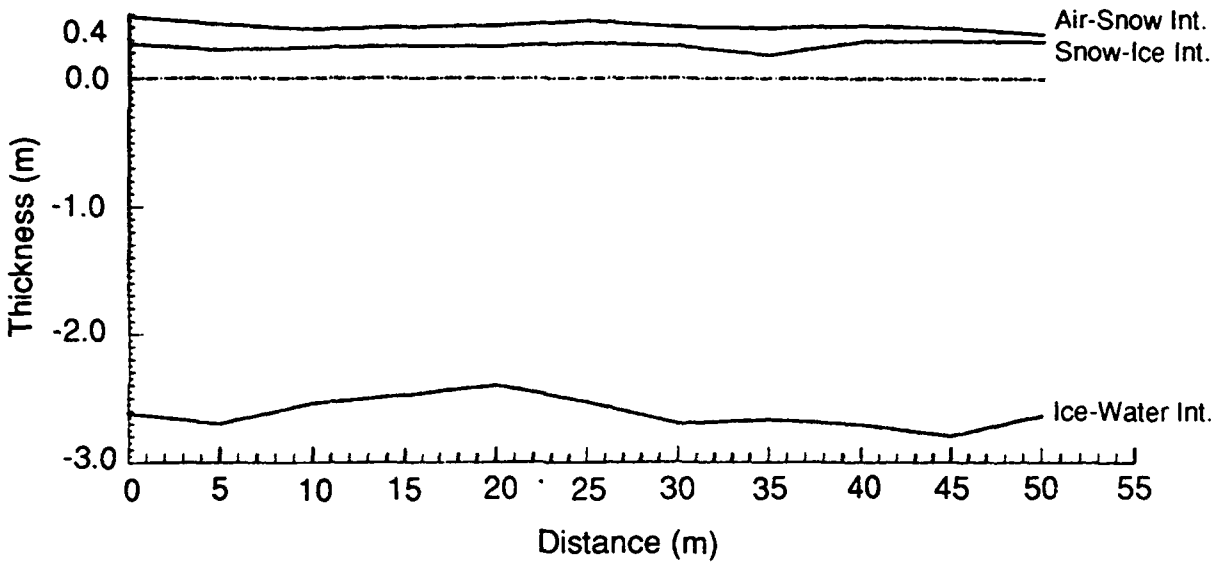

Figure 1a. Thickness profile of a level portion of an ice floe sampled in the Arctic Basin at 86°15'N 9°37'E (holes spaced 5 m apart).

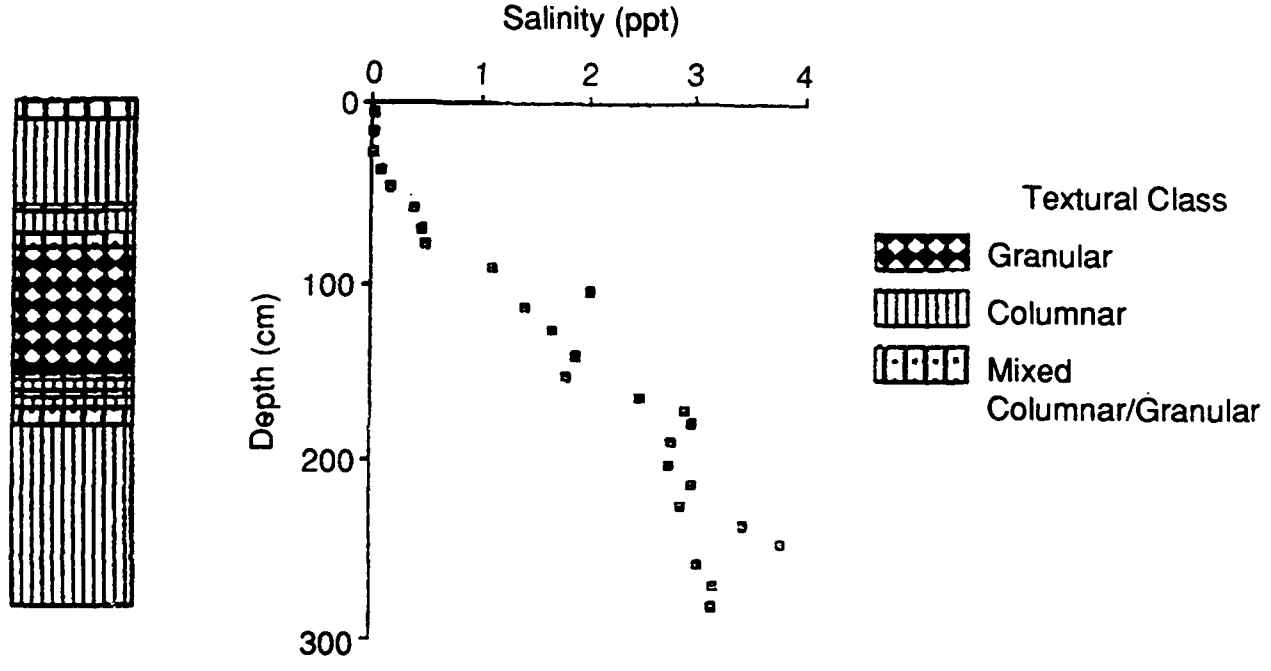

Figure 1b. Textural stratigraphy and salinity profile of an ice core extracted along the profile shown in Figure 1a.

B-II

Thickness Measurements of Arctic Multiyear Ice

Walter B. Tucker III

U.S. Army Cold Regions Research and Engineering Laboratory

The mesoscale (10–1000 m) topography of multiyear ice has been examined using closely spaced drill hole measurements on a number of floes. The emphasis was to determine the amounts of deformed ice contained by each floe and to assess relationships between ice surface and bottomside topography. Ice thickness measurements were obtained from eight floes, six of which were in the southern Beaufort Sea, and two in the eastern Arctic, north of Svalbard. On each floe, rectangular grid patterns were established with drill holes located from 5 to 10 m apart. The sizes of the grids ranged from 50 × 50 m to 30 × 750 m. The locations of the grids were chosen to be representative of the surface topography observed on the floe.

Drilling was carried out with a portable hot water drilling system which makes 5 cm diameter holes at penetration rates of 4–5 m min^{-1}. Measurements of ice thickness, freeboard (surface height above the water level), and snow depth were recorded at each drill hole. The accuracy of these measurements is estimated to be ± 2 cm.

The total number of measurements, mean thickness, draft, ice freeboard, snow depth, and calculated ice density are shown in Table 1. Floe thicknesses ranged from 3.0 m to 5.4 m. Drafts closely paralleled the thicknesses, with the draft values being 90% of the thickness for every floe. Freeboards, in contrast, were generally about 10% of the ice thickness but varied from 8.5% to 10.9%. The average snow depths on the floes ranged from 8 to 35 cm, and these depths were 25 to 80% of the ice freeboards. Those floes in the eastern Arctic (7 and 8), had larger snow depths than did the Beaufort Sea floes. Ice densities were calculated from the simple isostatic relationship using assumed snow and seawater densities of 0.35 and 1.025 Mg m^{-3}, respectively. The mean densities determined in this manner showed relatively little variance, ranging from 0.911 to 0.919 Mg m^{-3}. The mean density for all samples was 0.913 which agreed well with measured multiyear ice densities. It is imperative that the snow cover be accounted for when determining ice density in this manner.

Figure 1a shows the histogram of the thickness distribution for all measurements. Those for individual floes contained more variability but major features of the distribution are similar. The pdf has a single mode and appears to have an exponential decay of the larger thicknesses. The variability of thicknesses between and within floes

is demonstrated in the percentile plot in Figure 1b. This type of plot is a coarse synopsis of individual probability distribution functions. This figure emphasizes the ranges of thicknesses that may be encountered on single floes. For instance, floes 2, 3, and 8, have relatively narrow ranges while the others have substantially larger ranges due to the thick ice from deformation. This variability was verified by the determination of correlation lengths (1/e), which ranged from 25 to 50 m for thickness and draft and 10 to 30 m for freeboard.

Table 1. Mean thickness (h), draft (d), freeboard (f) , snow depth (s), and density (ρ) for each of the floes. Units of depths and thicknesses are m and density is Mg m^{-3}. N is the number of measurements.

Floe	1	2	3	4	5	6	7	8
N	225	225	144	1001	451	451	789	484
h	5.58	3.13	3.00	3.83	5.39	4.13	5.16	2.62
d	5.01	2.82	2.70	3.43	4.82	3.68	4.72	2.36
f	0.57	0.30	0.30	0.39	0.57	0.45	0.44	0.26
s	0.17	0.13	0.08	0.12	0.11	0.08	0.35	0.19
ρ	0.913	0.914	0.919	0.912	0.917	0.911	0.915	0.916

One objective of this investigation was to estimate the amount of deformed ice found in multiyear ice. The sampling strategy sought to choose typical multiyear ice topography and to avoid biasing the sample with an excess of ridged ice or smooth ice. There are two simple first-order techniques for estimating the amount of deformed ice. The equilibrium thickness of Arctic multiyear sea ice determined from detailed thermodynamic simulations by Maykut and Untersteiner (1971) is 3.0 to 3.5 m. Thus a reasonable threshold thickness might be the high end of the simulated equilibrium thickness. For these data, 67% of the thicknesses exceeded 3.5 m and 48% exceeded 4.0 m (Fig. 1a). Therefore, much of this ice exceeded thicknesses that could be expected from thermodynamic growth alone. An alternative method of attempting to estimate the amount of deformed ice is to examine the slopes between adjacent draft points, and again assume that any slope larger than a selected threshold must have been created by a deformation process. Wadhams (1981) and McLaren (1989) selected a slope of 1:40 to designate level ice from submarine top sounder profiles of ice draft. For the measured drafts reported here, 69% of the slopes exceeded 1.5° (~1:40) and 49%

exceeded 3.0° (~1:20). These percentages are very similar to those obtained from the thickness thresholds. We conservatively estimate that a minimum of 50% of the ice sampled in our surveys had previously been deformed.

It is worthwhile to examine the relationship of ice elevations with drafts. Simple isostasy dictates that the mass above sea level must be accounted for by a much larger mass below sea level. It is well known, however, that not every surface feature will have a corresponding feature on the bottomside at some established ratio. Nonetheless, it is of major interest to successfully predict the thicknesses from topside elevations alone as this would enhance ice thickness monitoring from aircraft or satellite. For these data, draft correlates with thickness with a coefficient of 0.99, which is no surprise given the close correspondence shown earlier. Correlations between the topside and thicknesses were decidedly less but still reasonable. The coefficient between ice freeboard and thickness was 0.74 and that between snow plus ice freeboard (total elevation) and thickness was 0.76.

For effective freeboard and thickness the correlation coefficient was 0.77. Effective freeboard is simply the ice freeboard plus the snow converted to an equivalent ice thickness. In order to attempt to predict ice thicknesses from surface elevations, a simple linear transformation was applied by multiplying the snow plus ice elevations by the ratio of the mean thickness to mean snow plus ice elevations (7.12 in this case). The resulting predicted thickness distribution was a good approximation to the observed distribution. This exercise lends encouragement to the use of techniques that can accurately profile surface elevations (e.g., airborne laser) for determining the ice thickness distribution.

This investigation has provided insight into the variability of topography on the top and bottomside of multiyear ice floes. The hot water drilling method is a rapid, reliable technique for examining the small scale variations. The variability of ice thicknesses observed on single floes was quite large due to the incorporation of deformed ice in multi-year floes. It comes as no surprise that the bottomside is significantly rougher than the topside. Using snow plus ice elevations to predict ice thicknesses appears to be a promising technique for obtaining the ice thickness distribution. Finally, this study leads us to believe that a minimum of 50% of multiyear ice is deformed ice. This finding indicates that any program designed to monitor ice thickness must consider more than thermodynamic processes. For example, a warmer climate may be accompanied by higher winds, which could actually increase the thickness of the ice in the central Arctic through increased ridging. For this reason, it is imperative that

modeling studies of ice dynamics and thermodynamics and techniques of monitoring ice dynamics (buoys or satellite SAR) be incorporated into any program that addresses long-term monitoring of ice thickness.

References

Maykut, G. A., and N. Untersteiner, 1971. Some results from a time-dependent thermodynamic model of sea ice, *J. Geophys. Res.*, **76**, 1550–1576.

McLaren, A. S., 1989. The under-ice thickness distribution of the Arctic Basin as recorded in 1958 and 1970, *J. Geophys. Res.*, **94**, 4971–4983.

Wadhams, P., 1981. Sea-ice topography of the Arctic Ocean in the region 70°W to 25°E, *Philos. Trans. R. Soc. London, Ser. A*, **302** (1464), 45–85.

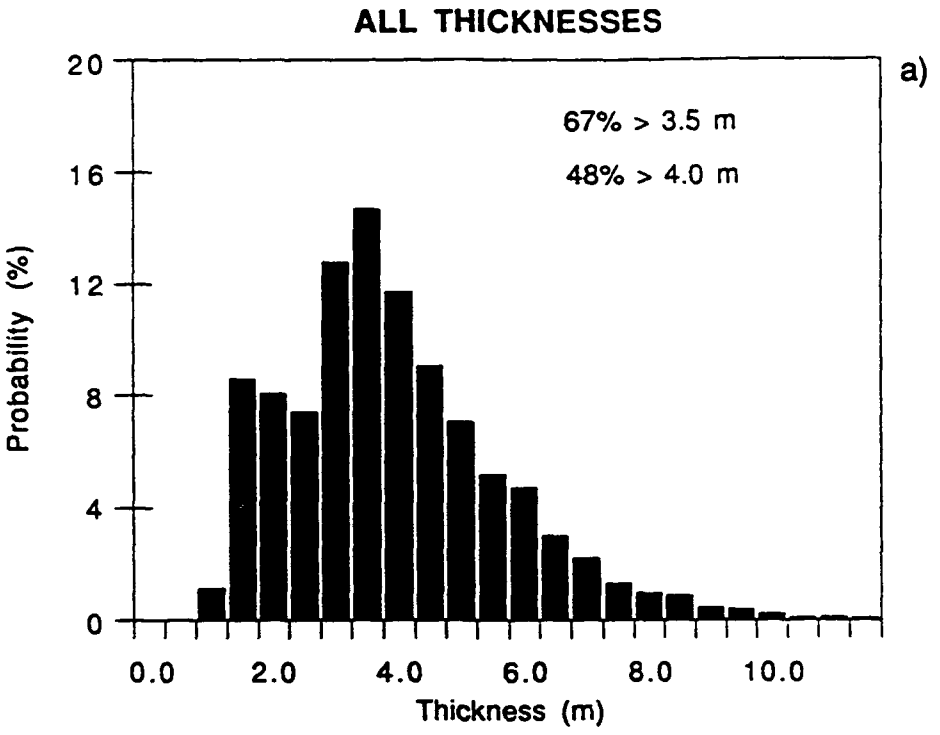

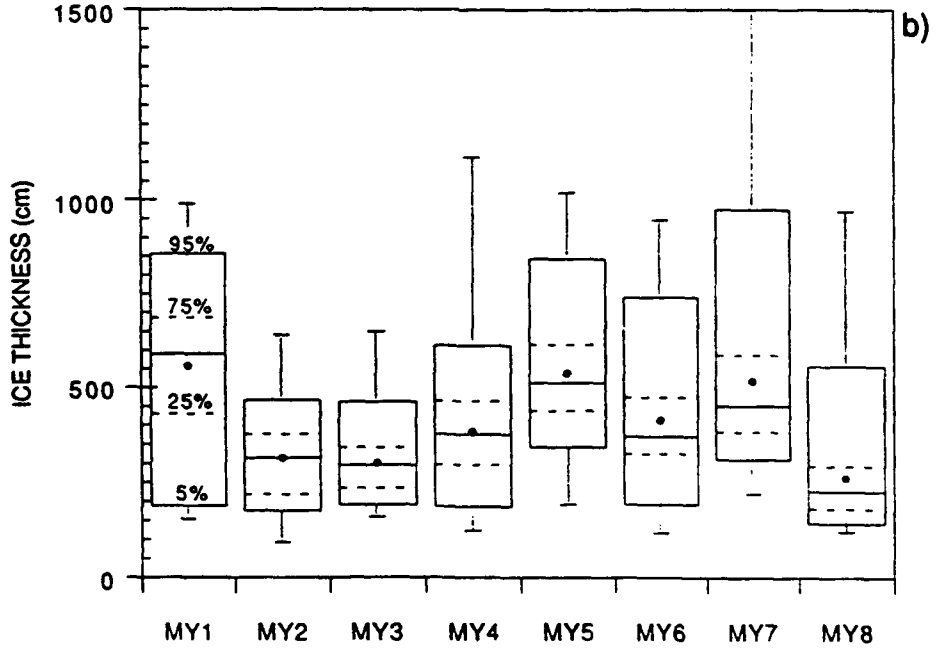

Figure 1. (a) Histogram of thickness distribution for all data. b) Percentile plot of thicknesses for all floes. Lines show ranges of data, horizontal bars designate percentiles as labeled, center solid bar is median, and dot is mean.

B-III

Sea Ice Thickness Distributions Derived From Archived Aerial Photographs of the Arctic Sea Ice Pack

D. T. Eppler and L. D. Farmer
Polar Oceanography Branch Office
Naval Research Laboratory (NRL)

Introduction

Gray tones that characterize new and young sea ice in aerial photographs vary as a function of ice thickness. This characteristic, which arises from the fact that albedo, reflectivity, scattering, and absorption of ice at optical wavelengths depend on its thickness, permits the thickness distribution of these thinner ice types (thickness less than approximately 30 cm) to be derived from black and white aerial photographs. The thickness–gray tone relationship is a fortuitous one since accurate information concerning the thickness distribution at this thin end of the spectrum is difficult to obtain with comparable accuracy using alternative methods that have proven effective for thick ice [submarine top-sounder profiles (McLaren, 1989); airborne laser profiles (Comiso et al., 1991)]. Photographs thus represent one of the best sources of this information.

Method

At NORDA in the early 1980s methods were developed for deriving ice thickness distributions from aerial photographs of the Arctic pack using computer-assisted image classification techniques (Farmer and Eppler, 1985). Similar techniques have since been used by CRREL to derive thickness distributions and ice characteristics of the Antarctic pack (Ackley et al., Appendix B-IV). These routines, which run on personal computers, use gray-tone differences to classify areas of different ice thickness.

Photographic prints or negatives are digitized to a frame buffer using a scanner or a TV camera. With the digitized image displayed on a monitor from memory, the analyst defines ranges of image intensities that correspond to different ice types. Look-up tables in the hardware are set such that pixels in each ice category are shown in a different tone or color. The process is interactive: the classified image is displayed in real time so that adjustments to breakpoints that define different ice types can be evaluated visually through comparison with the original photograph.

This classification strategy works only if different ice types show distinct gray-tone signatures. In cases where classification is confounded by different ice types of similar gray tone (for instance, snow-covered first-year and multiyear ice), software provides the analyst with the option of outlining regions of the image manually using a mouse or light pen, or by controlling the position of a cursor on the screen with keystrokes. These regions are recognized as different surface types and are assigned to appropriate ice categories designated by the analyst. When, in the analyst's opinion, ice in the scene is classified accurately, the computer counts pixels that fall into each category to determine the percent of the scene covered by each ice type. These percentages are saved on disk where they can be accessed subsequently for specific applications.

Basis for Classification

Ice types are classified using the World Meteorological Organization (WMO) scheme as a guide (WMO, 1970). The WMO system is well suited to this application in several regards. First, it is designed to be used for visual observations. Second, WMO ice types are associated with discrete thickness ranges, which enables thickness distributions to be derived from ice classification data. Third, identification of ice types is based on interpretation of sea ice tones, textures, and features and, as such, is directly applicable to inferences made from gray-tone signatures like those rendered in photographs (Table 1) (WMO, 1970; Steffen, 1986). Although gray tones represent the primary information used by the analyst (and the computer program) to classify each scene, the presence and morphology of deformational features such as rafts, ridges, folds, and fractures depend on ice thickness and provide important secondary information. For thicker ice types (gray-white ice, thin, medium, and thick first-year ice, multiyear ice), the snow-covered characteristics also are important.

Available Data

NRL, NORDA, and the Naval Oceanographic Office have accumulated a substantial archive of aerial photographs of Arctic regions. These data, which are now held by NRL in Hanover, New Hampshire, were gathered over the past 25 years in conjunction with Project Birdseye Arctic reconnaissance flights, the AIDJEX experiment, and numerous other arctic field experiments conducted or supported by the Navy. Most of the data consist of negatives on 9-1/2 inch aerial film, although in a few instances some data exist only in the form of large-format contact prints. All data are black-and-white. Images in the data set document ice conditions in the central Arctic Basin and in waters

adjoining the United States, Canada, Greenland, Iceland, and Norway (Figure 1, Table 2). Insofar as these data depict ice conditions over a wide range of geographic regions in most seasons over more than two decades, information concerning regional, seasonal, and annual variation in ice conditions is present in the archive. Individual photographs have been used for specific projects, but the data set has never been analyzed as a whole for the synoptic information it contains.

These types of data represent one of the best sources of information about ice thickness distribution in the range between 0 and 30 cm. Analysis of the NRL archive, and others like it in Canada, Europe, and the Commonwealth of Independent States, can provide baseline data of importance to studies of arctic heat flux, pack divergence, and ocean mixed-layer dynamics. In addition to thin ice thickness distributions, concentrations of the first-year ice and multiyear ice fractions of the pack also can be derived, although accurate thickness distribution information cannot be inferred for these thicker ice types using photographs alone. Melt pond coverage can be derived readily from summer images of the pack in melt, and information concerning ridge and lead density and orientation can be derived during all seasons.

References

Comiso, J. C., P. Wadhams, W. B. Krabill, R. N. Swift, J. P. Crawford, and W. B. Tucker III, 1991. Top/bottom multisensor remote sensing of Arctic sea ice, *J. Geophys. Res.*, **96**, 2693–2709.

Farmer, L. D., and D. T. Eppler, 1985. A method for determining sea ice type and inferred ice thickness distributions from aerial photographs, *Proceedings of the Arctic Oceanography Conference and Workshop*, Naval Ocean Research and Development Activity, Stennis Space Center, Mississippi, 205–213.

McLaren, A. S., 1989. The under-ice thickness distribution of the Arctic Basin as recorded in 1958 and 1970, *J. Geophys. Res.*, **94**, 4971–4983.

Steffen, K., 1986. Atlas of the sea ice types, deformation processes, and openings in the ice, Zurcher Geographische Schriften Heft 20, Geographisches Institut, Eidgenossische Technische Hochschule, Zurich, 55 pp.

WMO, 1970. WMO sea ice nomenclature, Secretariat of the World Meteorological Organization, Geneva, Switzerland, 147 pp.

Table 1. Sea ice classification scheme (World Meteorological Organization, 1970).

Ice Type	Thickness	Gray Tone	Features
open water	0 cm	black	
new			
frazil	0 cm	black	unconsolidated
slush	0- 50 cm	very dark gray to gray	unconsolidated
shuga	0- 50 cm	dark gray to gray	unconsolidated
grease	0-100 cm	dark gray to gray	unconsolidated
nilas			
dark nilas	0- 5 cm	very dark gray	rafts
light nilas	5- 10 cm	dark gray to gray	rafts
young			
gray	10- 15 cm	gray to light gray	rafts
gray-white	15- 30 cm	light gray to almost white	rafts or ridges
first-year			
thin	30- 70 cm	white	ridges
medium	70-120 cm	white	ridges
thick	120-200 cm	white	ridges
old			
second-year	200-400 cm	white	ridges
multiyear	200-400 cm	white	ridges, hummocks

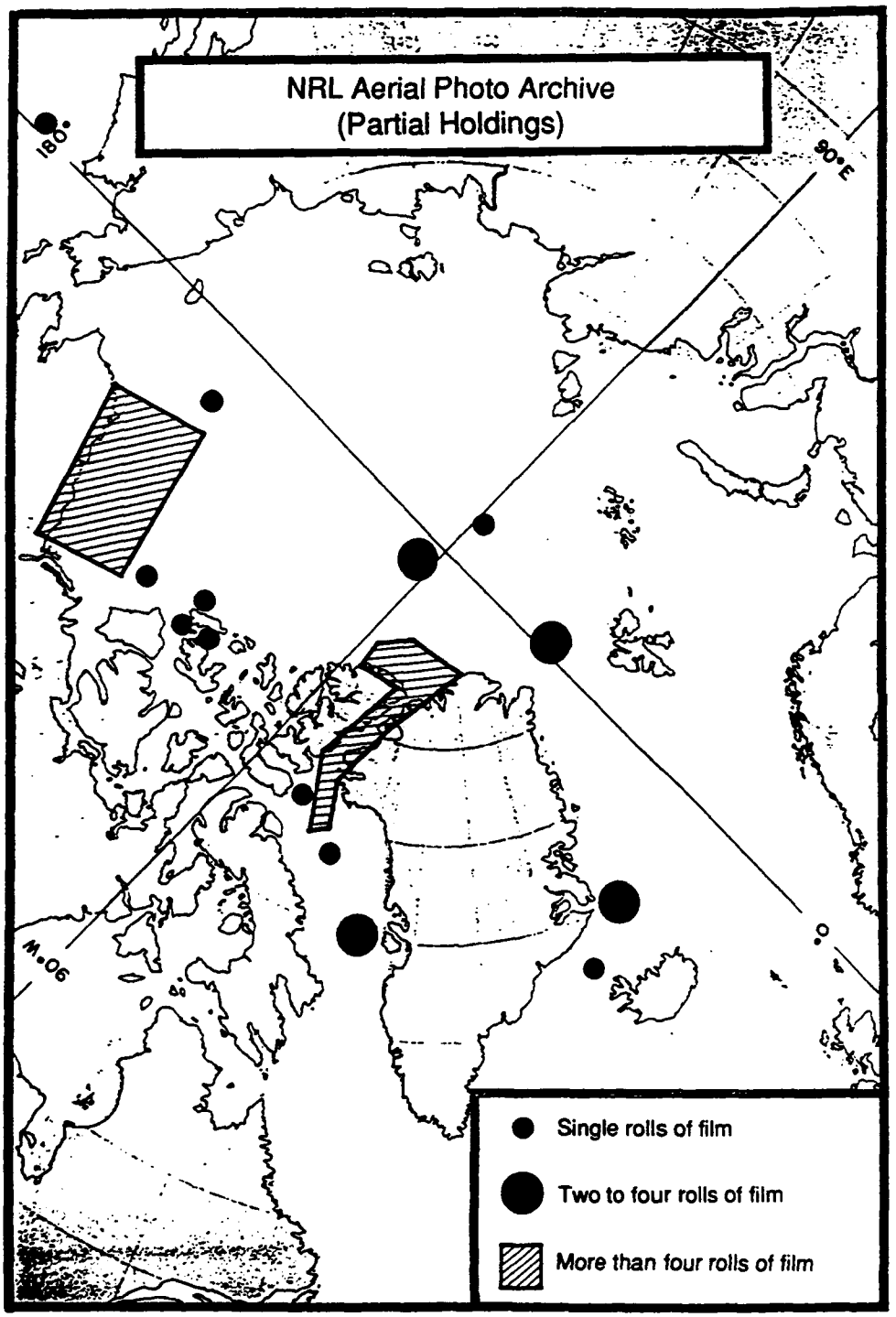

Figure 1. NRL aerial photo archive (partial holdings).

Table 2. Summary of data in the NRL archive of Arctic aerial photographs.

WATER BODY	MAR	APR	MAY	JUN	JUL	AUG	SEP	OCT	TOTAL ROLLS
GREENLAND	4	14	12			1		8	39
LABRADOR		2							2
BAFFIN BAY	8	12	13						33
ARCHIPELAGO		2	1		1				4
BEAUFORT	11	7	6	2	1	12			39
BERING	1	7	1						9
CHUKCHI	3		4					6	13
SIBERIAN									0
LAPTEV									0
KARA									0
BARENTS									0
SOVIET ARCTIC									0
GREENLAND ARCTIC		4	11			5			20
AMERICAN ARCTIC		1	2						3
EUROPEAN ARCTIC						2			2
KANE BASIN			8			1			9
TOTAL ROLLS	27	49	58	2	2	21	0	14	173

Numbers indicate rolls of 9" wide , black-and-white aerial film.

B-IV

Antarctic Ice Thickness Distributions Obtained From Aerial Photography

S. F. Ackley, P. Wadhams and M. Lange

During the 1986 Winter Weddell Sea Project, aerial photographs were taken from a helicopter on over 20 occasions. These flights obtained photographs over approximately 20 to 50 km of track with a nominal frame size of 0.75 km × 0.75 km. The approximately 10,000 frames are being analyzed using a relatively inexpensive PC-based image processing system. Using a frame-grabber option, the images have been digitized as 512 × 512 pixel files. As each roll is digitized, the data have been transferred to an optical disk (256 Mbytes/side). Some selection was made depending on the amount of overlap in the photography so that the resulting digitized images represent independent samples of the regions, i.e., no duplication or overlap of the images. This has resulted in 2600 frames being digitized, representing 24 different sea ice regions in the eastern Weddell Sea.

We have processed most of these sets into ice thickness distributions using an interactive image processor on a PC. Each image is brought up and, if needed, anti-biasing is applied to account for nonuniform illumination. A histogram of the gray scales is then obtained and the histogram is used to choose approximate gray scale ranges for the ice types shown on the image. The six categories vary from black for open water, through dark gray (thin nilas of 5 to 10 cm thickness), gray (nilas to young ice of 10 to 20 cm thickness), gray to gray-white (young ice of 20 to 30 cm thickness), gray-white (young ice of 30 to 40 cm thickness), and white (snow-covered floes of 40 to 80 cm mean thickness, measurements obtained by surface drilling in the region). Using the false-coloring option on the image processor, each ice type can be illuminated interactively and the corresponding gray scale range identified for each ice type. The digital histogram then identifies the number of pixels or, equivalently, the percentage of the frame that corresponds to that ice type. From these percentages, the ice thickness distribution can be computed for each set of images by summing each category's percentages and dividing by the total number of frames for that set.

Figure 1 shows an Ice Thickness Distribution obtained on 19 July 1986 for the Antarctic Marginal Ice Zone while the ice edge was advancing. All the ice represented in the distribution was pancake ice. This particular distribution gives a significantly lower open water fraction than expected for the Marginal Ice Zone, in fact, a surprisingly

small open water percentage of less than 2%. Over the three lowest categories, however, corresponding to ice of less than 20 cm, the sum of the total area is nearly 20%. These results are similar to other distributions we have obtained away from the Marginal Ice Zone that suggest the actual open water fraction is generally very low in the pack ice but the combination of open water and thin ice is generally about 10 to 30% of the total coverage. Each set of images samples an area corresponding to one to a few pixels of passive microwave satellite data. We feel these data may be a limited but not trivial calibration against which to check the various algorithms for microwave imagery being tested for ice concentration in the Antarctic. Upcoming field programs will make further use of aerial photography from both fixed-wing aircraft and helicopters. The technology described here gives a relatively straightforward quantitative method of analyzing these data, both for the characterization of the region for the particular experiment and for validation comparisons with satellite and ground-based data.

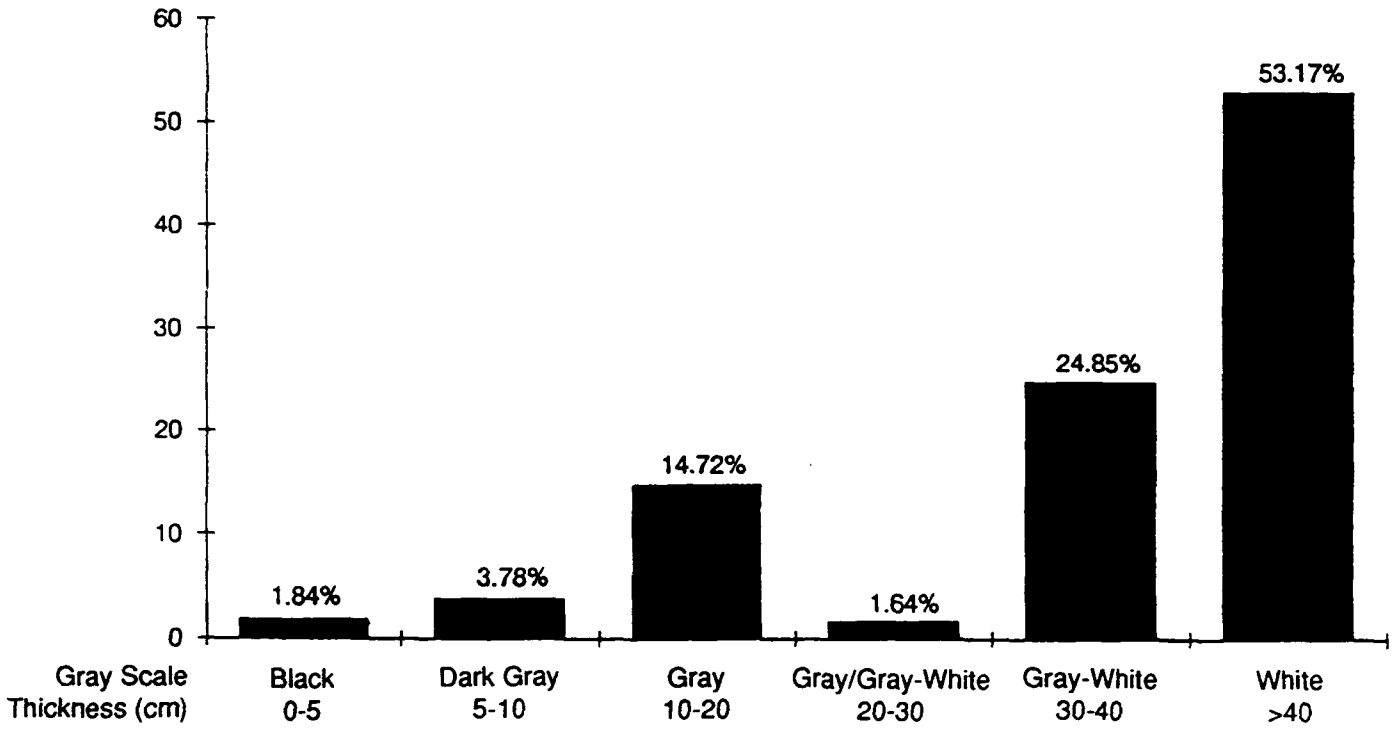

Figure 1. Ice thickness distribution obtained on 19 July 1986 for the Antarctic Marginal Ice Zone.

B-V

Ice Thickness Observations From British Submarines

P. Wadhams
Scott Polar Research Institute, University of Cambridge

Submarine data have been collected from British submarines since 1971, mainly from the Eurasian sector of the Arctic Basin and from Fram Strait and the Greenland Sea. Three cruises have carried scientists from Scott Polar Research Institute, Cambridge, and the data from six cruises have been released for analysis and publication. The dates and locations are as follows:

1971	Mar.	HMS *Dreadnought*	Fram Strait – North Pole
1976	Oct.–Nov.	HMS *Sovereign*	80-90°N, 25°E-70°W
1979	Apr.–May	HMS *Sovereign*	Fram Strait 79°–84°N
1985	June–July		Fram Strait northwards
1987	May		Greenland Sea and repeat of 1976
1989	Spring		Greenland Sea

From 1989 onwards, annual spring cruises have been carried out, a process we plan to continue, and the data are being, or will be, released for analysis. This does offer the opportunity, at least for the Greenland Sea and European sectors of the Arctic, to develop systematic analyses of interannual variability for testing against the predictions of models.

A large number of papers have been published on the statistical analysis of upward sonar data from these cruises (see references). Normally the track is divided into sections 50 or 100 km long, to achieve statistical stability, and the following statistics developed:

mean draft of all ice

probability density function (pdf) of draft

percentage and pdf of draft of undeformed ice

distribution of pressure ridge depths and spacings

distributions of lead widths and spacings

autocovariance, power spectrum, and fractal dimension of bottom.

Submarines: Advantages and Drawbacks

The chief advantages of submarine sonar surveys as a way of generating ice thickness distributions are:

1. Upward sonar (mobile or moored) is still the only *direct* and *accurate* means of measuring the draft of sea ice, from which the thickness distribution can be inferred with very little error.
2. Submarine-mounted (as opposed to moored) sonar allows *basin-scale* surveys to be carried out on a single cruise, providing data on the geographical variation in ice thickness characteristics.
3. Submarine-mounted sonar detects the *shape* of the ice bottom more accurately than moored sonar does, including identifying pressure ridges and rough, undeformed multiyear ice. It permits spectral and fractal studies, with which we gain an understanding of the mechanics of the ridge-building process.
4. By the use of additional sensors and concurrent airborne studies, a submarine can be used as a powerful vehicle for *validating* remote sensing techniques, including laser and passive and active microwave.

The chief drawbacks are:

1. Unlike moored sonar, a submarine profile cannot generate a systematic *time series* of ice thickness at a point in space.
2. Military submarines are constrained in their frequency of cruises and areas of operations, so that *systematic grid surveys* with regular repetition, the ideal, are seldom attained. Airborne or satellite sensors would be better for this, although the *initial role* of the submarine is very important in carrying out the necessary validation (e.g., for laser).
3. Submarines cannot carry out surveys in *shallow water*, so that many interesting aspects of ice deformation near shore cannot be studied.
4. It is unlikely that a military submarine would be available in the *Antarctic*, although this is a very suitable region for the use of sonar on an autonomous underwater vehicle (AUV).

The key application is to the understanding of seasons and interannual changes in the pdf, and hence in the distribution of undeformed and deformed ice types, as a way of testing the predictions of climate models and of ice-ocean-atmosphere models. However, there are other applications, including

boundary layer studies

internal wave generation

estimation of ocean-atmosphere heat flux

estimation of fresh water fluxes (e.g., Greenland Sea)

estimation of mass transport

frequency of ice scour

sonar propagation and scattering loss.

In the case of two of the cruises (1976 and 1987) the submarine carried a side scan sonar as well as an upward looking sonar, and qualitative analyses of the imagery obtained have been published. In the same two cruises one or more remote sensing aircraft co-operated with the submarine, running along the same track at a coincident time so as to permit validation of remote sensing systems over considerable lengths of track. The 1976 cruise involved a laser profilometer and a SLAR; the 1987 cruise involved an X-band SAR, the NASA AOL (airborne oceanographic lidar, an advanced laser profilometer), multifrequency passive microwave radiometers, an infrared radiometer, and a camera. Results of these validations have been recently published, with a third paper in press on the laser-sonar comparison which offers possibly the best opportunity for replacing submarine cruises by a more synoptic technique.

Future prospects for British submarine data collection include the following:

1. Further systematic studies of the same region of the Arctic (Greenland Sea and Eurasian Basin) at the same season of each year
2. The capability of validating satellite passive microwave and ERS-1 SAR imagery, and of comparison with moored upward sonar data
3. Development of AUVs for mesoscale, and eventually basin-scale, sonar profiling tasks.

References

Wadhams, P., 1981. Sea-ice topography of the Arctic Ocean in the region 70°W to 25°E, *Philos. Trans. R. Soc. London, Ser. A*, **302** (1464), 45–85.

Wadhams, P., 1990. Evidence for thinning of the Arctic ice cover north of Greenland, *Nature*, **345**, 795–797.

B-VI

Accuracy of Submarine Ice Draft Measurements

W. Tucker, R. Anderson, J. Newton, C. Wales, G. Newton, and T. Luallin

The majority of our knowledge of ice thickness in the Arctic basin has resulted from measurements of ice draft made by transiting nuclear submarines equipped with upward looking sonar profilers. At present, this is the only feasible means of obtaining basin-scale ice thickness information. It is worthwhile to consider the possible errors that may be inherent in such data. It should be immediately understood that the upward looking sonar systems were not designed to be used as scientific data gathering instruments. Rather the profiler is used in an operational mode. In the case of U.S. Navy submarines, the profiler is primarily utilized for locating potential surfacing sites. As such, the elimination of errors in the data collection system has not been a major goal. Another important point regarding these data is that the system measures ice draft, not thickness. Unfortunately, frequently in discussions and occasionally in the literature, the words are used interchangeably. While isostasy dictates that ice draft be approximately 90% of the thickness, local isostatic imbalances prohibit exact conversion of draft to thickness. Bourke and Paquette (1989) discuss limitations of converting draft to thickness.

The spatial resolution of the upward looking sonar is an important system parameter that significantly affects the statistics calculated for the ice drafts. The resolution is a function of the beamwidth of the sonar sounder. Early cruises used sonars with very wide beams, wider than 10°. Most data collected recently, however, have been obtained with sonars having a beamwidth of about 3°. The effect of beamwidth is that the ice nearest the sounder within the illuminated area provides the first and strongest return, thus is recorded as the ice draft. Unless the ice is essentially flat, the system generally does not measure the depth of that ice directly above the sounder. The net effect, then, is to make ridge keels appear wider, possibly eliminating some troughs between closely spaced ridges. This will affect the statistics by overestimating the mean draft and underestimating the number of independent keels. Wadhams (1984) discusses this problem and presents a method for comparing data collected by different beamwidth sounders.

On U.S. Navy submarines, data are currently recorded on analog paper rolls, as well as digitally with the Digital Ice Profiling System (DIPS). The digital data are stored on PC-compatible floppy disks. Prior to 1986, most data were recorded only on analog

paper rolls, although a few cruises were equipped for recording on digital magnetic tape. Lacking digital data, the analog paper records must be manually digitized, an extremely labor intensive procedure. Certainly some error is inherent in this hand digitizing process, but McLaren (1989) believes this to be quite small if care is taken during the procedure.

There are several possible sources of error associated with the upward looking ice draft measurement system. These include the assumed sound velocity, the determined depth of the upward looking sounder, and the trim angle of the submarine. The repeatability of the system from ping-to-ping has been verified to be about 0.1 m. This accuracy was determined by positioning the submarine beneath a level ice floe and making continuous measurements of the same ice.

Without question, the largest single source of error within the system is the sound velocity. An average sound speed must be assumed for the seawater layer between the submarine and the ice. The sound velocity is not continually monitored by the submarine, although a capability exists to obtain a sound velocity profile between the submarine and the ice at infrequent occasions. A sound velocity error of 100 ft s^{-1} results in an ice draft error of 1.6 m for a submarine at a depth of 250 ft. For a constant sound speed error, the ice draft error increases linearly with depth. On the DIPS, the sound velocity is selected from one of four switch selectable settings, ranging from 4712 to 5000 ft s^{-1}. The setting most frequently selected for use in the Arctic is 4712 ft s^{-1}. Average sound speeds for the upper 200 to 500 ft in the Arctic have been observed to vary from 4700 to 4820 ft s^{-1}. The very high sound speeds are apparently restricted to the Fram Strait and the region north of the Barents Sea shelf where warm Atlantic water enters the Arctic Basin near the surface. For the majority of the central Arctic Basin, sound speeds in the upper layers range from 4700 to 4750 ft s^{-1}. Thus some ice draft error due to incorrect sound speed is likely.

Small errors can be caused by the submarine not being in perfect trim such that the sounder is not pointed absolutely vertical. The errors caused by a 1° or 2° trim offset (most common) are nearly insignificant. Much larger errors are induced by the inaccuracy of the known depth of the sounder. The ice draft measurement is the difference between the depth below the sea surface and the sonar measured range to the ice bottom. Errors in the depth of the sounder are related to the accuracy of the submarine depth detector, the location of the depth detector relative to the profiler, and changes in atmospheric pressure. Combined, these sources could produce depth errors as large as 1.2 m.

The potential combined errors of raw unprocessed data could, then, be as large as 2.8 - 3.0 m. This large error represents a maximum potential limit on totally unprocessed data. Normal processing of the data can eliminate most of this error, however. During the data reduction procedure, a major effort is directed at elimination of the system errors. The U.S. Navy Arctic Submarine Laboratory uses a computer algorithm to correct the raw digital data. Described briefly, the algorithm searches the data for minimum draft points that occur sequentially in the record. These sequentially occurring minima are designated as open water or very thin ice and are assigned a depth of zero. The surrounding data are then corrected for the calculated offset. During the processing, the simultaneously obtained analog records are frequently consulted to verify the identification of open water areas, which are more easily recognized on the analog recordings. Data processed in such a manner are estimated to have ice draft errors of 0.3 to 0.5 m (Bourke and Garrett, 1987). During processing of profiles for which only the analog data exist, open water areas are noted and assigned zero depth during the manual digitization of the record. Surrounding drafts are corrected to the zero datum. It is anticipated that errors would be about the same as with the digital data.

The bottom line is that system errors are to be expected, and while care exercised during data collection can help reduce these errors, a major effort will be required to eliminate or significantly reduce them. Careful data processing appears to be the best, most cost effective method at present to deal with the possible errors.

References

Bourke, R. H., and R. P. Garrett, 1987. Sea ice distribution in the Arctic Ocean. *Cold Reg. Sci. Technol.* **13**, 259-280.

Bourke, R. H., and R. G. Paquette, 1989. Estimating the thickness of sea ice, *J. Geophys. Res.*, **94**, 919-923.

McLaren, A. S., 1989. The under-ice thickness distribution of the Arctic as recorded in 1958 and 1970. *J. Geophys. Res.*, **94**, 4971-4983.

Wadhams, P., 1984. Arctic sea ice morphology and its measurement. In *Arctic Technology and Policy* (I. Dyer and C. Chryssostomidis, Eds.), Washington, DC, Hemisphere Publishing Corporation, 179-195.

B-VII

Upward Looking Sonar Ice Draft Series From the Greenland Sea

A. S. Kvambekk and T. Vinje
Norsk Polarinstitutt
1330 Oslo Lufthavn, Norway

Three ice thickness series using moored upward looking sonars (ULS) have been retrieved from the Greenland Sea. The first series was recorded at 75°N and 12°W during the period June 1987 to June 1988. The next two series were obtained at 78°N - 05°W and 79°N - 03°W from August 1990 to August 1991. The instruments used were prototypes developed at Chr Michelsens Institute, Bergen (Fig. 1).

The ULS is also equipped with a pressure transducer, a tilt meter, and a temperature sensor. For each recording, four sonar shots are taken of which the two showing drafts with a difference less than 0.5 m are stored. The number of recordings over a period of one year amounts to about 60,000 or 130,000, depending on whether the sampling interval is set to 4 or 8 minutes.

There are a number of controls and corrections that have to be applied to the series. The varying atmospheric pressure is corrected for by pressure readings from weather maps, while the wave effects and varying temperature in the water column have to be corrected for by adjusting the series to the pressure transducer depth during ice free conditions (Fig. 2).

The effect of currents on the vertical alignment of the ULS was tested by towing the instrument alongside a ship at a variable speed of about one knot. The ULS was kept at a visible depth. It turned out that the vertical alignment was very stable. This is also confirmed by the internal recordings of the tilt which, for the majority of cases, was less than 2°. The ULS is attached to the top of a mooring at a nominal depth of 50 m. As the length of the mooring may be 2000–3000 m, the tilt of such a long mooring due to variable currents may result in a variable instrument depth around 50 m. The pressure transducer therefore should have adequate range to cover the variable depth both due to currents and, more importantly, to cover the uncertainty of deployment depth when the mooring is deployed from the ship during difficult weather and ice conditions. Data may be lost if this range is not wide enough. We have chosen a pressure transducer range covering the interval of 30 to 150 m depth.

If the sonar beam width is 2° and the depth of the sonar head is about 50 m the footprint diameter is about 2 m. We assume that it is the return signals from the deepest draft within the footprint that are stored. This assumption implies a possible systematic error resulting in excess draft values. Based on this assumption the footprint effect has been evaluated from a special, detailed mapping of the underside of ice floes in the Fram Strait using a narrow-beamed scanning sonar. For footprints with a diameter of 2 m it turns out that this systematic effect may amount to an excess draft of roughly 20 cm. This estimate is based on 45 surveys applying the scanning sonar for the subsurface topographic mapping from a depth of about 15 m below the ice surface.

The annual average effective ice draft is defined as the average of all draft observations including open water. The annual average effective ice thickness can then be calculated by a multiplication of the relationship between the total thickness and draft, 1.136, which was found from drillings in Fram Strait (Vinje and Finnekåsa, 1986). The annual effective ice thicknesses at the three locations then become 2.54 m at 75°N, 1.58 m at 78°N, and 2.24 m at 79°N (Kvambekk and Vinje, 1992). A correction for the above systematic footprint error has not been included.

The annual average ice thicknesses (open water recordings excluded) are 3.37 m and 3.16 m at 75° and 79°, respectively. When comparing, one should note that the southern series was obtained in 1987–88, while the northern one was obtained in 1990–91.

References

Kvambekk, Å. S., and T. E. Vinje, 1992. Ice draft recordings from upward looking sonars (ULSs) in the Fram Strait and the Barents Sea in 1987/88 and 1990/91, Rapportserie Nr. 79 Norsk Polarinstitutt, Oslo.

Vinje, T. E., and O. Finnekåsa, 1986. The ice transport through Fram Strait, Norsk Polar Institutt Scrivener, NR. 186, Oslo, 39 pp.

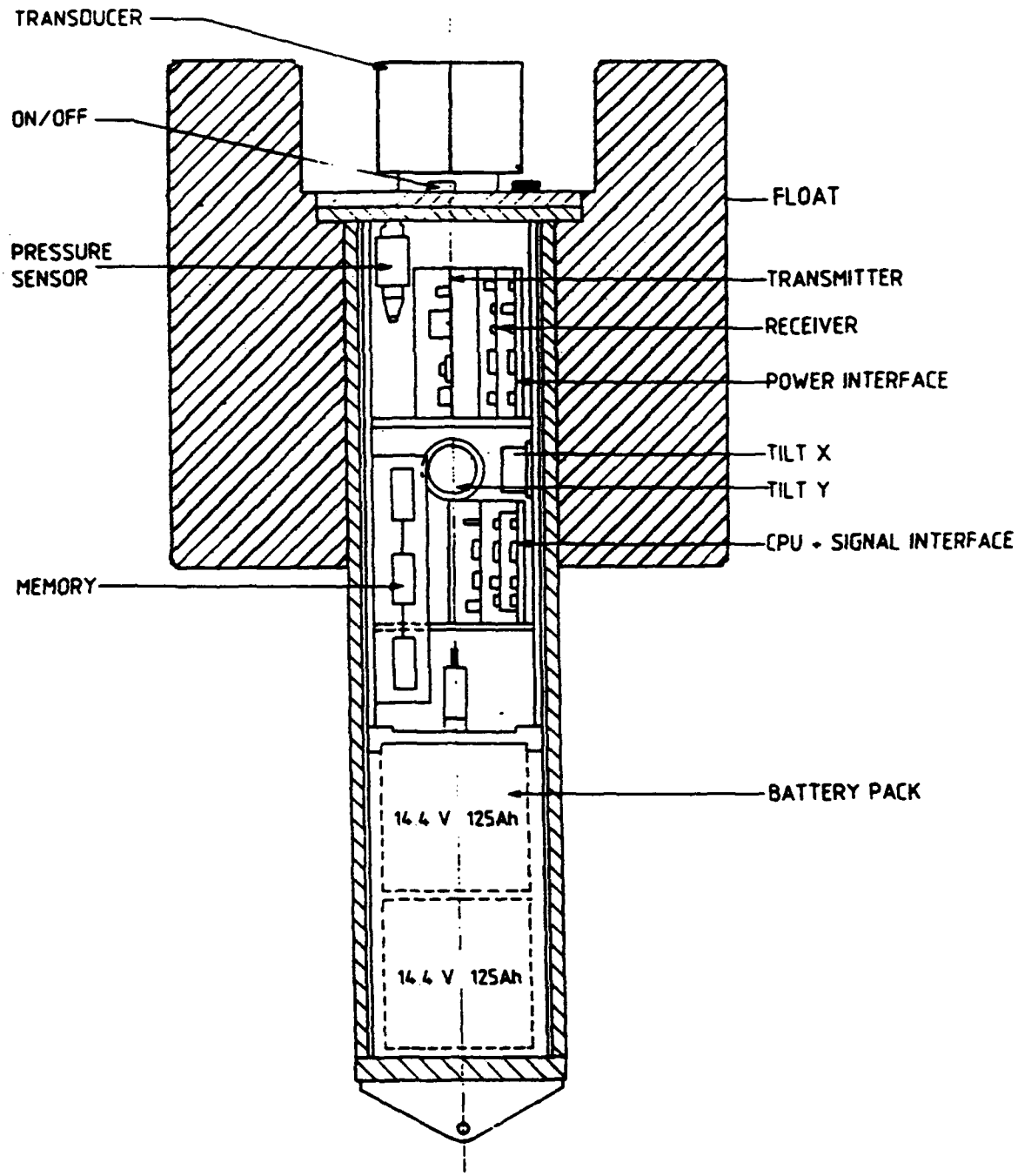

Figure 1. The Chr Michelsens Institute upward looking sonar, 300 kHz.

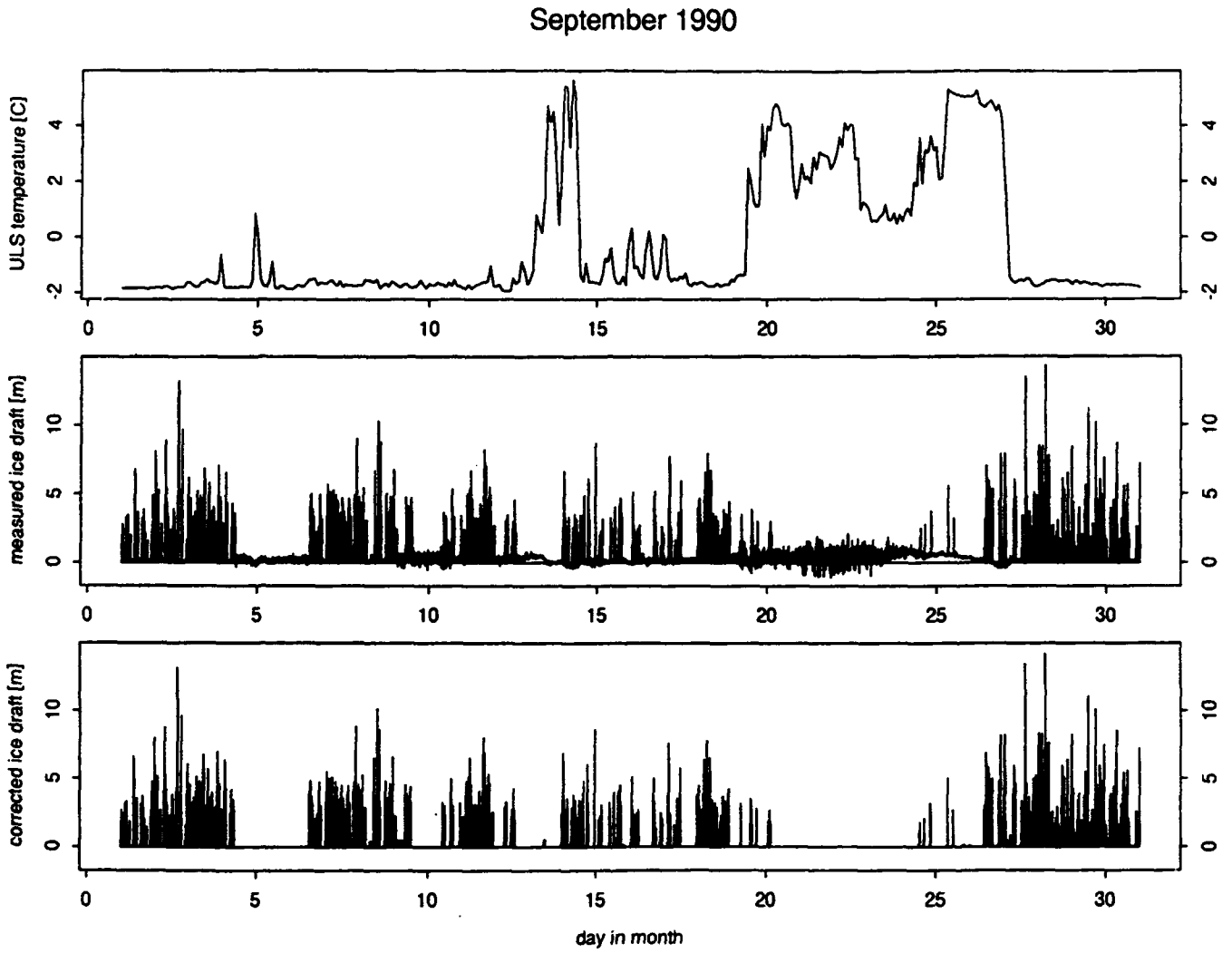

Figure 2. Temperature observations and raw and corrected ice draft recordings from the ULS at 78°N, September 1990. Note the wave effects on the recordings during the warm water influx event 18–24 September.

B-VIII

Sampling the Temporal Variability of Sea Ice Draft Distribution

Richard E. Moritz
Polar Science Center, Applied Physics Laboratory
University of Washington

The cumulative ice thickness distribution $G(h)$ is defined as the fraction of the surface area A covered by ice whose thickness ζ is less than h (Thorndike et al., 1975). The corresponding density distribution $g(h) \equiv \partial G/\partial h$ specifies the probability of occurrence $g(h)dh$ of ice with thicknesses in the range h, $h + dh$ in the area A. It is well known that some physical phenomena such as air-sea fluxes of heat, radiation, and momentum depend on properties of $g(h)$ that are not well represented by its mean value $\bar{h}$. In addition to their relevance to ice physics, distributions averaged over area are most useful for comparing *in situ* measurements to remote sensing data. In general, g depends on the time t and the position x of the area A that is sampled, thus $g = g(h, x, t)$. This temporal and spatial variability of g is central to problems of ocean-atmosphere-ice interaction. For example, $\partial g/\partial t$ and ∇g appear in the basic conservation equation developed by Thorndike et al. (1975). On the time scale of years to decades, it is of interest to study possible climatic changes Δg that might be related, for instance, to changes in the radiation balance arising from changes in the chemical composition of the atmosphere.

Observational approaches to the study of $g(h)$ must address two fundamental issues:

1. Estimating sample distributions averaged over an area A from a finite set of measurements in A.
2. Evaluating whether the observed variability of the sample distributions corresponds to temporal change in the true distribution in A.

The approach sketched here is motivated by a particular measurement setup. Assuming that useful estimates of ice thickness follow from accurate measurements of ice draft, we monitor ice draft at a fixed location X_o at regular time intervals $\Delta t = 5$ min, using a narrow-beam upward looking sonar (ULS) moored to the seafloor (Figure 1). The horizontal motion of the ice past the fixed mooring provides a sample of the ice

drafts in the region A near the mooring. After a time interval $N\Delta t$, one has a discrete time series $\tilde{h}_j$ $j = 1, N$ of measured ice draft $\tilde{h}$. The measured ice drafts may be grouped into bins of width Δh_m , $m = 1, M$, and a frequency count $F(m)$ of observations in each bin may be plotted as a histogram. The histogram may be normalized (and smoothed if necessary) to provide an estimate $\hat{g}(h_m)$ which we call the "sample ice draft distribution." Sample parameters, such as the mean and variance of the ice draft, may be estimated directly from the series $\tilde{h}_j$ using standard formulas. Examples are shown in Section IV of this report.

The relationship between the sample time series statistics and the area average definition of $g(h)$ is illustrated in Figure 2, where the envelope representing A encloses a set of points on the ice surface that were directly above a fixed location $\mathbf{X}_o$ at successive 5-minute intervals during a 4-day period. The points on the sketch are based on real sea ice motions measured by an ARGOS buoy in the Chukchi Sea during May 1988. We regard the time series as a random sample of the ice draft within the sketched region. There are $N = 1{,}152$ measurement points on Figure 2, spread over a region of about 10 km by 20 km and over a 4-day period. If the statistics of ice draft are stationary in time and homogeneous in space, then each of the N points is a sample of a single random process whose ice draft distribution is $g(h)$. In this case, one expects distinct sample distributions $\hat{g}_N$ to exhibit large *sampling variability* for small N, and to converge to the true distribution g for sufficiently large N. But we are interested in the temporal and spatial variations of $g(h, x, t)$.

Given a nonstationary, inhomogeneous process h, and the obvious increase with N of the time period and area to which the sample refers, the true and sample distributions g and $\hat{g}_N$ would be expected to change continually as $N \rightarrow \infty$, in response to local and advective processes. We call the latter changes *geophysical variability* of the distribution. Given a time series of total duration $N \times \Delta t \times K$, construct a sequence of K distinct sample distributions $\hat{g}_N(k)$, $k=1, K$. The variability among all these sample distributions arises from the combined effects of sampling variability and geophysical variability, and both sources of variability depend on time. Whether the geophysical variability is resolved depends on how the sampling variability decreases with N and how the geophysical variability increases with N and K.

Therefore, the crux of the sampling problem is whether the draft and the horizontal velocity of natural sea ice vary in such a way that the sampling variability becomes small during a time period in which the geophysical variability is negligible. If so, it should be possible to measure real temporal and spatial changes in $g(h, x, t)$ by monitoring time series of ice draft at a set of fixed locations. It is assumed here that if $\hat{g}$ converges to something, it is converging to the area averaged distribution g. Other sampling issues, such as anisotropy in the fields of ice draft and velocity, and correlation between ice speed and ice draft, are important, but are mooted if the sample distributions do not converge. These secondary issues are beyond the scope of the present note.

A simple example serves to illustrate the ideas outlined above. Let $\bar{\hat{h}}(k)$ be the sample mean of the kth set of N ice draft measurements spaced at equal time intervals Δt and drawn from a stationary ensemble with variance σ_h^2. The *variance of the sample means* about the true mean is

$$VSM = \frac{\sigma_h^2}{D} \tag{1}$$

where

$$D \approx \frac{(t + \tau_s)}{\tau_s} \tag{2}$$

is the number of degrees of freedom for estimating the mean, $t = N\Delta t$ and τ_s is the integral autocorrelation time scale for h (Bendat and Piersol, 1971). For large N, $VSM \rightarrow 0$ and the sample mean converges to the true mean. Equations (1) and (2) characterize the sampling variability associated with the mean ice draft.

A simple model for the *geophysical variability* of the mean over time t is

$$\mu(t) = \mu(0) + \frac{\partial \mu}{\partial t} t + O(t^2) \tag{3}$$

where $\mu(t)$ is the true (area) mean ice draft:

$$\mu(t) \equiv \int_0^\infty h\, g(h, t) dh .$$

In large-scale sea ice models (Coon et al., 1974; Thorndike et al , 1975; Hibler, 1980) $\partial\mu/\partial t$ results from the processes of advection, thermodynamic growth, and velocity

divergence. Over a sufficiently small time interval, $\alpha \equiv \partial\mu/\partial t$ may be taken as a constant parameter. Introducing a *running time average*

$$<\mu(t)> \equiv \frac{1}{t}\int_0^t \mu(s)ds \tag{4}$$

we find the time-dependent, *geophysical standard deviation* of μ,

$$\sigma_\mu(t) \approx \frac{\alpha t}{\sqrt{12}}. \tag{5}$$

Equation (5) models the time evolution of the geophysical variability of area mean ice draft during times short enough for the forcing processes represented by α to remain essentially constant. For larger times, a simple way to prevent σ_μ from diverging as $t \to \infty$ is to put

$$\sigma_\mu^2(t) = \sigma_\mu^2(\infty)[\,1 - \exp(-t/\tau_g)\,]^2 \tag{6}$$

which satisfies $\partial\sigma_\mu/\partial t = \alpha/\sqrt{12}$ at $t = 0$ if

$$\tau_g = \frac{\sqrt{12}\,\sigma_\mu(\infty)}{\alpha}\ . \tag{7}$$

The time scale τ_g characterizes geophysical changes in the mean ice draft, and $\sigma_\mu^2(\infty)$ is the long-term geophysical variance of the running mean ice draft.

If the sampling variability described by equation (1) is independent of the geophysical variability described by equation (3), then the *total measured variance of the mean ice draft* becomes the sum

$$TMVM = VSM + \sigma_\mu^2(t). \tag{8}$$

Introducing the nondimensional parameters $q \equiv \tau_g/\tau_s$, $p \equiv \sigma_\mu^2(\infty)/\sigma_h^2$, $t/\tau_g \to t$, and $V \equiv TMVM/\sigma_h^2$ yields

$$V = \frac{1}{1+qt} + p[1 - \exp(-t)]^2\ . \tag{9}$$

Figure 3 illustrates the behavior of the nondimensional sampling and geophysical and total variance for different values of the parameters p and q. The contribution of sampling variability to TMVM diminishes with time, whereas the contribution of geophysical variability grows. For large q, sample means converge before geophysical

variability becomes significant, and the total variance displays an obvious minimum. p measures the geophysical variance of the area mean ice draft in units of the variance of ice draft at a single point. By definition, both p and q are positive. Because p is the ratio of the variance of mean values to the variance of individual realizations of ice draft, it is reasonable to expect $p < 1$. If observations of ice draft exhibit a pronounced minimum $V(t_m)$, then t_m provides a natural averaging time for the estimation of sample mean ice draft. Sampling variability dominates for $t < t_m$ and geophysical variability dominates for larger times. The time t_m decreases with increasing p and q. The geophysical variance resolved by distinct samples averaged over t_m is $\xi \equiv p - V(t_m)$. ξ increases with increasing p and q.

Measurements made by the ULS in the Chukchi Sea during 1988–1989 provide a basis for direct observational estimates of $TMVM(t)$ and $V(t)$. A segment of the time series $\tilde{h}_j$ is divided into K distinct samples. Each sample contains N measurements, so the segment as a whole contains $K \times N$ measurements. The K sample means and sample variances are computed, together with a grand mean for the entire segment. The variance TMVM of the K sample means about the grand mean is estimated directly as the average sum of squared deviations. The sample variances are averaged over the K values to provide a normalizing variance σ_h^2. The ratio $TMVM/\sigma_h^2$ is an estimate of $V(t)$, where $t = N\Delta t$. The procedure begins with $N = 1$ and is repeated for $N = 48, 96, 144 \cdots$ (4-hour increments) holding the number of samples fixed at K in each case.

Figure 4 shows dimensional results, when the computations are carried out through various portions of the 1-year Chukchi ice draft time series. The variability shown in Figure 4a (days 110–450) samples the entire year. There is a minimum TMVM of about 0.4 m^2 at $t_m \approx 3\,d$. The variance of the geophysical change (about 1 m^2) is small compared with the variance of h (about 7 m^2). Shorter subsegments reveal different behavior. Very little variance of sample means occurs during days 120–200 (Figure 4b), so, although the sampling variability decays after about 3 days, the geophysical change in the mean is too small to be detectable. By contrast, a significant advective event brings polar pack ice and large sample means over the ULS during days 200–280. Again, 3 days is an adequate sampling time but now the geophysical signal is large. Figure 4d (days 160-240) derives from the melt season, when the sample mean ice draft decreases systematically

from about 2.5 m to less than 1 m. It is worth noting that the sample mean ice draft is usually significantly larger than the modal ice draft. The mode changes from about 1.8 m to zero during days 160–240.

The observational estimates of TMVM cited above suggest that the sample mean ice drafts estimated from segments of a ULS time series converge to quasi-stationary values for segments of about 3 days' duration. They also show that geophysical processes such as melting, freezing, and advection are large enough to be resolved from a sequence of 3-day samples. Obviously this kind of calculation can be extended to other parameters, such as sample variances and individual bins of the histogram of ice draft distribution. The basic sampling model can be adapted to any sample statistic that is a sum of random variables. Even for other parameters, such as the modal ice draft, the qualitative behavior of sampling variance curves should be instructive.

Based on the results of the Chukchi ULS analysis, it is recommended that the ULS time series be aggregated in segments of about 3 days' duration for comparison with area-average quantities such as the mean ice draft. Comparisons between ULS sample statistics and remote sensing data are appropriate for roughly 3-day ULS averages, and roughly 20 by 20 km remote sensing footprints. Slightly different intervals and footprints may be appropriate in other regions where the ice velocity and spatial variability of ice draft are significantly different than in the Chukchi Sea.

References

Bendat, J.S. and A.G. Piersol, 1971. *Random Data: Analysis and Measurement Procedures,* Wiley Interscience, New York, 407 pp.

Coon, M.D., G.A. Maykut, R.S. Pritchard, D.A. Rothrock, and A.S. Thorndike, 1974. Modeling the pack ice as an elastic-plastic material. AIDJEX Bulletin, No. 24, 1-105.

Hibler, W.D. III, 1980. Modeling a variable thickness sea ice cover. *Mon. Wea. Rev.,* **108** (12), 1943-1973.

Moritz, R.E., 1991. Sampling the temporal variability of sea ice draft distribution (abstract), *Eos* Supplement, Fall AGU mtg., 237-238 (manuscript in prep).

Thorndike, A.S., G.A. Maykut, D.A. Rothrock, and R. Colony, 1975. The thickness distribution of sea ice. *J. Geophys. Res.* **80**, (33), 4501-4513.

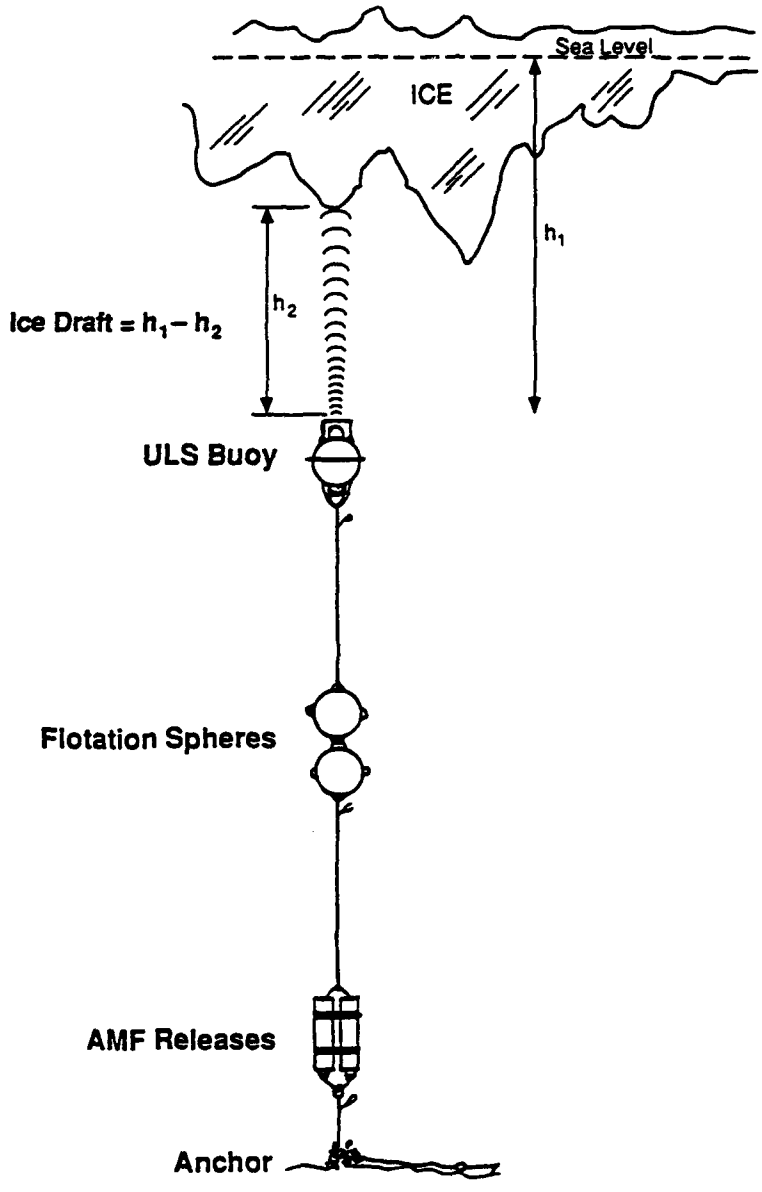

Figure 1. ULS mooring configuration. h_1 is estimated hydrostatically from measurements by a pressure gauge on the ULS buoy. h_2 is estimated from the round-trip travel time of the reflected acoustic pulse. Data are stored in a 2 Mb EPROM inside the ULS buoy. The ULS rises to the surface for recovery when the acoustic release is activated.

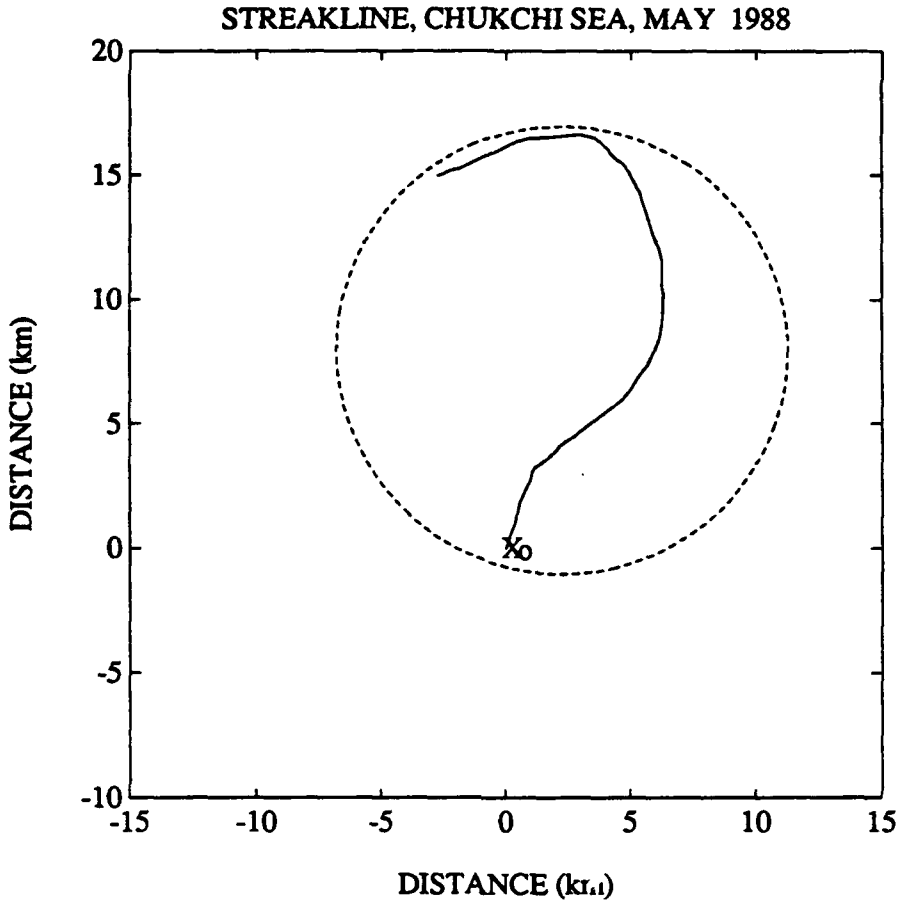

Figure 2. Relationship between time series sample points and area on the ice surface. Solid line shows positions at time t = 4 d of 1152 points that passed over the fixed position X_o during a 4-day period. Positions are estimated from ARGOS buoy measurements interpolated to 5-minute intervals. The time series statistics are regarded as estimates of averages over the area enclosed by the dashed line.

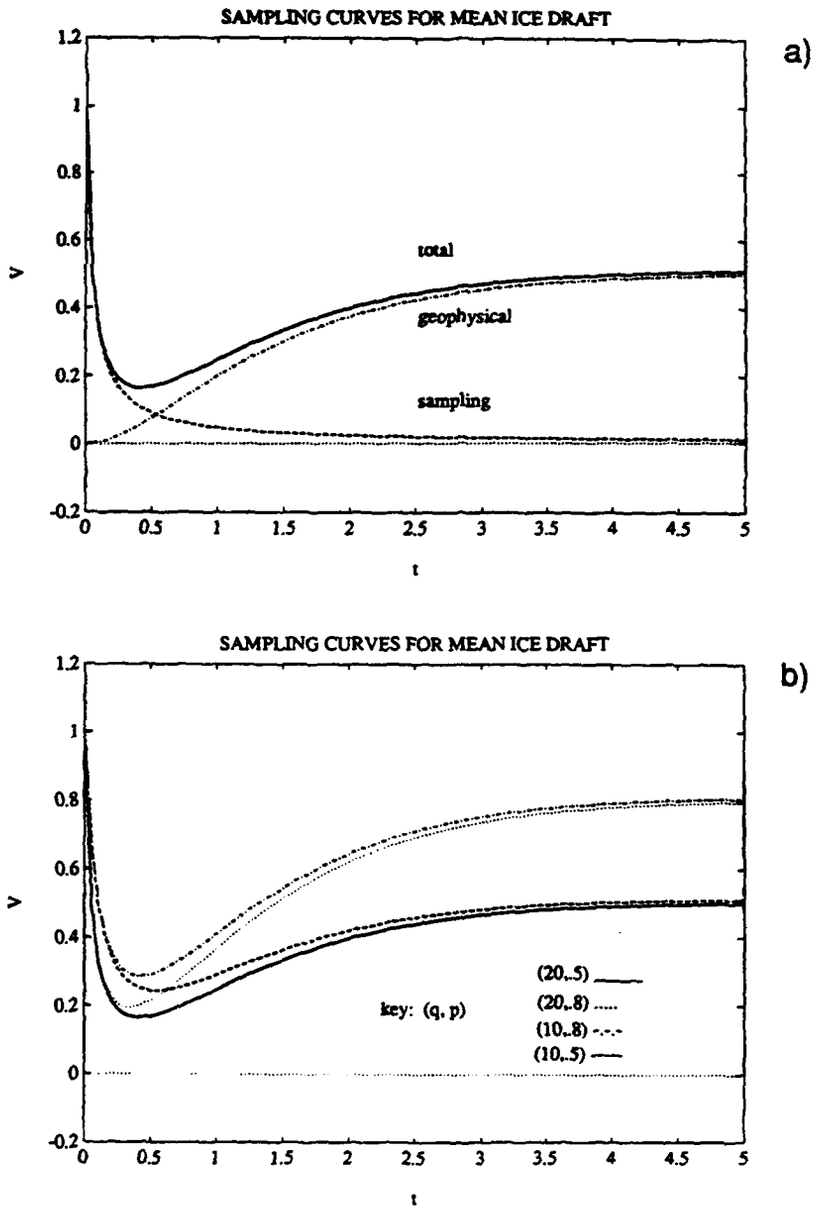

Figure 3. (a) Sampling curves illustrating the time evolution of sampling variability, geophysical variability, and their sum, the total variability $V(t)$. (b) Sampling curves illustrating the dependence of $V(t)$ on the parameters p and q.

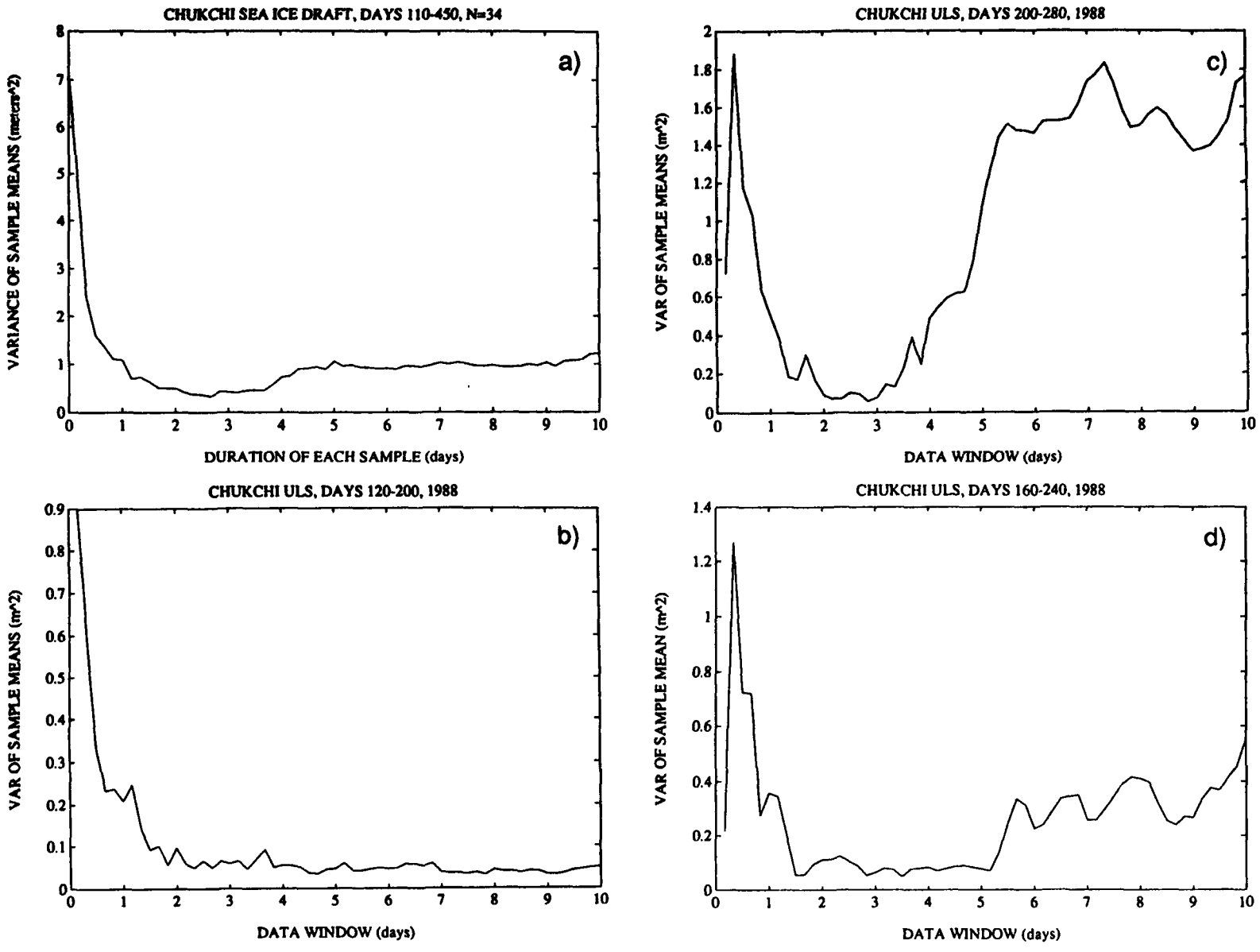

Figure 4. Estimates of TMVM (t) from ULS measurements in the Chukchi Sea, 1988-1989. (a) 340-day sample from April 1988 to March 1989; (b) Late winter sample, days 120–200; (c) Late summer sample, days 200–280; (d) Melt season sample, days 160–240.

B-IX

Airborne Laser Altimetry Measurements for Sea Ice Thickness

William B. Krabill
Observational Science Branch, Code 972
Laboratory for Hydrospheric Processes
Directorate of Earth Sciences
Wallops Flight Facility
NASA Goddard Space Flight Center

Airborne remote sensor technology and associated data processing techniques can be used to make reliable estimates of sea ice thickness over large areas. One such system is NASA's Airborne Oceanographic Lidar (AOL), which has been utilized for topographic measurement technique development since the late 1970s. Data collected by the AOL on the NASA P-3 mission to the Arctic Ocean in 1987 have demonstrated that high precision ice topography measurements can be obtained with a state-of-the-art laser profiling system. The 1987 results also illustrate the two major problems that have hampered the application of airborne lidar systems for measuring sea ice thickness in past experiments. These problem areas are associated with (1) the adjustment of range measurements for systematic errors resulting from extreme changes in backscatter from ice and water targets and (2) the removal of aircraft motion from the laser ranging data. Future measurement projects utilizing this technology will require coincident data from an airborne Global Positioning System (GPS) receiver for removal of aircraft motion and for geographical referencing of the laser data.

Light Detection And Ranging (LIDAR) systems, the light analog of RADAR, have been used for a number of ice measurement projects in the past. The primary measurement error source associated with many previous experiments involves the ranging instrumentation. The hardware used by most pulsed-laser lidars to perform the time-of-flight range measurement is a "clock" or timer, which is started by the exiting laser pulse and stopped by the returning energy reflected from the target. The discriminators that create these start and stop signals are "leading edge/threshold" devices, in which a logic pulse is created when the amplitude of the detected energy crosses a predetermined threshold. Changes in the backscattered energy from the ice or water target affects the timing of the threshold crossing for the stop pulse leading to "range walk" for pulses from lower reflectivity surfaces. This technology is adequate for a measurement with errors of a few tens of centimeters or less in applications where the

reflectivity of the target is relatively constant. However, the reflectivities for sea ice and seawater are very different, making this application especially challenging. The freeboard measurement must be accomplished by averaging a series of lead elevation measurements to establish a local mean sea level. The ice surface, on a pulse-to-pulse basis, has a reasonably constant albedo. The open water of the lead, however, can present a drastically varying reflectivity to the lidar. If the surface winds are very light, or a portion of the lead is sheltered by tall ice, the water surface will act like a mirror. For direct nadir pulses almost all of the energy is reflected back to the receiver. For pulses that have an incidence angle slightly off-nadir (due to aircraft pitch and roll variations), the mirror-like surface can forward-scatter most of the energy, leaving a very small amount (or none at all) for the receiver optics. A freshening wind can further perturb the process, producing patches of capillary waves that are effective reflectors of laser energy. The entire spectrum of signal intensities from this process can vary by four or five orders of magnitude, requiring more auxiliary measurement capability than would be found in the typical "off-the-shelf" lidar system.

The second principal error source in past experiments stems from knowledge of aircraft vertical position relative to a mean sea level that is mostly covered by ice. Recent advances in differential carrier phase GPS applications have substantially reduced this error source. Differential carrier phase tracking involving short baselines is now capable of positioning an aircraft with an accuracy of 2–3 cm relative to the location of a fixed receiver. For longer baseline experiments, such as flights over a large section of the Arctic Basin, these errors would grow to the ~5 cm range owing to ephemeris errors and different ray paths. However, since these errors are systematic in nature, the laser range measurements to leads can be used to correct the differential trajectories, so that the aircraft trajectory, and thus the ice topographic profile, will be relative to local mean sea level. As it turns out, this process is also necessary to remove ellipsoid-to-geoid differences between the GPS trajectory and local sea level.

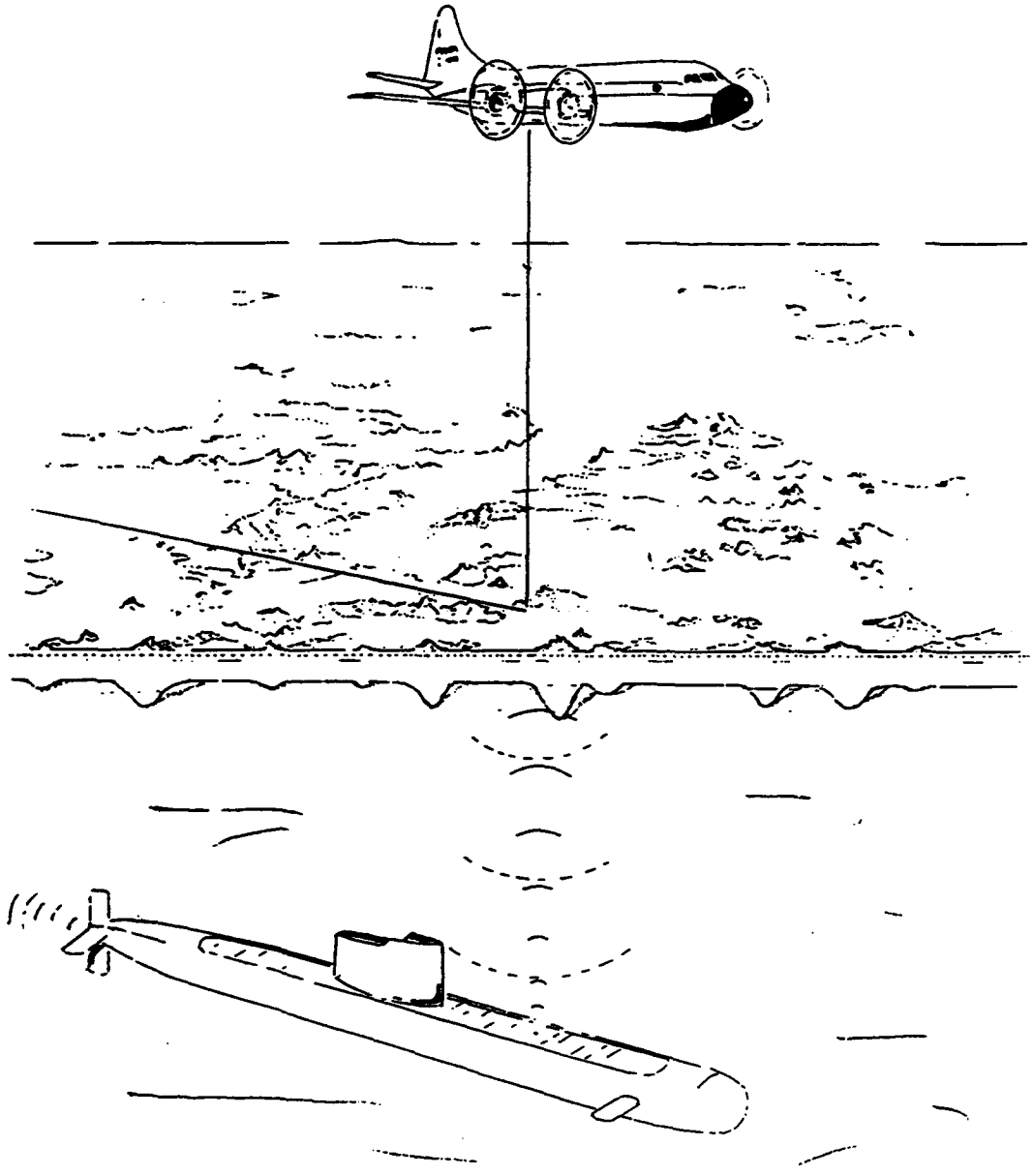

Figure 1. Airborne laser altimetry.

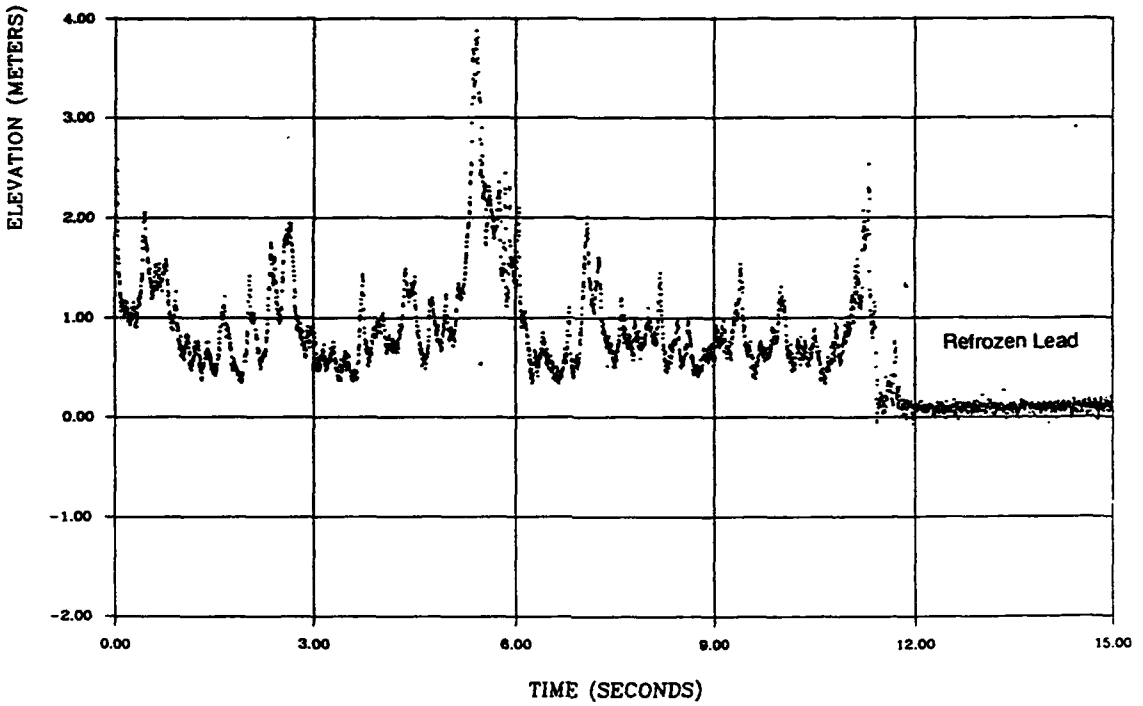

Figure 2. Laser profile of Arctic Sea ice, 10 April 1992.

B-X
Inferring Ice Thickness Distribution From Airborne Laser Profiling

P. Wadhams and J. C. Comiso

During the last two decades, laser profiling of sea ice has been carried out extensively in the Arctic (e.g., Ketchum, 1971; Weeks et al., 1971; Tucker et al., 1979; Krabill et al., 1990), and on a more limited basis in the Antarctic (Weeks et al., 1989). The main objective has been to delineate the frequency and height distributions of pressure ridge sails and the spatial distribution of surface roughness. On at least two occasions it has been possible to match a laser profile against a coincident profile of ice draft over substantial lengths of joint track. One of these was a joint aircraft-submarine experiment (Wadhams and Lowry, 1977; Lowry and Wadhams, 1979; Wadhams, 1980, 1981) while the second was a similar aircraft-submarine experiment in May 1987 involving a NASA P-3A aircraft equipped with an Airborne Oceanographic Lidar (AOL) and a British submarine equipped with a narrow-beam upward-looking sonar (Wadhams, 1990; Comiso et al., 1991; Wadhams et al., 1992, in press). Only the more recent experiment permitted a direct comparison of the pdf (probability density function) of draft and freeboard, since the AOL (see Appendix B-IX) has a superior capability over earlier lasers in the removal of the sea level datum from the record.

In a recent paper on the results of this experiment, Comiso et al. (1991) showed that over a 60 km track north of Greenland the overall pdfs of ice freeboard and draft could be brought to a close match across the entire range of data by a simple coordinate transform of the AOL data based on the ratio of mean densities of ice and water (buoyancy factor). Specifically, they showed that if R is the ratio of mean draft to mean freeboard, then matching of the freeboard pdf with the draft pdf is achieved by expanding the elevation scale of the freeboard pdf by a factor of R, and diminishing the magnitude of the pdf per meter by the same factor. This is equivalent to saying that if a fraction $F(h)$ of the ice cover has an elevation in the range h to $(h + dh)$, then the same fraction $F(h)$ will have a draft in the range $R(h)$ to $R(h + dh)$. R is related to mean material density (ice plus snow) ρm and near-surface water density ρw by

$$R = \rho m / (\rho w - \rho m) . \qquad (1)$$

Figure 1 shows the result of applying this transformation, with $R = 7.91$, showing a semilogarithmic plot of sonar draft pdf and laser pdf after application of the coordinate transformation. The two plots lie basically on top of each other except at high draft values where the number of data points is very limited.

The success of this correlation prompted an analysis of the entire data set of coincident tracks, the results of which are reported in Wadhams et al. (in press). It was found that 400 km of track contained coincident data of good enough quality to be analyzed, but of these 100 km were rejected after initial analysis because they lay in the Fram Strait marginal ice zone, where conditions change rapidly with distance, and were displaced laterally from one another by some 40 km. The remaining 300 km were divided into six 50 km sections, where the lateral displacement from the submarine track ranged from virtually zero to some 30 km. The location was north of Greenland, within the zone 80.5 – 85°N, 2 – 35°W. The results of the analysis were as follows:

1. Despite variations in mean draft from 3.6 to 6 m, the six values of R all lay within a narrow range, of mean 7.89 ± 0.18. This corresponds to a mean material density of 908.8 ± 2.3 kg m^{-3}, which is reasonable given that typical sea ice densities lie in the range 910–915 kg m^{-3}, with the mean density being reduced by the snow cover, which is sensed by the laser.
2. When each section was subjected to a coordinate transform based on its own value of R, the pdf's matched the sonar pdf's extremely well plotted on a semilogarithmic scale (Figure 2).
3. When plotted on a linear scale, the agreement was not as good, because mid-range depth probabilities are enhanced by the transformation while very thin and very thick ice probabilities are reduced (Figure 3). This is comprehensible on the basis of considering a uniform snow cover, which would give a low value of R for thin ice and a high value for thick ice. The use of a single average value for the transformation causes thin ice to be moved into thicker categories, and thick ice into thinner, thus making the converted distribution narrower and more peaked than the real ice draft distribution. In principle, a freeboard-dependent R could be used for the transform, but this would involve a sacrifice of simplicity.

How might R vary with time of year and location? To study this question, a simple model for the seasonal variation of R, based on the best available data on seasonal snow thickness, the mean density of snow, and the mean density of ice and near-surface water displaced by the ice cover, was developed. Unfortunately, current knowledge of some key parameters is inadequate. Seasonal snow thickness appears to be over-estimated in the source used for our model (Maykut and Untersteiner, 1971), with few more recent data available. There are few systematic measurements of ice density, especially of any fundamental difference between the densities of first-year and

multiyear ice. Near-surface water density is not known with the accuracy that is required for the model (since R depends on the difference between water and ice density), although it is known that it diminishes during summer because of dilution by meltwater. However, the results, a set of which is shown in Figure 4, provide useful insights about time and the spatial variability of R. The plots in Figure 4 show large seasonal variation in R, mainly due to snow load. R is at its highest value on 20 August, at the start of the snow season, with bare ice. R falls rapidly during the autumn snowfalls of September and October, then diminishes only very slowly from November to the end of April, when little snow falls. A further onset of spring snow brings R to its lowest level at the beginning of June. As soon as surface snow melt begins, R rises rapidly until by the end of June it has risen again almost to its August value. The final slow drift is due to surface water dilution. In fact there will be one or more higher peaks for R during the summer period, as meltwater pools form on the ice surface (increasing R), then drain (decreasing R), but no useful data exist on mean meltwater pool coverage, mean depth, or draining dates. In any case, the results show that snow load is a critical parameter, and that the best time to carry out surveys is when dR/dt is at its lowest value, i.e., between November and the end of April.

In conclusion, the use of an airborne laser may provide a good alternative procedure for surveying both the mean ice thickness and the thickness distribution of sea ice cover. The model suggests that a survey during early spring would be useful, with annual repetition in order to examine interannual fluctuations and trends (possibly climate-induced) in the mean ice thickness or the form of the distribution. Better data are required on the seasonal and spatial variability of snow load, ice density, and surface water density, and it would be valuable to make at least one more attempt at a coincident airborne-submarine profile, covering as many different ice regimes as possible, for validation purposes. However, even in the absence of improved background data, the present results suggest that in regions with mean ice thickness in the range 4–6 m, the ratio R will lie in the vicinity of 8.0 in spring and can be estimated to an accuracy of ±2.4% in 300 km of track. This yields an accuracy of about ±12 cm in mean thickness over 300 km of track (30 cm in 50 km), neglecting other sources of error. This is an acceptable accuracy for detecting and mapping variability. In the Antarctic much more validation would be needed before the laser could be employed in this way, since snow has a much stronger influence on mean density there than in the Arctic, and there is a major difference between snow load on first-year and multiyear ice (since the snow cover does not all melt in summer). However, if such validation were

done, this technique could be a highly effective mapping tool for the vast expanse of sea ice cover in winter.

References

Comiso, J. C., P. Wadhams, W. B. Krabill, R. N. Swift, J. P. Crawford, and W. B. Tucker III, 1991. Top/bottom multisensor remote sensing of Arctic sea ice, *J. Geophys. Res.*, **96**, 2693–2709.

Ketchum, R. D., 1971. Airborne laser profiling of the Arctic pack ice, *Remote Sensing Environ.*, **2**, 41–52.

Krabill, W. B., R. N. Swift, and W. B. Tucker III, 1990. Recent measurements of sea ice topography in the Eastern Arctic. In *Sea Ice Properties and Processes* ed. by S. F. Ackley and W. F. Weeks, U.S. Army Cold Regions Res. & Engng. Lab., Hanover NH, Monograph 90-1, 132–136.

Lowry, R. T., and P. Wadhams, 1979. On the statistical distribution of pressure ridges in sea ice, *J. Geophys. Res.*, **84**, 2487–2494.

Maykut, G. A., and N. Untersteiner, 1971. Some results from a time-dependent thermodynamic model of Arctic sea ice, *J. Geophys Res.*, **76**, 1550–1575.

Tucker, W. B. III, W. F. Weeks, and M. Frank, 1979. Sea ice ridging over the Alaskan continental shelf, *J. Geophys. Res.*, **84**, 4885–4897.

Wadhams, P., 1980. A comparison of sonar and laser profiles along corresponding tracks in the Arctic Ocean, In *Sea Ice Processes and Models* (ed. R. S. Pritchard), Univ. Washington Press, Seattle, 283–299.

Wadhams, P., 1981. Sea-ice topography of the Arctic Ocean in the region 70°W to 25°E, *Philos. Trans. R. Soc., London*, **A302**(1464), 45–85.

Wadhams, P., 1990a. Evidence for thinning of the Arctic ice cover north of Greenland, *Nature*, **345**, 795–797,

Wadhams, P., 1992. Sea ice thickness distribution in the Greenland Sea and Eurasian Basin, May 1987, *J. Geophys. Res.*, **97**, 5331–5348.

Wadhams, P., and R. T. Lowry, 1977. A joint topside-bottomside remote sensing experiment on Arctic sea ice, *Proc. 4th Canadian Symp. on Remote Sensing*, Quebec, 16-18 May 1977, Canadian Remote Sensing Soc., 407–423.

Wadhams, P., W. Tucker, W. Krabill, R. Swift, J. Comiso, and N. Davis, in press. The relationship between sea ice freeboard and draft in the Arctic Basin, and implications for ice thickness monitoring, *J. Geophys. Res.*

Weeks, W. F., A. Kovacs, and W. D. Hibler III, 1971. Pressure ridge characteristics in the Arctic coastal environment, In *Proc. 1st Intl. Conf. Port & Engg. under Arctic Conditions*, ed. by S. S. Wetteland and P. Bruun), Tech. Univ. Norway, Trondheim, 152–183.

Weeks, W. F., S. F. Ackley, and J. Govoni, 1989. Sea ice ridging in the Ross Sea, Antarctica, as compared with sites in the Arctic, *J. Geophys. Res.*, **94**, 4984–4988.

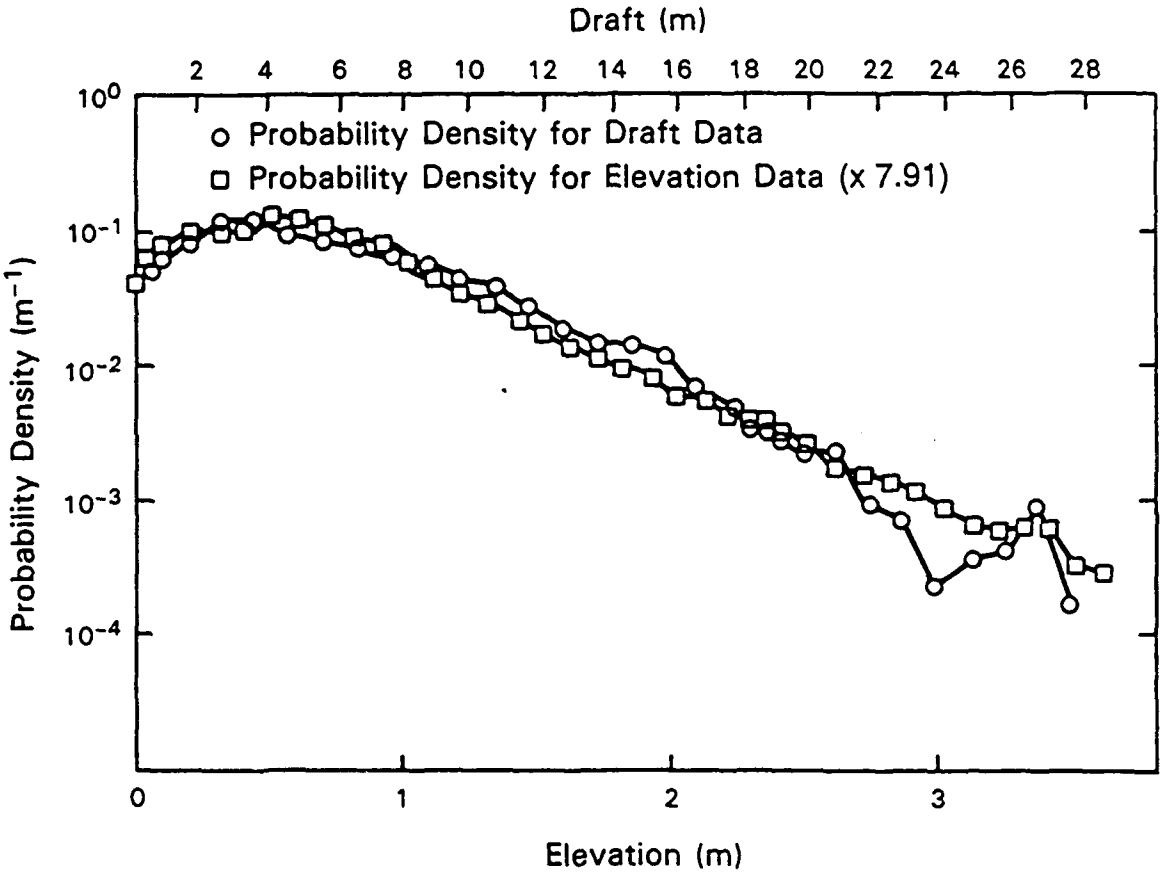

Figure 1. Results of a matching between 60 km of sonar and laser profile, in which freeboard pdf is stretched along abscissa by mean draft/freeboard ratio of 7.91 and reduced in magnitude by same factor (from Comiso et al., 1991).

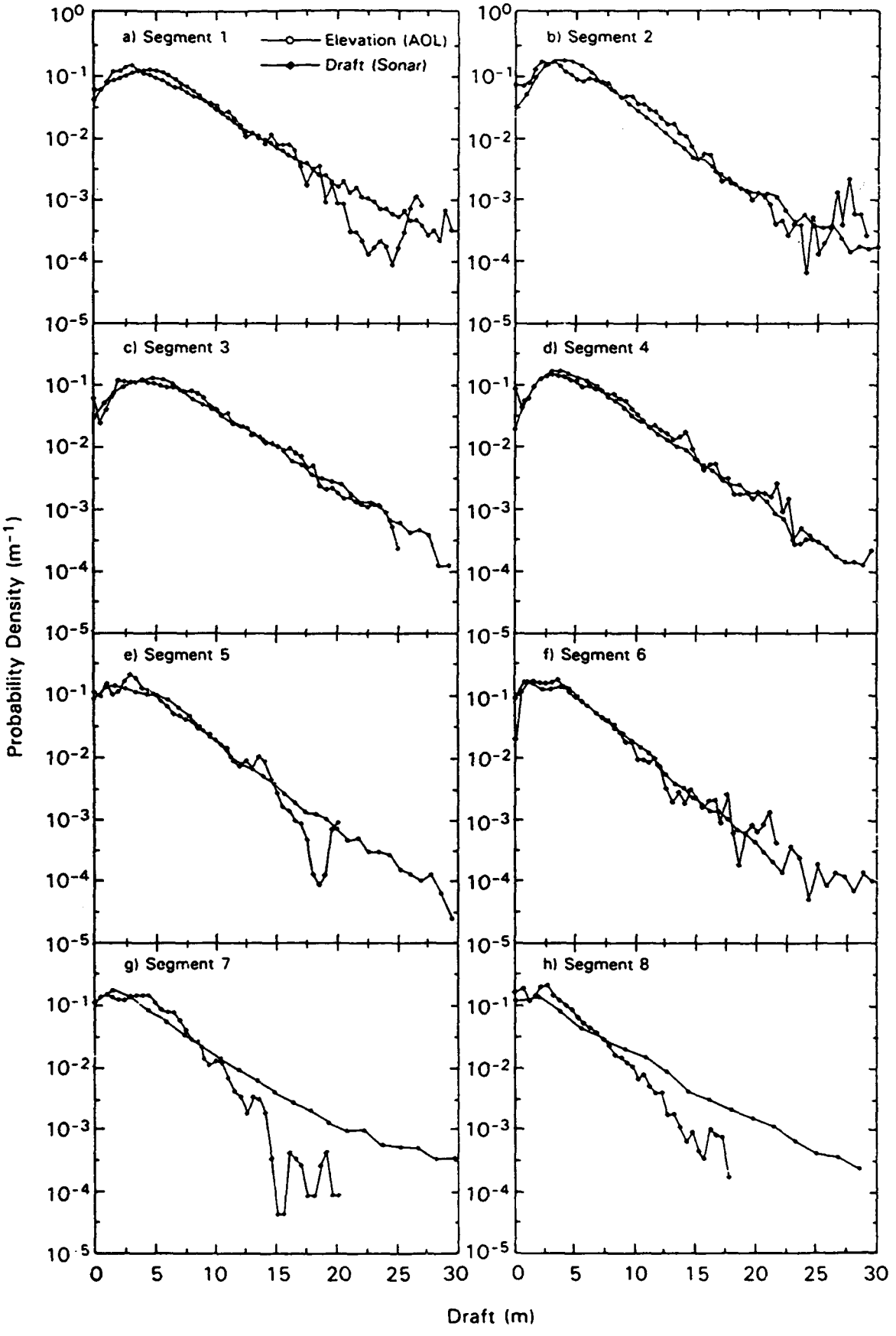

Figure 2. Results of carrying out similar transformation to Figure 1 on eight 50 km sections of coincident track (from Wadhams et al., in press).

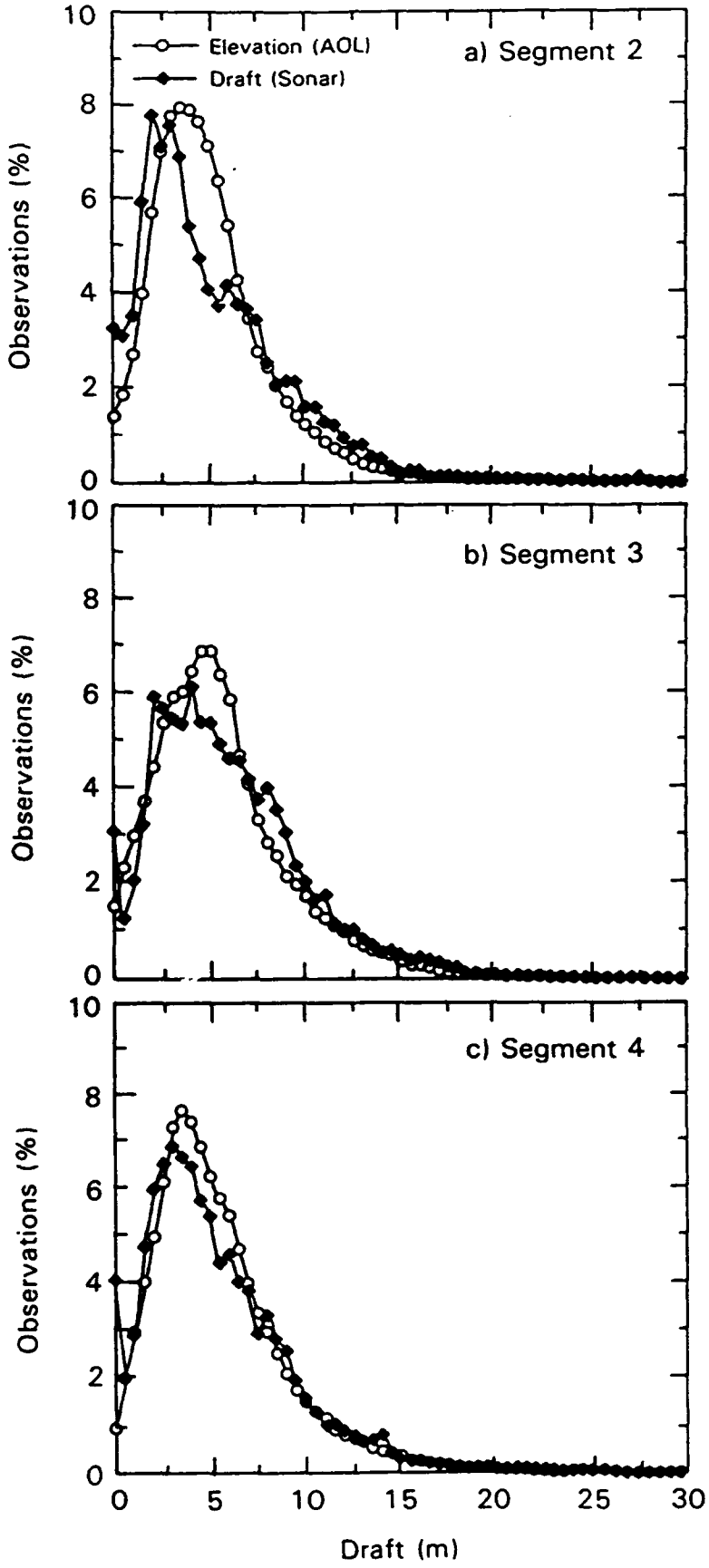

Figure 3. Real and converted pdf's of ice draft plotted on linear scale (from Wadhams et al., in press).

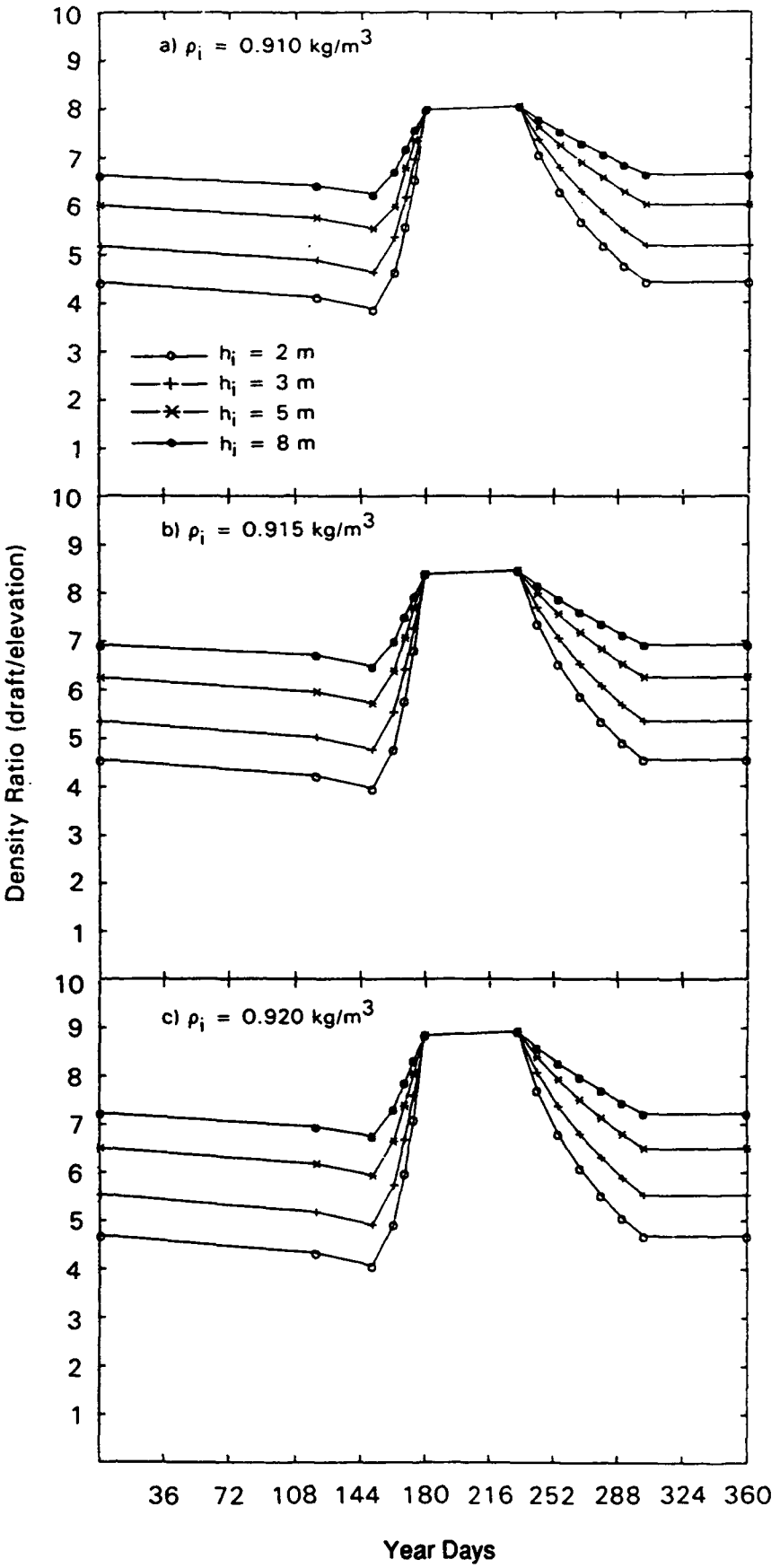

Figure 4. Results of a model of the variation of draft/freeboard ratio R with season (from Wadhams et al., in press).

B-XI

Remote Measurement of Sea Ice Thickness Using Electromagnetic Sounding

Austin Kovacs

U.S. Army Cold Regions Research and Engineering Laboratory

Sea ice is a multicomponent medium. Its constituent parts are fresh ice, liquid brine inclusions, gas pockets, and, depending upon eutectic factors, solid salt crystals. The volume of fresh ice is by far the largest fraction, typically in excess of 95%. Sea ice is classified by age (first-year, second-year, and multiyear) and by morphology. Variations in growth, melt, and deformation processes result in ice formations of complex shape, structure, and brine and gas contents. The complex structure and liquid inclusion variations have greatly limited our ability to measure sea ice thickness remotely. This is especially true for sounding systems operating at VHF frequencies and above. At these frequencies, the propagation of electromagnetic energy in sea ice suffers high attenuation as a result of the conductive brine inclusions that increase in volume with depth. The conductivity of sea ice varies with ice depth, temperature, and brine volume. However, the bulk conductivity of arctic sea ice seldom exceeds 0.03 S/m. Only during the early part of the melt season, when the solid salts that precipitated out during the cold winter months redissolve to increase the sea ice brine volume, might the bulk conductivity reach about 0.07 S/m.

Various airborne radar sounding systems have been used to profile sea ice thickness, with mixed results. Cold first-year sea ice between about 0.5 and 2.5 m thick has been successfully profiled, but not "warm" sea ice or sea ice with a high brine content. Deformed first-year sea ice cannot be profiled at VHF-UHF frequencies because of the presence of highly conductive seawater within the submerged ice rubble. In addition, loss of bottom reflection can be experienced in areas where selective ice crystal platelet growth occurs in which the c-axis of the crystals becomes aligned with the current. Under these conditions when the E field of the sounding radar's transceiver antenna is parallel to the preferred horizontal sea ice crystal c-axis orientation, a strong reflection from the bottom of the ice sheet occurs. When the antenna E field is perpendicular to the preferred horizontal crystal c-axis alignment, a weak or intermittent reflection (or none at all) may be detected from the ice bottom.

Airborne radar sounding of multiyear sea ice has been successful. The sounding of second-year sea ice floes has met with only limited success, however, because the

relatively high brine content of this ice type causes high attenuation of the EM wavelet energy within the ice structure.

The above factors have limited the usefulness of sounding sea ice thickness at VHF and UHF frequencies.

Airborne electromagnetic (AEM) systems operating in the VLF frequency band at about 1 to 200 kHz overcome many of the limitations associated with VHF-UHF sounding of sea ice thickness. In particular, the electromagnetic fields are governed by a diffusion rather than a wave equation. The result is that the energy "reflected" from the ice–water interface is not seen as temporally compact reflection events at the receiver, but rather is spread out over a wide time window. More importantly, AEM sounding is not significantly affected by the conductivity of the sea ice. Unlike radar sounding, where a discrete reflection is recorded from the ice surface and the ice bottom, only the distance to the ice–seawater interface is determined with the AEM system. This is because sea ice is transparent at AEM sounding frequencies. A laser is used to measure the distance from the AEM antenna to the ice surface. Subtracting this distance from that determined by the AEM system gives the apparent ice thickness.

An airborne electromagnetic sea ice sounding system has been designed to measure the distance from a towed antenna platform to the ice–water interface by means of electromagnetic induction (EMI). The towed cigar-like platform has a transmitter and receiver antenna spaced about 3 m apart. The wideband EMI system allows for the transmitting of frequencies over a range of about 1 kHz to 250 kHz. At the lower frequencies sea ice is relatively resistive and thus quite transparent. Therefore, during sea ice sounding the transmitted (primary) electromagnetic field induces eddy currents primarily in the conductive seawater. These currents in turn produce a secondary electromagnetic field that is sensed, along with the primary electromagnetic field, by the receiver antenna. The EMI system is designed to measure the in-phase and quadrature components of the secondary magnetic field. These components are normalized by dividing them by the magnitude of the received primary electromagnetic field component. The resulting response measured by the EMI system is a strong function of antenna platform height above the conductive seawater. An accurate measurement of this response and a full solution analysis of the data provide for a good estimate of the antenna platform to seawater distance (Kovacs et al., 1987). A laser sounding system, mounted in the antenna platform, provides the range to the ice surface. Subtracting this distance from the distance to the seawater, determined by the EMI system, gives an estimate of sea ice thickness.

EMI sounding produces an integrated depth-volume measurement with a quasi-circular footprint having a diameter of about one to four times the antenna height above the surface depending on antenna configuration. Therefore, the resulting EMI-determined distance to the sea surface is an "average" one for the area below the antenna platform. Because of signal-to-noise considerations, the antenna needs to be flown about 20 to 30 meters above the surface.

The EMI system has been under development since 1984. Five field tests have been made. The recent results indicate that the technology has developed to where average ice thickness can be determined to within about 5% of the true thickness. No other remote sea ice thickness sensing system has been proved to achieve this accuracy. The EMI results were achieved when system drift and noise levels were small or where they could be compensated for. To date, long (tens of kilometers), continuous sounding runs have not been possible because of excessive nonlinear drift. This problem is currently being addressed and should be resolved in the very near term.

The significant advantage of EMI sounding is the fact that it provides an average thickness under the antenna as well as providing a capability to measure thin ice only a few centimeters thick.

The EMI system is currently deployable only by helicopter. This restricts sounding runs to about 200 km. Fixed wing aircraft deployment is being considered. In the near term it would be extremely useful to do repetitive ice thickness measurement surveys off selected coasts. An excellent initial starting location would be off the Alaskan coast. The resulting geographic ice thickness data would be extremely useful for validating ice dynamic models and interpreting sea ice remote sensing imagery related to this coastline as well as providing baseline data for use in an assessment of climate change.

References

Kovacs, A., N. C. Nalleau, and J. S. Holladay, 1987. Airborne electromagnetic sounding of sea ice thickness and sub-ice bathymetry, CRREL Report 87–23.

B-XII

Operational Airborne Sea Ice Thickness Measurement System

Scott Holladay
Aerodat Limited and Canpolar Inc.
Ontario, Canada

Research and development of airborne sea ice thickness measurements has been conducted in Canada for over 15 years, particularly aimed towards development of a sensor that could support icebreaker activities. Current efforts are focused on a combined electromagnetic (EM)-radar-laser sensor which is towed about 30 m below a helicopter and about 30 m above the ice surface. It is anticipated that this system will become fully operational within about two years.

The instrument uses a laser to measure its height above the snow surface, a radar to detect the snow–ice interface, and electromagnetic methods to detect the distance to the ice–water interface (Figure 1).

Tests of this technology have been performed both in the Arctic and off Canada's east coast over a wide variety of ice types. Comparisons with surface measurements have been very good.

The system is housed in a bird about 0.4 m in diameter and 4 m long, weighing about 125 kg, which can be flown at up to 150 kph. Operator electronics weighing about 50 kg are housed in the helicopter and can easily be removed for other missions. Ice thickness output is real time. Ice thickness measurement range is approximately 0.2 to 20 m with an accuracy of the greater of ± 5% or ±0.1 m. Dry snow thickness can be measured to within ±10%. Ice strength can also be estimated from the electrical conductivity of the ice.

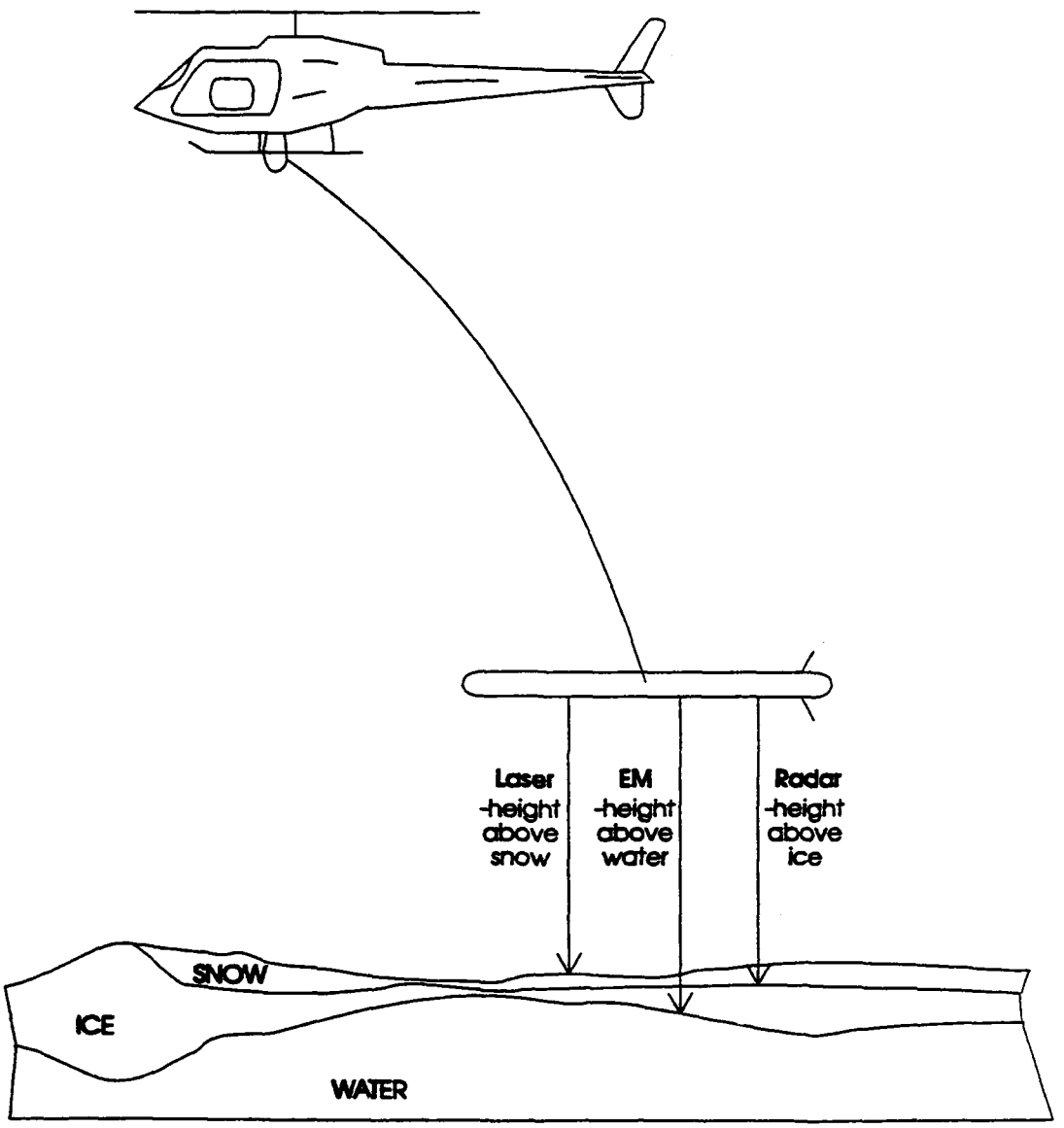

Figure 1. A combined electromagnetic (EM)-radar-laser sensor towed about 30 m below a helicopter and 30 m above the ice surface.

Aerodat - Canpolar Ice Thickness Sensor System Characteristics - Ice

Parameter	Specification
Ice types	All level sea ice, most ridges
Ice thickness range	0.2 to 20 m
Ice thickness accuracy	$\pm$ 5% or 0.1 m (greater of)
Minimum resolvable variation	0.05 m
Snow thickness range	0.3 to 5 m (dry snow only)
Snow thickness accuracy	$\pm$ 10%
Minimum resolvable variation	0.05 m
Ice strength range	Warm, saline to cold, fresh (?)
Ice strength accuracy	$\geq$ 3 categories (?)

Aerodat - Canpolar Ice Thickness Sensor System Characteristics - Equipment

Parameter	Specification
Aircraft	MBB BO105, Bell 206B, or larger
Installation on aircraft	Bolt on, bolt off
Flying conditions	< 40 knots wind speed
Flying altitude - helicopter	40 to 70 m
Flying altitude - bird	< 30 m
Flying speed	≤ 150 kph
Horizontal footprint	Approximately bird altitude
Horizontal sampling rate	10 - 20 samples/second
Electronics size	0.5 x 0.5 x 1.0 m
Electronics weight	50 kg
Power requirement	20A @ 28 VDC
Bird size	< 0.4 m diameter x 4 m long
Bird weight	Approximately 125 kg
Tow cable	30 m, hook deployable

AERODAT
Future Plans

- PRE-PRODUCTION PROTOTYPES AVAILABLE FOR FEASIBILITY DEMONSTRATIONS

- PRODUCTION PROTOTYPE BEING PLANNED FOR APPROXIMATELY 1993

- FUNCTIONALLY SIMILAR, BUT HARDENED FOR OPERATIONAL USE

B-XIII
Ice Thickness Observations From Satellites

D. A. Rothrock
Polar Science Center, Applied Physics Laboratory
University of Washington

What use can we make of visible, infrared, and passive and active microwave sensors to estimate sea ice thickness? Satellites do not see the lower surface of sea ice. They see only radiation emitted or scattered from the top surface or the volume of the top few tens of centimeters of the ice. We try to relate these surface radiative properties through a mixture of physics and empiricism to ice thickness, often through the intermediary of "ice type." This chain of relationships—of surface radiative properties to ice type to ice thickness—involves large uncertainties. The standard algorithm in the microwave part of the spectrum is to estimate the ice "type"—new or first-year or multiyear—from the microwave signal. The signal is affected by the roughness of the surface, the dielectric constant of the ice, and the number, sizes, and spacings of brine pockets within the ice sheet. A perfect electromagnetic theory might tell us a great deal about these properties from a microwave signal, however even this connection is somewhat tenuous at present. Even if the link between surface ice properties and microwave signals were perfectly understood, it would still be something of an extrapolation to deduce information about ice thickness. For thin ice, the surface temperature and the albedo have a more direct relation to ice thickness, especially as long as the ice is snow-free. In general, though, satellites provide only a proxy measurement of ice thickness.

Representative of the utility of SAR data for determining ice thickness is the ice classification algorithm in the Geophysical Processor System at the Alaska SAR Facility. The algorithm depends on distinct peaks—separated by about 6 dB in winter—for first-year and multiyear ice in the histogram of C-band VV-polarization backscatter. New ice and open water are another 4 dB less bright than first-year ice (Kwok et al., 1992). In other seasons, first-year and multiyear ice are barely distinguishable. Look-up tables with the mean and standard deviation of backscatter for these types have been constructed for each of four seasons from scatterometer and SAR aircraft observations. The appropriate table is selected depending on the month and air temperature. The nominal range of ice thickness assigned to each of these types in winter and late spring

is: open water and new ice, 0 to 0.2 m; first-year ice, 0.2 to 2.2 m; and multiyear ice, > 2.2 m. In fall, the cutoff between first-year and multiyear ice is 1.5 m instead of 2.2 m.

This algorithm will be routinely applied to the ERS-1 SAR data, providing a data base of total ice concentration and ice type concentration for much of the northern and substantial portions of the southern ice cover for several years. The algorithm will be improved as experience dictates. A similar algorithm will be applied to JERS-1 SAR data. The data will be spotty in the sense that the ground swaths are narrow and will not be continuously sampled. Analysis of time series of these data along with validation experiments will help us assess the accuracy of these concentration estimates.

Polarimetric SAR data are better able to discriminate ice thickness for thin ice types. L-band VV and HH intensities and their ratio, and copolar (VV-HH) phase difference contain most of the useful additional information. Present data from JPL aircraft experiments are promising though scanty. They show that the polarization ratio distinguishes open water from new ice, and that the copolar phase can distinguish about two thin ice categories from ice thicker than about 1 m (Winebrenner and Farmer, in preparation). It would be wise to include polarimetric SAR aircraft missions in any intercomparison experiment of ice thickness sensors. Unfortunately, there are no plans to fly a polarimetric SAR in space for at least the rest of this decade.

Passive microwave satellite data provide our longest sea ice data record. Their interpretation in terms of ice type concentrations rests on assumptions about the signatures of "pure" types: water, first-year ice and multiyear ice. They are more difficult to analyze, because the pixels are tens of kilometers across and contain a mixture of ice and water. (The SAR pixels are small and are classified as a single ice type.) There is some uncertainty about selection of pure type signatures, and the resulting concentrations of water and ice types. The NASA algorithm selects pure type signatures that tend to be extremal values and minimize the number of pixels lying outside the mixture triangle or having concentrations greater than one or less than zero (Cavalieri et al., 1984). Rothrock and Thomas (1990) examine the continuity of ice types through several annual cycles, finding that there is probably more multiyear ice than estimated by the NASA algorithm. Further analyses with different assumptions about the pure ice signatures provide a more self-consistent picture of how first-year and multiyear ice are kept in balance (Thomas, submitted; Thomas and Rothrock, submitted). In these analyses the multiyear ice concentration of the Arctic Ocean is about 0.7 in early winter, compared with an estimate of 0.4 with the NASA algorithm. These are differences in interpretation that need to be reconciled.

We can consider a crude conversion of ice type concentrations into ice thickness data. Consider the mean for the whole Arctic Ocean, for most of which we have ice concentration estimates from passive microwave satellites. Suppose ice types have ice in the following ranges of ice thickness: water, 0 to 0.1 m; first-year ice, 0.1 to 2.0 m; multiyear ice, 2 to 4 m. Then compute the range of the mean Arctic Ocean ice thickness by weighting each type by its concentration. After freezeup, the NASA algorithm concentrations (of 0.02, 0.63, and 0.35 for water, first-year, and multiyear ice) give a mean ice thickness range of 0.8 to 2.7 m. The Thomas and Rothrock concentration estimates (of 0, 0.27, and 0.73) give a mean ice thickness range of 1.5 to 3.5 m. These are large differences. I reiterate, we must resolve what passive microwave satellites are telling us about ice types.

Turning to visible and infrared imagery, we know that leads are warm and dark and that thick ice is cold and bright. How well can we harness that general idea to estimate the thickness of ice in leads? Think of the satellite data such as AVHRR as providing maps of surface temperature $T(x,y)$ and albedo $\alpha(x,y)$. Five channels may provide more than these two pieces of data, but let's think about only two variables. The surface heat balance Q for a snow-covered ice slab (net radiative and turbulent fluxes) must balance the conductive heat flux C_S through the snow layer of thickness s and the flux C_i through the ice layer of thickness h. Assume linear temperature profiles through the snow and the ice. Suppose in addition to having a map of surface temperature we know the surface heat balance Q; then we have two equations $Q = C_S = C_i$ with three unknowns: h, s, and snow-ice interface temperature T_i. We also have a third equation, for now empirical, for albedo as a function of ice thickness and snow thickness. This gives useful information only for very thin snow thicknesses; snow depths over a few centimeters are "saturated" in albedo (that is, they are at an asymptotic, bright value). These three equations allow us to map snow and ice thickness to the albedo and temperature plane of the satellite data (for fixed Q). Such a mapping defines a curvilinear region in the (T,α)-plane such that $0 < h < h_{\text{thick ice}}$ and $0 < S$, as shown in Figure 1. This curvilinear region contains the AVHRR data points from a region several hundred kilometers square, so it is likely that this model provides a useful representation of the data. Disregarding snow thickness and summing all pixels that lie between two ice thickness contours (say, 0.1 to 0.2 m) gives an estimate of the concentration of ice in that thickness range. The procedure is likely to have useful accuracy for ice thicknesses up to about 0.5 m and snow depths less than 0.05 m when this thin ice is embedded in 3 m thick ice. It will not be applicable for thick ice, because the albedo can tell us nothing about the thicker snow cover on older

ice, and we are left with no way to solve for h or s or the snow-ice interface temperature. This is a new and unproven application of temperature and albedo data; its utility remains to be evaluated (see Lindsay and Rothrock, 1992). There are other suggestions that thin ice concentrations can be estimated from albedo—that is, from gray tone in photographs (Eppler, in these proceedings).

Satellites may allow us to estimate the concentration of a few thin ice categories. Polarimetric SAR and thermal and visible data are the most promising. There are also some results concerning new ice signatures in passive microwave data (Wensnahan et al., 1991). There is a continuing need to improve the ability of passive microwave sensors and single-channel SAR to estimate ice type concentrations to be used as proxy data for ice thickness. A complementary point of view is that sea ice models should compute the distribution of ice age since this provides a more direct comparison with microwave satellite data.

References

Cavalieri, D. J., P. Gloersen, and W. J. Campbell, 1984. Determination of sea ice parameters with the Nimbus 7 SMMR, *J. Geophys. Res.*, **89**(D4), 5355-5369.

Kwok, R., E. Rignot, B. Holt, and R. Onstott, 1992. Identification of sea ice types in spaceborne synthetic aperture radar data, *J. Geophys. Res.*, **97**, 2391-2402.

Lindsay, R., and D. A. Rothrock, 1992. The calculation of surface temperature and albedo of Arctic sea ice from AVHRR. Presented at the Int'l Glac. Soc. Symp. on Remote Sensing of Snow and Ice, Boulder, May 1992. To appear in *Ann. Glaciol.*

Rothrock, D. A., and D. R. Thomas, 1990. An Arctic Ocean ice balance with assimilated satellite and buoy data. *Proc. Int. Symp. on Assim. of Obs. in Met. and Oceanog.*, Clermont-Ferrand, France, 1-13 July, 1990, 461-466.

Thomas, D. R., submitted. Global pure type signatures for passive microwave sea ice algorithms, submitted to *J. Geophys. Res.*

Thomas, D. R., and D. A. Rothrock, submitted. The Arctic Ocean ice balance: A Kalman smoother estimate, submitted to *J. Geophys. Res.*

Wensnahan, M. R., T. C. Grenfell, G. A. Maykut, and D. Winebrenner, 1991. Microwave emission from thin saline ice: Field observations and their implications for remote sensing, *Eos*, **72**, 259.

Winebrenner, D., and D. Farmer, in preparation. On the L-band polarimetric SAR response to ice thickness in new and thin sea ice types, to be submitted to *J. Geophys. Res.*

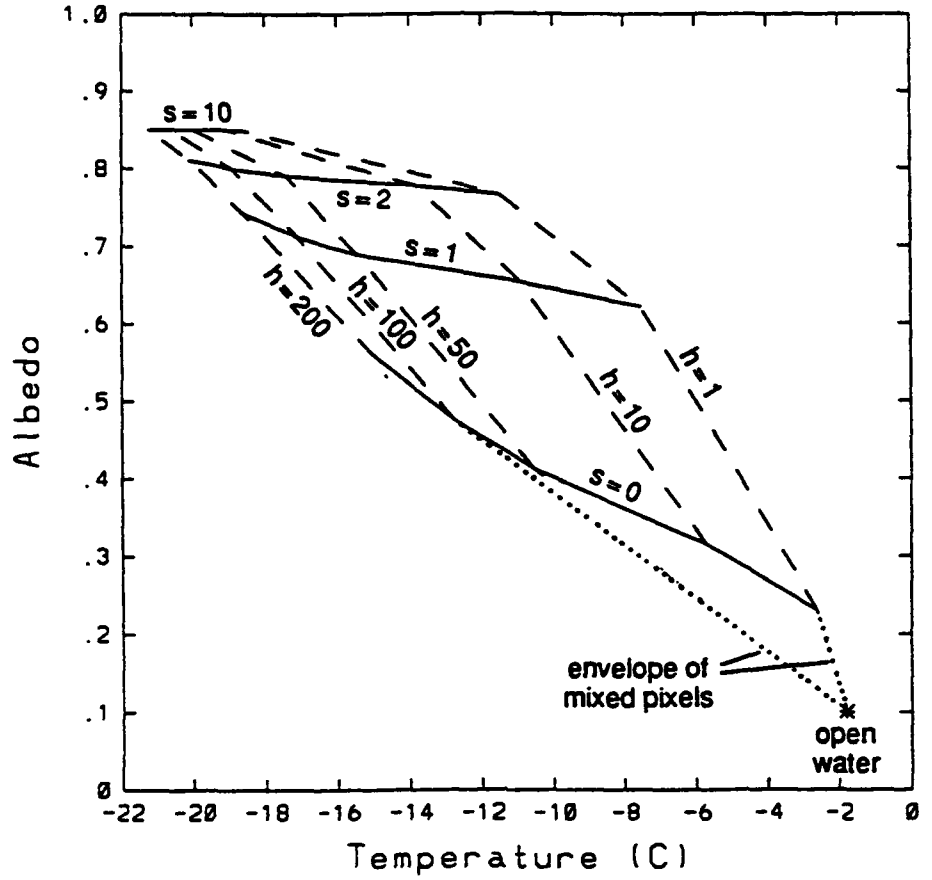

Figure 1. A mapping of ice thickness h *and snow thickness* s *onto the temperature-albedo plane. The heat flux* Q *assumes an air temperature of −15°C, wind speed of 5 m* s^{-1}*, and downward longwave and shortwave fluxes of 100 and 370 W* m^{-2}*. Thicknesses are in centimeters. The satellite data generally fall within the envelope of all (h,s) values (after Lindsay and Rothrock, 1992).*

B-XIV
Active and Passive Microwave Signatures and Relationship to Ice Thickness

J. C. Comiso and P. Wadhams

Previous attempts to measure the thickness distribution of sea ice directly using both active and passive microwave sensors have not been very successful, partly because of the complexity in the electrical properties of sea ice and partly because of very demanding requirements on electronic instrumentation (e.g., large antennas and heavy equipment). Imaging active and passive microwave systems, such as the synthetic aperture radar (SAR) and SSMI, are not expected to do any better, especially because the frequencies associated with these systems have not been at the proper wavelength (i.e., a few meters). However, it may be possible to extract from the microwave data at least an indirect link to the thickness distribution since these data are observed to discriminate some of the principal ice types and surfaces. For example, the ability to assess the distribution of first-year ice, multiyear ice, and ridged ice (the average thicknesses of which are different) would enable statistical analysis of overall thickness characteristics of the ice cover.

Results from the 1987 experiment described by Comiso et al. (1991) afforded an opportunity to test the direct relationship between the backscatter from an X-band SAR and the draft distribution from an upward looking sonar along the same track of sea ice. An example of a 10 km track of the multisensor data including SAR, sonar, and passive microwave data is shown in Figure 1. The question that can be addressed is, to what extent can SAR backscatter variability be used to infer the shape of the ice thickness distribution. First, a qualitative examination of the profile of SAR backscatter along the tracks of the submarine and P-3 (Figure 2) suggests that there is a clear positive correlation with the draft profiles. This is to be expected since pressure ridges associated with thick ice give strong returns on account of their geometry (Onstott et al., 1987; Livingstone, 1989; Burns et al., 1987). An examination of the correlation between SAR backscatter and sonar ice draft shows that on a whole there might be thickness distribution information from the SAR backscatter. A scatter plot of draft versus SAR backscatter over a restricted 22 km section of track (Wadhams et al., 1991) where there was excellent matching between tracks is shown in Figure 3. The correlation coefficient of draft versus SAR backscatter was about 0.68, for an averaging length of about 252 m (or 15 SAR pixels). The correlation coefficient is in fact better

than that found between ice draft and elevation as derived from lidar (the latter correlation being less than 0.5). This is partly because the draft distribution offers a greater range of depth discrimination for undeformed ice and a better representation of ridges, so a higher correlation can be developed over a shorter averaging length than for elevation. Furthermore, there is evidence that SAR responds to the whole width of a ridge, rather than its narrower surface sail alone. Also, the snow surface roughness which the lidar sees may not necessarily be associated with the ice surface roughness to which the SAR is sensitive.

It is obviously an advantage that the SAR backscatter matches the draft distribution, since the latter is close to the thickness distribution. However, it is clear that SAR alone cannot be used to infer the complete shape of the ice thickness distribution because only 46% of the variance of the SAR can be explained by draft variations. Furthermore, this correlation is developed over averaging lengths of 252 m, indicating that to some extent we are relating a mean ice draft to a mean SAR backscatter, rather than obtaining an algorithm that can generate a fine-resolution ice thickness distribution as in the case of the laser technique (Krabill, Appendix B-IX). It should be noted that the experiment described above was specific to X-band SAR (9.6 GHz HH), whereas the types of satellite SAR that will be producing routine synoptic data from the polar oceans are of different frequencies (e.g., C-band, 5.3 GHz, on ERS-1).

Another way to use SAR data for evaluating ice thickness is through ice type classification. Since the strength of the SAR backscatter is a function of roughness, multiyear ice and ridge ice have been observed to have significantly higher backscatter than first-year ice, young ice, and new ice. Techniques have been developed based on the unique backscatter properties of the different types to classify the arctic ice pack into multiyear ice, first-year ice, and open water (or young ice) (Kwok et al., 1992) using C-band SAR data. The potential for this technique is very good, partly because of good resolution that enables delineation of different floes. However, there are ambiguities (e.g., classification of new ice and young ice) and further validation is needed to establish regional and temporal consistency. Also, with the ERS-1 system, global coverage is difficult because of limited daily coverage.

The use of passive microwave data for a similar purpose is worth exploring because the data provide good global coverage at a good temporal resolution. Because of brine drainage each summer, multiyear ice shows passive microwave signatures that differ from those of first-year ice (Wilheit et al., 1972, Gloersen et al., 1973). Figure 1g illustrates how multichannel passive microwave brightness temperatures could be used

to discriminate different ice types. In Figure 1h, the brightness temperatures at 37 GHz are lower than those of the 18 GHz for multiyear ice, the brightness temperatures at 37 GHz and 18 GHz are approximately the same for first-year ice, while over open water the brightness temperatures at 18 GHz are lower than those of 37 GHz. This information partly provides the basis for some algorithms that estimate first-year and multiyear ice concentrations (Swift et al., 1985; Svendsen et al., 1983). A similar concept was utilized by Cavalieri et al. (1984) but using polarization and gradient ratios from the 18 GHz and 37 GHz channels. It is, however, not clear that the signature of multiyear ice is entirely stable (Thomas and Rothrock, 1989). Tooma et al. (1975) observed that second-year ice has signatures different from those of the older ice. In a cluster analysis of multispectral emissivities of arctic sea ice, Comiso (1983) observed nonlinearities in the distribution of clusters in the consolidated ice region, suggesting different signatures in different regimes of the Arctic Basin. The existence of different signatures for multiyear ice has been confirmed by in-situ measurements and implied by high resolution aircraft measurements (Comiso et al., 1991). For satellite passive microwave systems, because of very large footprints (about 30 by 30 km), a mixing algorithm has to be applied to recover multiyear ice fraction from the data. If there is more than one signature for multiyear ice, this procedure does not give very accurate results.

Results of a statistical study of the spatial distribution of arctic sea ice cover based on age are shown in Figure 4 (Colony and Thorndike, 1985). The analysis is based on several years of buoy data. The different contours correspond to the boundaries where different ages of sea ice are usually confined. In this study, the oldest ice floes are found in the Lincoln Sea region north of Greenland and the Canadian Arctic Archipelago. The next oldest ice floes are adjacent to this region but farther north. This pattern is followed to the seasonal sea ice region where most of the ice cover is first-year ice or new ice. While the actual distribution of ice of different ages may not be as clearly separated as indicated, because of oceanic and atmospheric processes which may affect the different ice types differently, the general pattern makes sense and correlates very well with different emissivity clusters as described by Comiso (1990). If this relationship between emissivity and age can be confirmed, the value of the microwave data would be further enhanced.

Additional information about multiyear ice coverage can also be obtained from studies of the summer ice cover. Since multiyear ice corresponds to floes that survive the summer, the multiyear ice distribution can be independently inferred from the ice

cover distribution during the summer (Comiso, 1990). While the summer minimum may not occur simultaneously throughout the Arctic Basin, a good approximation of multiyear ice coverage can be inferred from the data. Time series passive microwave data collected during the summer could provide information about interannual changes in the perennial ice cover. In combination with winter cluster maps, the summer ice data could provide a basis for improved interpretation of thickness distributions obtained by other means.

References

Burns, B. A., D. J. Cavalieri, M. R. Keller, W. J. Campbell, T. C. Grenfell, G. A. Maykut, and P. Gloersen, 1987. Multisensor comparison of ice concentration estimates in the marginal ice zone, *J. Geophys. Res.*, **92**, 6843-6856.

Cavalieri, D. J., P. Gloersen, and W. J. Campbell, 1984. Determination of sea ice parameters with the Nimbus 7 SMMR, *J. Geophys. Res.*, **89**, 5355-5369.

Colony, R., and A. Thorndike, 1985. Sea ice motion as a drunkard's walk, *J. Geophys. Res.*, **90**, 965–974.

Comiso, J. C., 1990. Arctic multiyear ice classification and summer ice cover using passive microwave satellite data, *J. Geophys. Res.*, **95**, 13,411–13,422, 13,593–13,597 (color plates).

Comiso, J. C., 1983. Sea ice microwave emissivities from satellite passive microwave and infrared observations, *J. Geophys. Res.*, **88**, 7686–7704.

Comiso, J. C., P. Wadhams, W. B. Krabill, R. N. Swift, J. P. Crawford, and W. B. Tucker III, 1991. Top/bottom multisensor remote sensing of Arctic sea ice, *J. Geophys. Res.*, **96**, 2693–2709.

Gloersen P., W. Nordberg, T. J. Schmugge, and T. T. Wilheit, 1973. Microwave signatures of first-year and multiyear ice, *J. Geophys. Res.*, **78**, 3564–3572.

Kwok, R., E. Rignot, B. Holt, and R. Onstott, 1992. Identification of sea ice types in spaceborne synthetic aperture radar data, J. *Geophys. Res.*, **97**, 2391–2402.

Livingstone, C. E., 1989. Combined active/passive microwave classification of sea ice. *Proc, IGARSS-89*, **1**, 376–380.

Onstott, R. G., T. C. Grenfell, C. Matzler, C.A. Luther, and E. A. Svendsen, 1987. Evolution of microwave sea ice signatures during early summer and midsummer in the marginal ice zone, *J. Geophys. Res.*, **92**, 6825–6835.

Svendsen, E., K. Kloster, B. Farrelly, O. M. Johannessen, J. A. Johannessen, W. J. Campbell, P. Gloersen, D. J. Cavalieri, and C. Matzler, 1983. Norwegian remote sensing experiment: evaluation of the Nimbus 7 scanning multichannel microwave radiometer for sea ice research, *J. Geophys. Res.*, **88**, 2781–2791.

Swift, C. T., L. S. Fedor, and R. O. Ramseier, 1985. An algorithm to measure sea ice concentration with microwave radiometers, *J. Geophys. Res.*, **90**, 1087–1099.

Thomas, D. R., and D. A. Rothrock, 1989. Blending sequential scanning multichannel microwave radiometer and buoy data into a sea ice model, *J. Geophys. Res.*, **94**, 10,907–10,920.

Tooma, S. G., R. A. Mannella, J. P. Hollinger, and R. D. Ketchum, Jr., 1975. Comparison of sea-ice type identification between airborne dual-frequency passive microwave radiometry and standard laser/infrared techniques, *J. Glaciol.*, **15**.

Wadhams, P., J. C. Comiso, J. Crawford, G. Jackson, W. Krabill, R. Kutz, C. B. Sear, R. Swift, W. B. Tucker, and N. R. Davis, 1991. Concurrent remote sensing of Arctic sea ice from submarine and aircraft, *Int. J. Remote Sensing*, **12**, 1829–1840.

Wilheit, T. T., W. Nordberg, J. Blinn, W. Campbell, and A. Edgerton, 1972. Aircraft measurements of microwave emission from Arctic sea ice, *Remote Sensing Environ.*, 2, 129–139.

Additional Reading:

Holt, B., J. Crawford, and F. Carsey, 1990. Characteristics of sea ice during the Arctic winter using multifrequency aircraft radar imagery. In *Sea Ice Properties and Processes* (eds. S. F. Ackley and W. F. Weeks), Monograph 90-1, US Army Cold Regions Res. & Engng. Lab., Hanover, NH, 224 (abstract).

Kovacs, A., and R. M. Morey, 1987. Estimating sea ice thickness from radar sounding time-of-flight data, In *Proc. 9th Intl. Conf. Port & Ocean Engng. under Arctic Condns*, eds. W. M. Sackinger and M. O. Jeffries, Univ. Alaska, Fairbanks, 1, 121–136.

Krabill, W. B., R. N. Swift, and W. B. Tucker III, 1990. Recent measurements of sea ice topography in the Eastern Arctic. In *Sea Ice Properties and Processes*, eds. S. F. Ackley and W. F. Weeks, U.S. Army Cold Regions Res. & Engng. Lab., Hanover NH, Monograph 90-1, 132–136.

Leppäranta, M., and T. Thompson, 1989. BEPERS-88 sea ice remote sensing with synthetic aperture radar in the Baltic Sea, *Eos, Trans. Am. Geophys. U.*, **70**, 698–699, 708–709.

Maykut, G. A., and N. Untersteiner, 1971. Some results from a time-dependent thermodynamic model of Arctic sea ice, *J. Geophys Res.*, **76**, 1550–1575.

Menashi, J., C. Swift, K. St. Germain, J.C. Comiso, and A. Lohanick, submitted. Passive microwave measurement of sea ice thickness, *J. Geophys. Res.*

Parkinson, C. L., J. C. Comiso, H. J. Zwally, D. J. Cavalieri, P. Gloersen, and W. J. Campbell, 1987. Arctic sea ice 1973-1976 from satellite passive microwave observations, NASA Spec. Publ. 489.

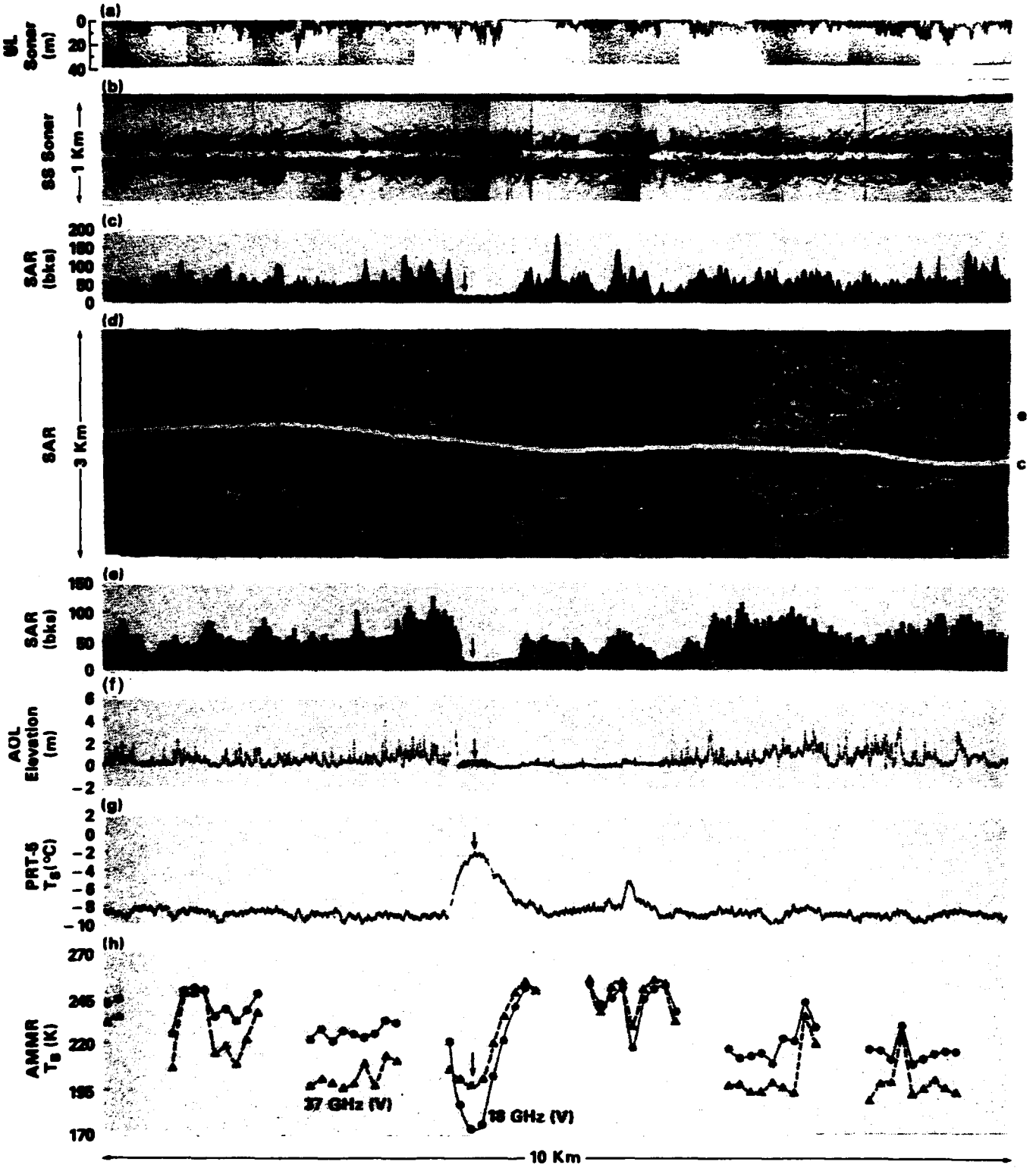

Figure 1. A 10-km section of imagery and profiles from the joint aircraft-submarine experiment of May 1987. (a) The upward looking sonar profile of ice draft. (b) Sidescan sonar imagery of the ice underside, with a 1000-m swath width. (c) The SAR backscatter values along the submarine track. (d) Contrast-stretched SAR imagery, with submarine and aircraft tracks overlaid. (e) The SAR backscatter values along the track of the P-3A. (f) The AOL laser profile of ice elevation. (g) PRT-5 infrared radiometer profile. (h) Microwave brightness temperatures at 18 GHz and 37 GHz from the AMMR (from Comiso et al., 1991).

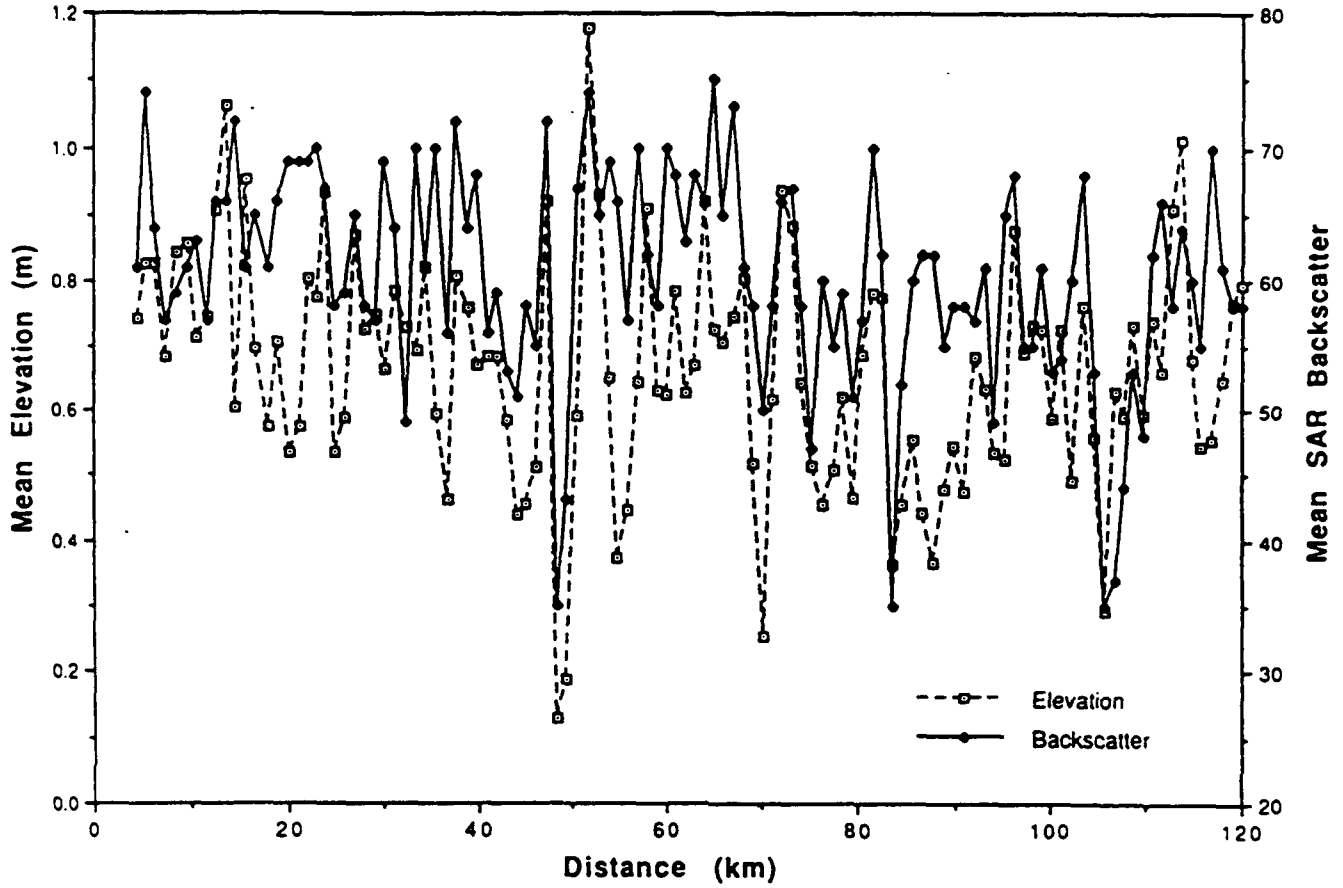

Figure 2. Mean elevation and mean backscatter for the 1-km window along a 120-km track. (from Comiso et al., 1991)

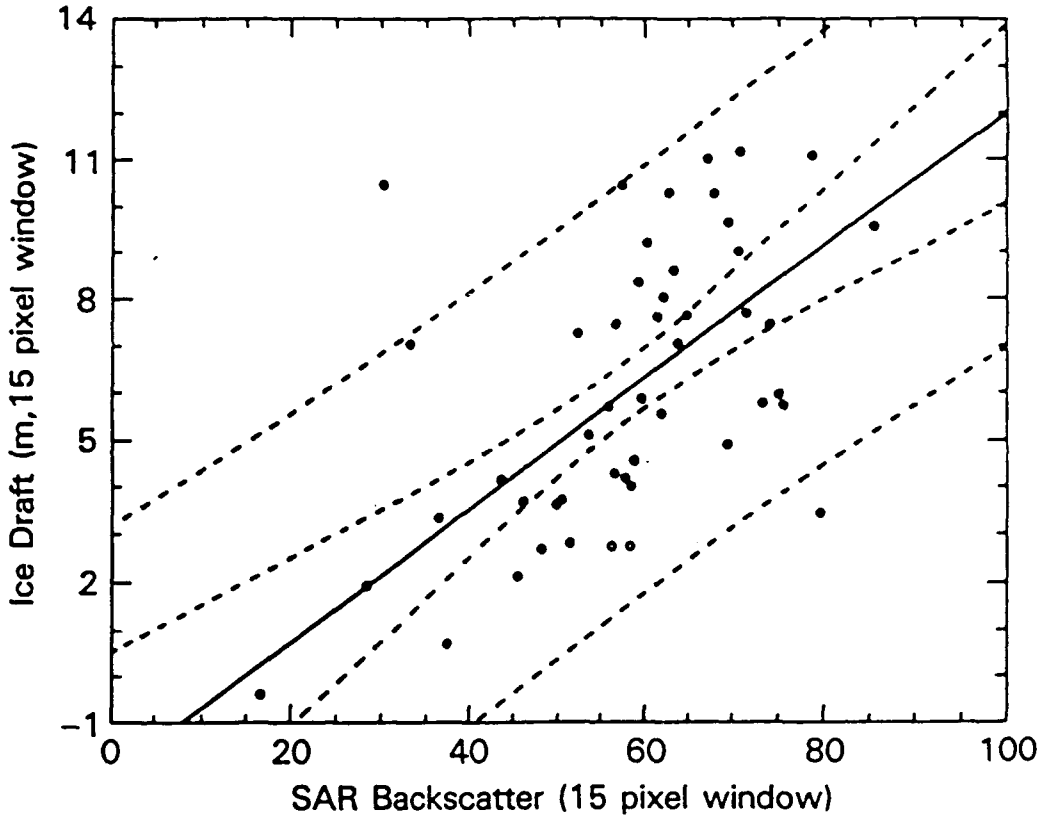

Figure 3. Scatter diagram of SAR backscatter versus ice draft, 252 m window, with 95% and 99% confidence limits added (from Comiso et al., 1991).

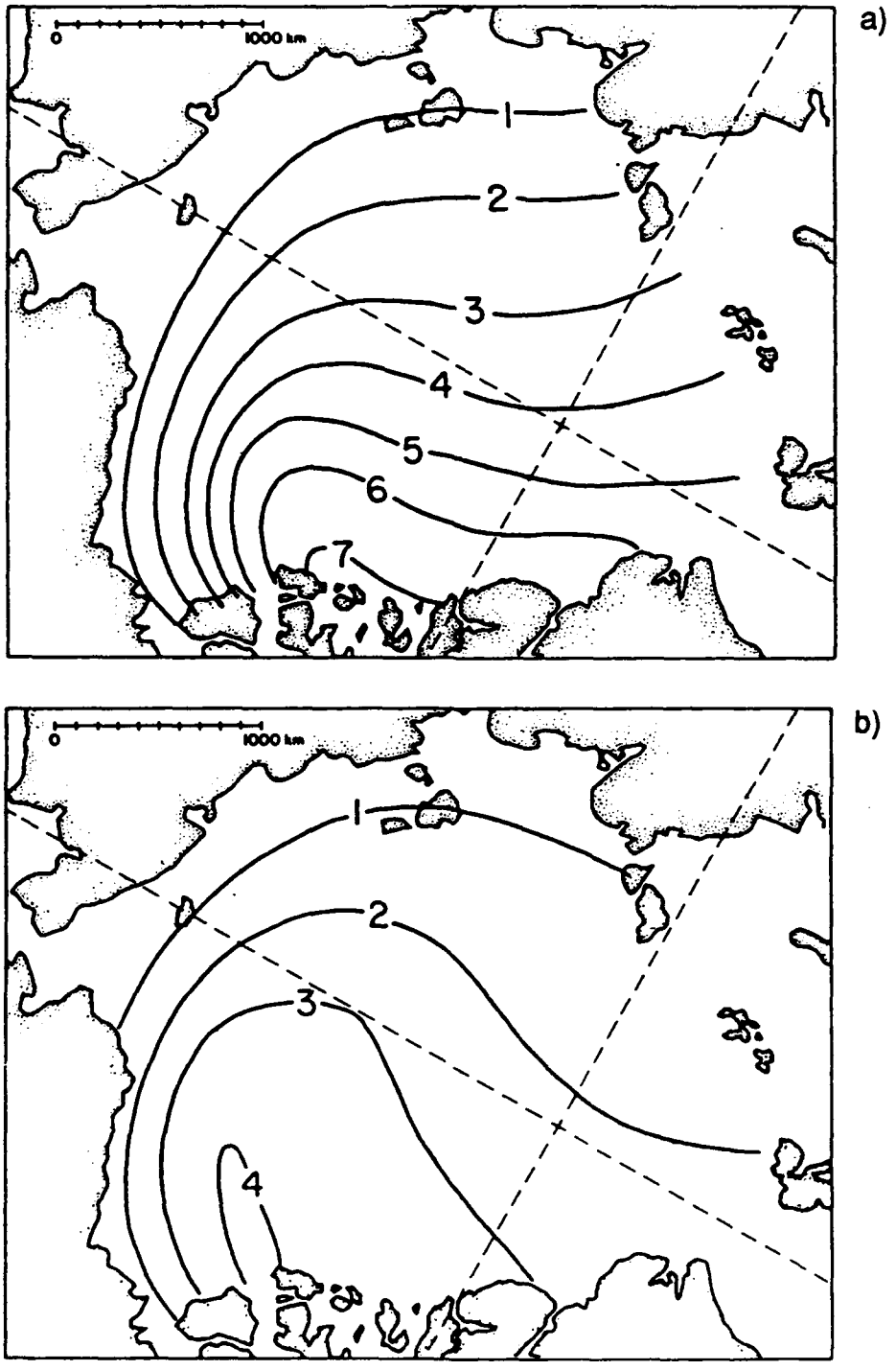

Figure 4. *(a) Contours of mean present age and (b) contours of the root of the variance of present age; the units are years (from Colony and Thorndike, 1985).*

B-XV

Some Impromptu Remarks Regarding Passive Microwave Measurements of Sea Ice Properties and Their Relationship to Sea Ice Thickness

Per Gloersen

A recent paper in *Nature* (Gloersen and Campbell, 1991) reported that the sea ice extent in the Arctic, defined as the area enclosed by the 15% ice concentration isopleth, decreased by about 2% over the 8.8-year lifetime of the Nimbus-7 Scanning Multichannel Microwave Radiometer (SMMR). This decrease is statistically significant at the 97% confidence level. At the same time, the Antarctic showed no statistically significant trend (see Figure 1). This raises some valid questions: Was there any corresponding decrease in sea ice thickness in the Arctic? Is there any hope of obtaining sea ice thickness information from passive microwave observations? There may be some useful answers to these questions, which I shall suggest later.

First, I should like to offer some caveats regarding techniques that have been described here today. Figure 3.1.33 in Gloersen et al. (1992) shows a large interannual variation in the distribution of multiyear ice in the Arctic Ocean. Thus, submarine sonar measurements of ice draft would be necessary over widely distributed areas during a given winter and at regularly-spaced time intervals in order to obtain a realistic picture of average ice thickness. That is to say, if repetitive measurements were made along only a select few transects from one year to another, then one might be observing merely shifts in the multiyear ice.

In principle, it is possible to infer ice thickness from observed microwave radiances for sufficiently thin sea ice. The calculated optical depth is on the order of a quarter of a wavelength or less (Figure 2), a severe limitation at even a wavelength of 21 cm. However, experimental points obtained at a wavelength of 21 cm (shown in Figure 2) imply an optical depth almost an order of magnitude larger than predicted. Unfortunately, these observations are contaminated by the formation of a highly-saline wet film on top of wintertime thin ice that persists until the ice is covered with snow (Ramseier et al., 1975) and serves to lower its microwave emissivity. A radio brightness temperature map obtained at the 1.55-cm wavelength by an imaging microwave radiometer on board the NASA CV-990 over the Bering Sea (Figure 19 in Ramseier et al., 1975) shows one of the measured thin and moist ice areas as an area of low-

brightness temperature at its center. A subsequent low-level pass over a nearby area obtained a multispectral view of thin ice (Figure 3).

Infrared techniques offer some hope of producing ice thickness data, but, as can be seen in Figure 4, the coincident surface air temperature must also be known in order to interpret the results. Although sparse, temperatures obtained from buoy observations might be useful in this regard.

A passive microwave technique not yet tested involves the comparison of subsurface sea ice temperature estimates obtained from passive microwaves (Cavalieri et al., 1984) with temperatures from buoys on the surface. Hypothetically, the radiance emitted from sea ice emanates largely from the snow-ice interface in the case of first-year sea ice and from near sea level for multiyear ice. This hypothesis is based on the knowledge that the freeboard portion of first-year ice contains brine, causing it to be a good microwave absorber, whereas the freeboard layer of multiyear ice contains empty brine pockets that entrap radiation (more for shorter wavelengths). The resulting volume scattering, however, is negligible at a wavelength of 4.6 cm used for the sea ice temperature calculation. Thus, the thicker (and older) the sea ice, the greater the difference between the ice temperatures derived from microwave radiances and those measured by surface buoys. It is suggested that a comparison such as this be made between ice temperatures derived from Nimbus-7 SMMR data and those obtained from the combination of Arctic Ocean Data Buoy Program and Soviet drifting station data. Estimates of ice thickness could be made with a heat transfer model and multiyear ice concentration maps, and compared with coincident measurements of ice draft from submarine data.

References

Cavalieri, D. J., P. Gloersen, and W. J. Campbell, 1984. Determination of sea ice parameters with the Nimbus 7 SMMR, *J. Geophys. Res.*, **89**, 5355–5369.

Gloersen, P., and W. J. Campbell, 1991. Recent variations in Arctic and Antarctic sea ice covers, *Nature*, **352**, 33–36.

Gloersen, P., W. J. Campbell, D. J. Cavalieri, J. C. Comiso, C. L. Parkinson, and H. J. Zwally, 1992. *Arctic and Antarctic Sea Ice, 1978–1987: Satellite Passive Microwave Observations and Analysis*, NASA SP511, National Aeronautics and Space Administration, Washington, D.C.

Gloersen, P., R. Ramseier, W. J. Campbell, P. M. Kuhn, and W. J. Webster, Jr., 1975. Ice thickness distribution as inferred from infrared and microwave remote sensing

during the Bering Sea Experiment, in *Proceedings of the Final Symposium on the Results of the Joint Soviet-American Expedition*, K. Ya. Kondratyev, Yu. I. Rabinovich, and W. Nordberg, eds., Gidrometeoizdat, Leningrad, pp. 282–293. (Republished as *USSR/USA Bering Sea Experiment*, by A. A. Balkema, Rotterdam, 307 pp., 1982.)

Ramseier, R. O., P. Gloersen, W. J. Campbell, and T. C. Chang, 1975. Mesoscale description for the principal Bering Sea Experiment, in *Proceedings of the Final Symposium on the Results of the Joint Soviet-American Expedition*, Leningrad, May 12–17, 1974, K. Ya. Kondratyev, Yu. I. Rabinovich, and W. Nordberg, eds., Gidrometeoizdat, Leningrad, 234–269. (Republished as *USSR/USA Bering Sea Experiment* by A. A. Balkema, Rotterdam, 307 pp., 1982.)

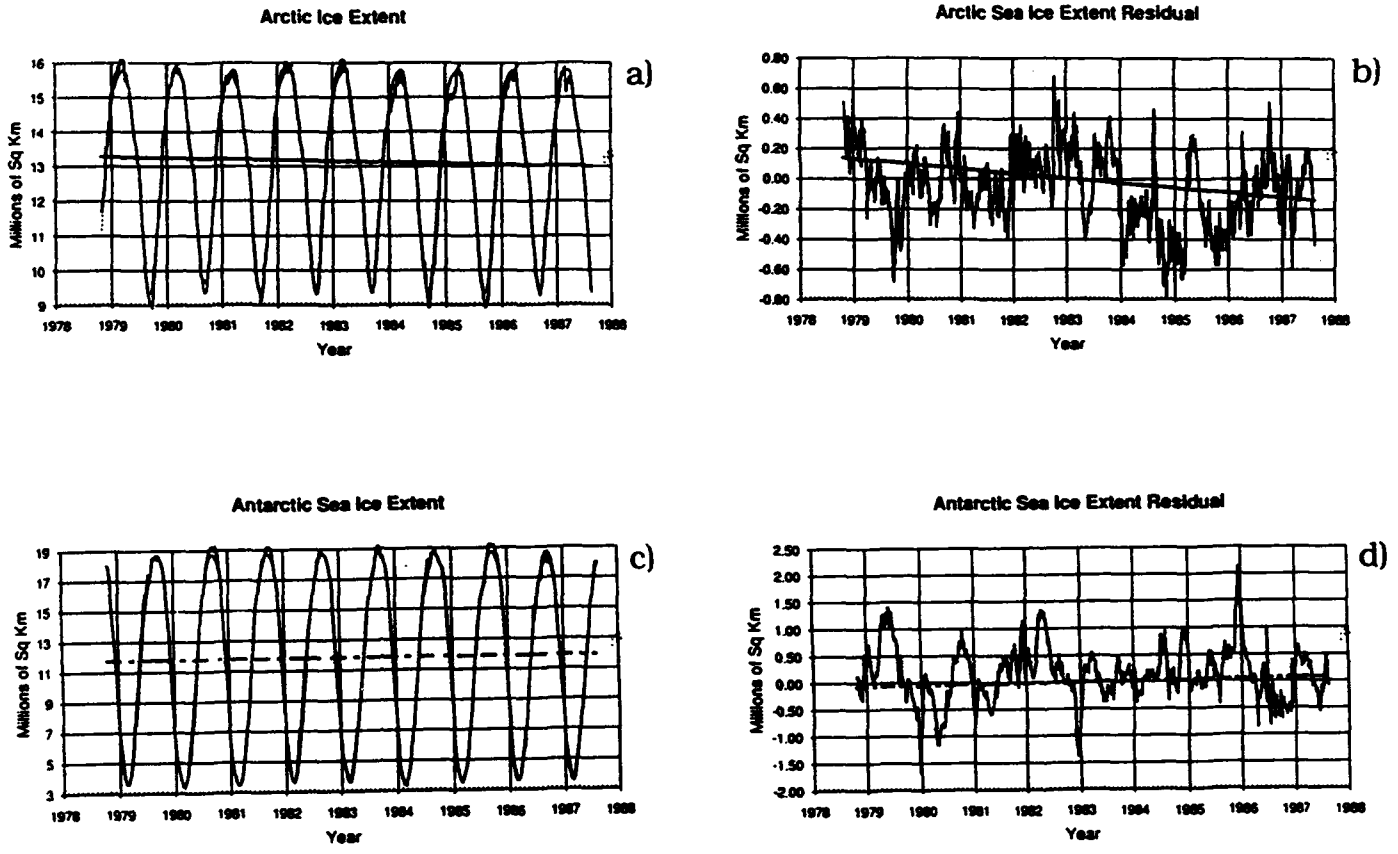

Figure 1. Sea ice extents (the areas enclosed by the margin of the sea-ice covers) and residuals for (a) and (b), the Arctic, and (c) and (d), the Antarctic, from 25 October 1978 to 20 August 1987, and their trends. The Arctic trend (solid line) is a 2.1% decline over the 8.8-year interval under discussion, and is significant to the 96% confidence level. The Antarctic trend (dashed line) is statistically insignificant. The extents are determined from the horizontally and vertically polarized radiances at wavelengths of 0.8 and 1.7 cm obtained by the SMMR on board the Nimbus-7 satellite. Also shown in (a) and (c) are the modeled seasonal oscillations composed of ten sinusoids comprising the first five harmonics of the annual cycle, whose amplitudes were obtained by an ordinary least-squares fit to the data. The residuals shown in (b) and (d) result from subtracting these modeled oscillations from the data, and emphasize the superimposed BLR trend lines. The radiances are corrected for long-term instrument drift and variations with ecliptic angle.

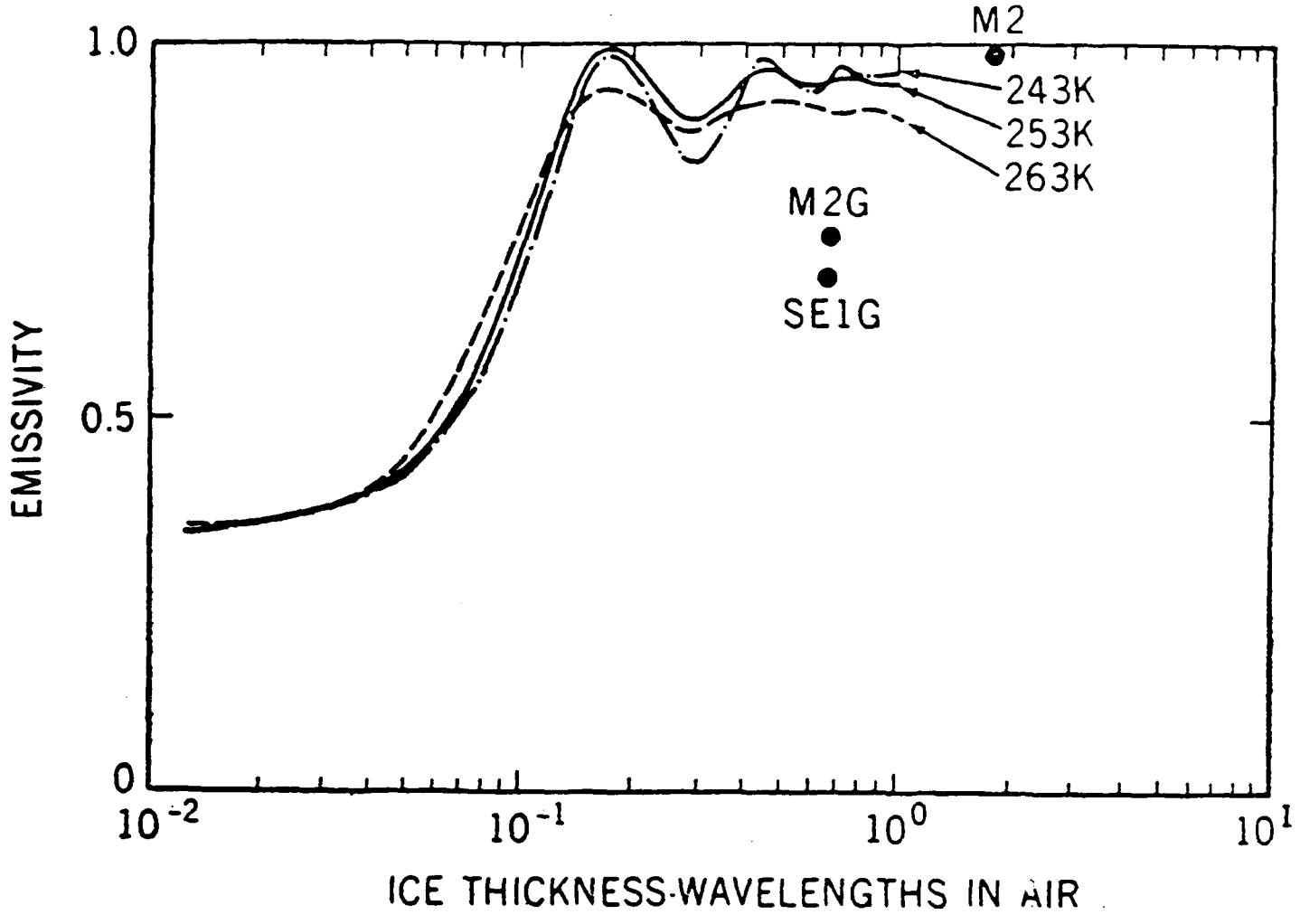

Figure 2. Microwave emissivity of sea ice as a function of ice thickness in units of microwave wavelengths in air, based on a simple three-layer theory. The dots are experimental points added for comparison (from Gloersen et al., 1975).

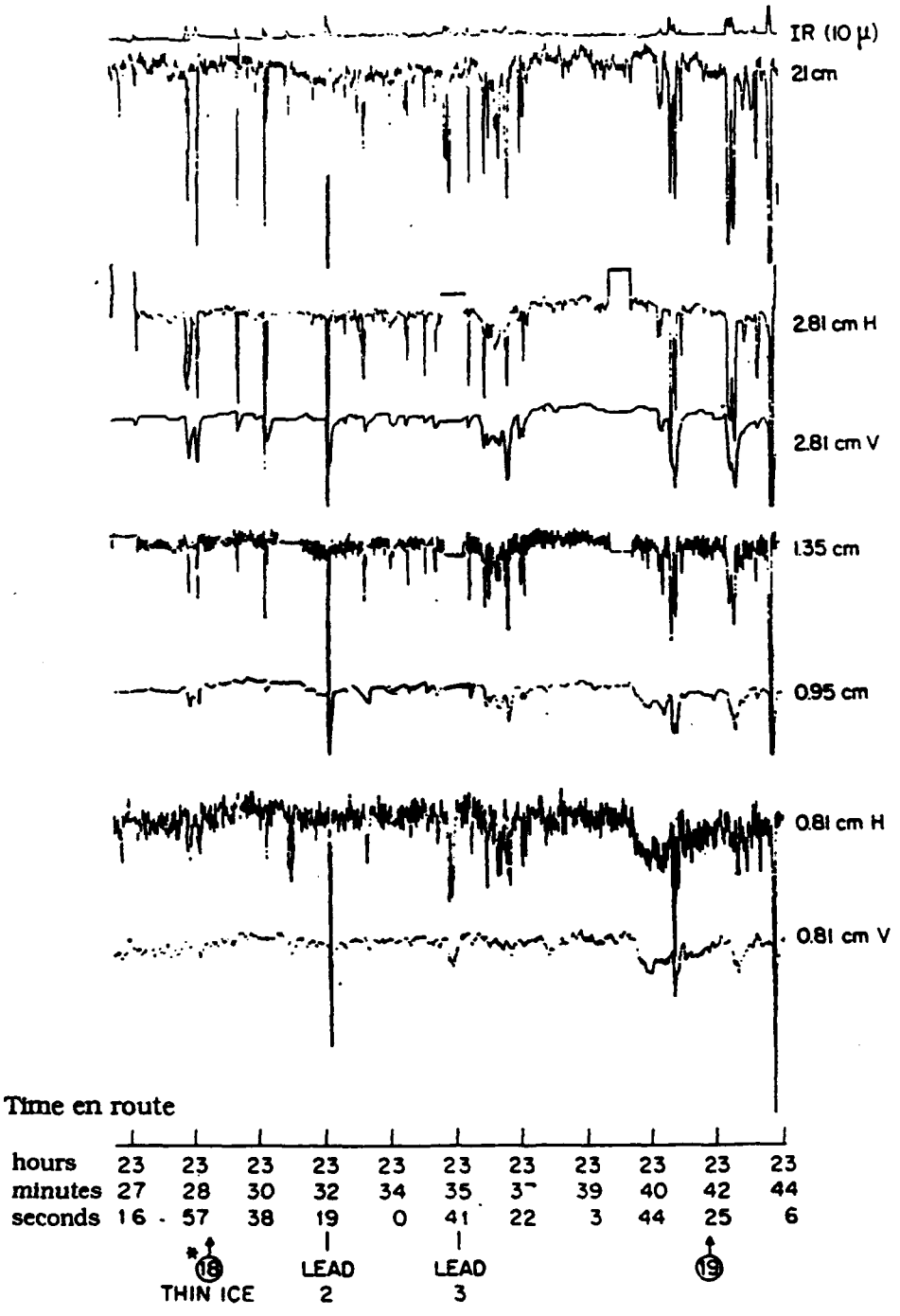

Figure 3. Multiwavelength data obtained during a low pass of the aircraft over the U.S. test area on 5 March 1973 (after Gloersen et al., 1975).

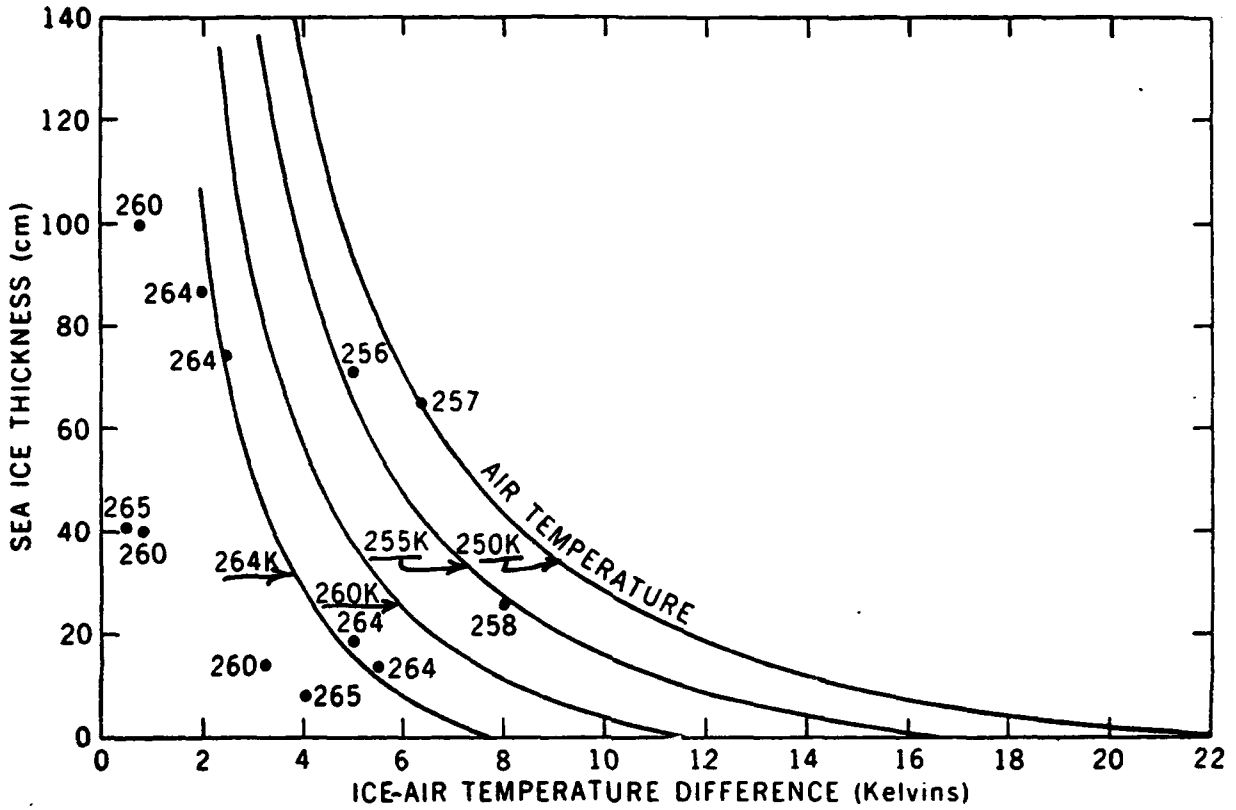

Figure 4. Modeled sea ice thickness vs ice–air temperature differences for four air temperatures, with experimental data also plotted for comparison. The numbers above the points refer to the air temperatures at which the observations were made. Air temperatures were obtained from concurrent measurements on board a surface vessel and helicopter (after Gloersen et al., 1975).

APPENDIX C
Models

C-I

Modeling the Thickness Distribution of Arctic Pack Ice

Gregory M. Flato

Thayer School of Engineering, Dartmouth College

Large-scale motion is responsible for the highly variable thickness of Arctic sea ice, producing areas of open water or leads and deforming the pack into pressure ridges tens of meters thick. A method of describing the large-scale dynamic and thermodynamic behavior of pack ice in terms of its thickness distribution (a probability density function of ice thickness) was developed by Thorndike et al. (1975). Flato (1991) has subsequently extended the thickness distribution theory by including ridged and level ice explicitly, and by investigating the behavior of the so-called ridge redistribution function and the role of the various parameters that describe the ridging process. Also investigated was the effect of including snowfall and a simple parameterization of brine pocket heat storage. The setting for this study was the sea ice model used by Hibler (1980).

A simulation of the entire Arctic ice pack has been performed for the years 1979–85. The first point to note is the relatively slow evolution of ridged ice volume over time from which the age distribution of ridged ice can be estimated. A simple model of ridged ice evolution indicates that the age of ridged ice is distributed exponentially with a mean and standard deviation of 3–4 years. Thus only about 14% (by area) of the ridged ice is older than 6 years, and only 0.03% older than 24 years.

Next, comparisons to observed thicknesses illustrate how well (or poorly) various aspects of the ice cover are modeled. An example of observed and computed thickness distributions is shown below in Figure 1 to illustrate the realistic nature of the model and the resolution in thickness achieved. This comparison is made difficult by the paucity of submarine sonar data during the time period for which the model was run. The comparisons of mean ice thickness do illustrate a feature seen in the model output for the entire Arctic, namely the large interannual variability — differences in the modeled mean thickness from one year to the next of well over a meter are not uncommon. One interpretation is that mean sea ice thickness may not be a particularly good indicator of gradual climatic change unless long time series are available. On the other hand, if the changes in modeled mean thickness are real, they imply sensitive response to details of the present climate. It is not known which features of the specified climate are responsible for the large ice thickness variations.

A number of sensitivity studies were conducted with this model to investigate the role of various parameters. It was found that neglecting snowfall (which affects both the surface albedo and conductivity) led to an increase in thickness of about 0.5 m, whereas the brine pocket heat storage parameterization had little effect except in the marginal ice zone where the onset of freezing and melting was delayed slightly. Of the parameters controlling the ridging process, the most important were the fraction of thin ice available for ridging and the height of the ridges produced. It was found that these parameters could be varied together in such a way as to produce little change in the mean thickness; further information (like the relative amounts of ridged and level ice) may be needed to eliminate this ambiguity. The ice strength parameter (the ratio of total energy losses to potential energy change during ridging — Rothrock, 1975) was adjusted in each case so as to give mean monthly ice drift that agreed closely with observed buoy drift; a value of 15–20 was required in most cases.

Finally, some comparisons between the present model and the widely-used two-level thickness formulation illustrate that the two-level scheme underestimates the mean thickness in all regions. The primary reason for this discrepancy appears to be the use of mean thickness in calculating thermodynamic growth and hence ignoring the strong dependence of ice growth rate on the details of the thin part of the thickness distribution.

References

Flato, G. M., 1991. Numerical investigation of the dynamics of a variable thickness Arctic ice cover, Ph.D. thesis, Dartmouth College, 185 pp.

Hibler, W. D. III, 1980. Modeling a variable thickness sea ice cover, *Mon. Wea. Rev.*, 108, 1943–1973.

Rothrock, D. A., 1975. The energetics of the plastic deformation of pack ice by ridging, *J. Geophys. Res.*, *80*, 4514–4519.

Thorndike, A. S., D. A. Rothrock, G. A. Maykut, and R. Colony, 1975. The thickness distribution of sea ice, J. *Geophys. Res.*, *80*, 4501–4513.

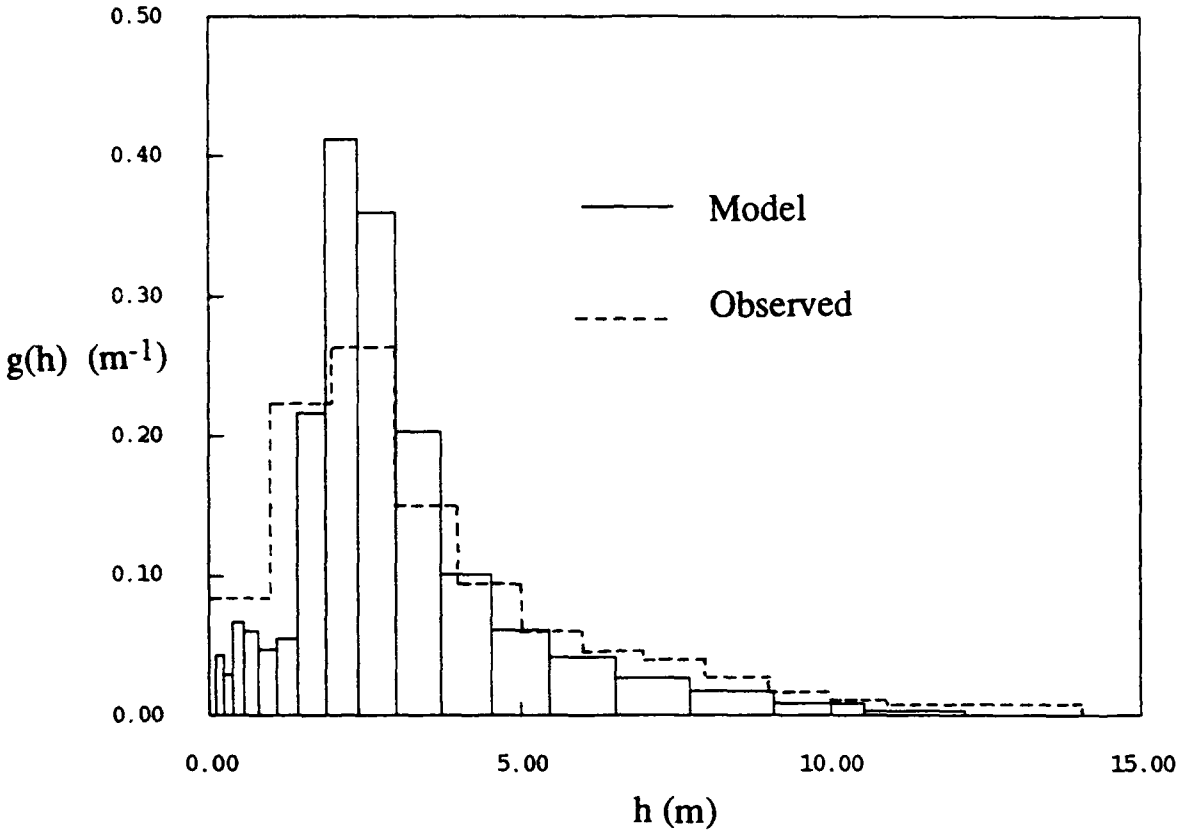

Figure 1. Observed (dashed line) and computed (solid line) thickness distributions at the North Pole for February 1960 and 1980, respectively.

C-II

Model Predicted Arctic Sea Ice Mass and Its Sensitivities

S. Hakkinen

NASA Goddard Space Flight Center, Code 971

A one-dimensional ice-ocean model was applied to predict Arctic sea ice mass based on monthly climatology. The thermodynamics of the ice were formulated according to the Semtner 3-level scheme modified to include effects of variable ice concentration. The ocean model consists of an 80-m thick layer with fine enough resolution to resolve the evolution of the mixed layer. The surface albedo is assumed to be 0.8 when the surface temperature is colder than –10°C, and 0.4 when it is warmer than 0°C. It varies linearly from 0.8 to 0.4 as the surface temperature increases from –10 to 0°C. This parameterization is not changed in the experiments discussed below.

The simulated equilibrium ice thickness, using the Maykut and Perovich (1987) longwave (LW) back radiation formula and assuming all meltwater drains off immediately, is 4.2 m. Using the Parkinson and Washington formulation (1979), the equilibrium thickness is 2.2 m. A short summary of the sensitivities to climate variables affecting the ice thickness follows, using Maykut and Perovich LW radiation, unless otherwise specified.

air temperature	equilibrium ice thickness
+ 2°C increase year-round	2.9 m
+ 5°C in winter (Nov.-Apr.)	3.6 m
+ 2°C in summer (May-Sept.)	3.2 m

cloudiness	equilibrium ice thickness
+ 10% increase year-round	5.4 m
+ 10% in winter	4.2 m (i.e., no effect)
– 10% in summer	3.4 m

snowfall	equilibrium ice thickness
double snowfall	3.4 m
triple snowfall	3.1 m

surface meltwater,

Parkinson and Washington LW radiation	equilibrium ice thickness
10 cm meltwater reservoir	2.7 m

From the above, it is obvious that the variables controlling the radiation balance have the strongest influence on the ice thickness. The choice of formulation (either Maykut and Perovich or Washington and Parkinson) of the LW back radiation has the largest sensitivity. Air temperatures mainly control the timing of the albedo change and thus shorten or extend the melt period, while cloudiness controls the incident solar radiation. This suggests that factors affecting the absorption of shortwave radiation make the major contribution to the evolution of the Arctic sea ice mass. Of course, the snowfall appears to strongly influence the ice thickness, but changes in this variable are about 100% while changes in cloudiness, for example, are about 10% or less.

Using the updated GISS temperature data for the period 1880 to 1990, the Arctic average ice thickness was predicted from the model. All other components of the forcing were assumed to be climatological. The annual average temperature anomaly is shown in Fig. 1a, the spatially averaged freezing period (Nov.–Apr.) anomaly in Fig. 1b, and the average melt season (May–Oct.) anomaly is shown in Fig. 1c. During the past 20 years the average annual or freezing period temperature anomalies do not show any clear trends. In the melt period anomaly, however, one might claim to see a slight trend towards warming. This trend is also detected by the model, which predicts a decreasing ice mass, shown in Fig. 2a. However, the simulated average ice mass at the end of 1990 is not nearly as thin as the model predicts for the 1930s.

To show the influence of the summer temperature variations, two model runs were done, one where freezing period anomalies were set to zero and another where the summer anomalies were set to zero. The corresponding ice thickness curves are shown in Fig. 2b for zero winter anomalies, and in Fig. 2c for zero summer anomalies. The Fig. 2b curve accounts for most of the variability in Fig. 2a, while the Fig. 2c curve has very modest modulation. This ice mass behavior is opposite to the temperature anomaly variability in which the winter anomalies are considerably larger than the summer anomalies. This emphasizes the importance of timing of the onset of the melt season and the accompanying change in albedo.

For improving our ability to model variations in the sea ice cover in the Arctic, it is essential to increase our knowledge of all components of the forcing, especially the air temperature and radiation fields. The remotely-sensed solar irradiance fields, which have become available recently from the ISCCP program, can offer an improvement to the prediction of the ice mass. However, the LW back radiation fields will still pose a problem. The remotely-sensed radiation fields, as well as the bulk parameterizations of

downwelling radiation fields, contain errors of 5–10 W m^{-2} which is approximately the net annual heat flux at the surface. Thus, a considerable uncertainty remains in determining the most important component of the surface forcing for the ice cover.

References

Maykut, G. A., and D. Perovitch, 1987. Role of shortwave radiation in summer decay of sea ice cover, *J. Geophys. Res.*, **92**, 7032–44.

Parkinson, C. L., and W. M. Washington, 1979. A large-scale numerical model of sea ice, *J. Geophys. Res.*, **84**, 311–337.

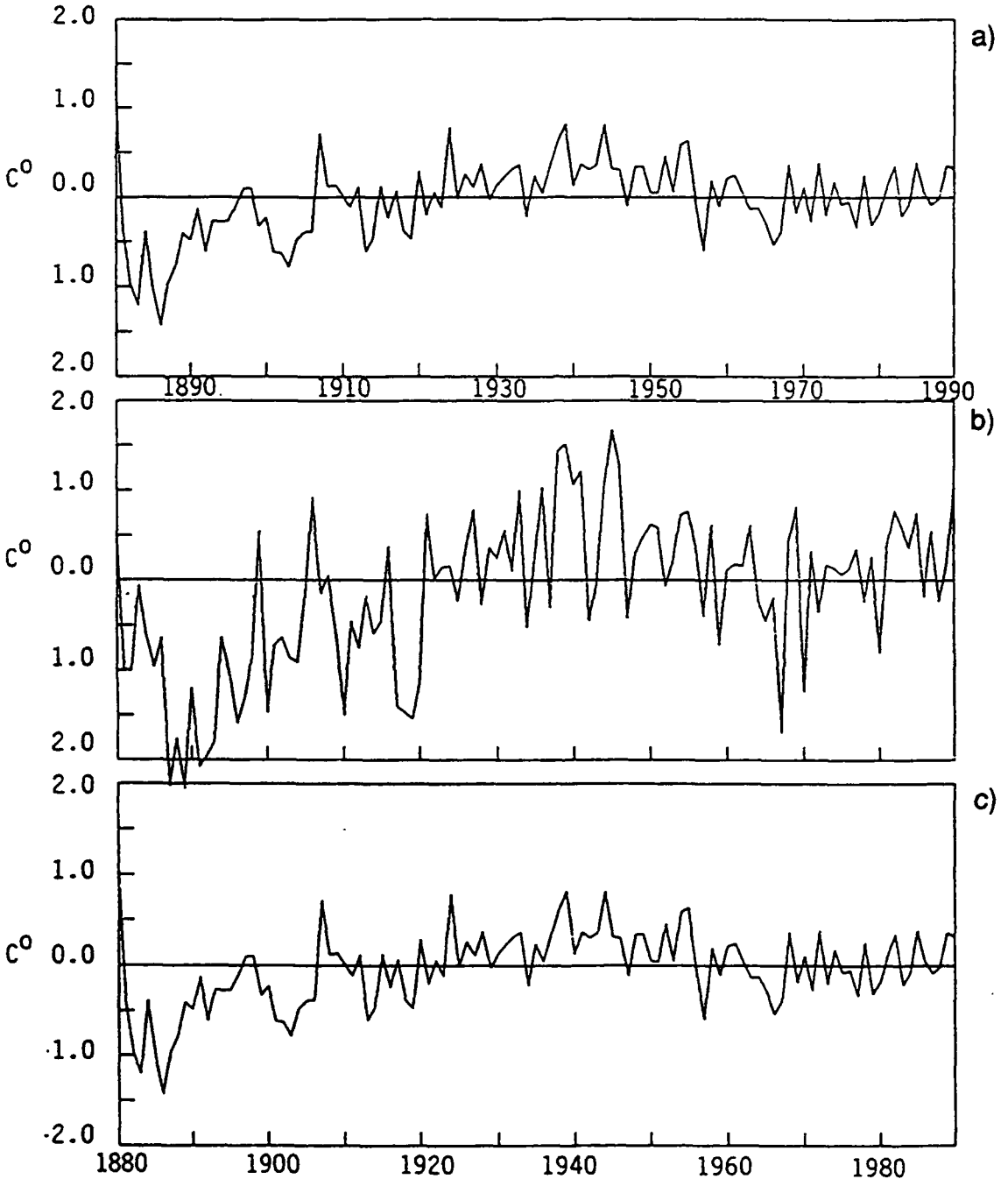

Figure 1. (a) Annual temperature anomaly from GISS; (b) freezing period (Nov.–Apr.) temperature anomaly; and (c) melting season (May–Oct.) temperature anomaly.

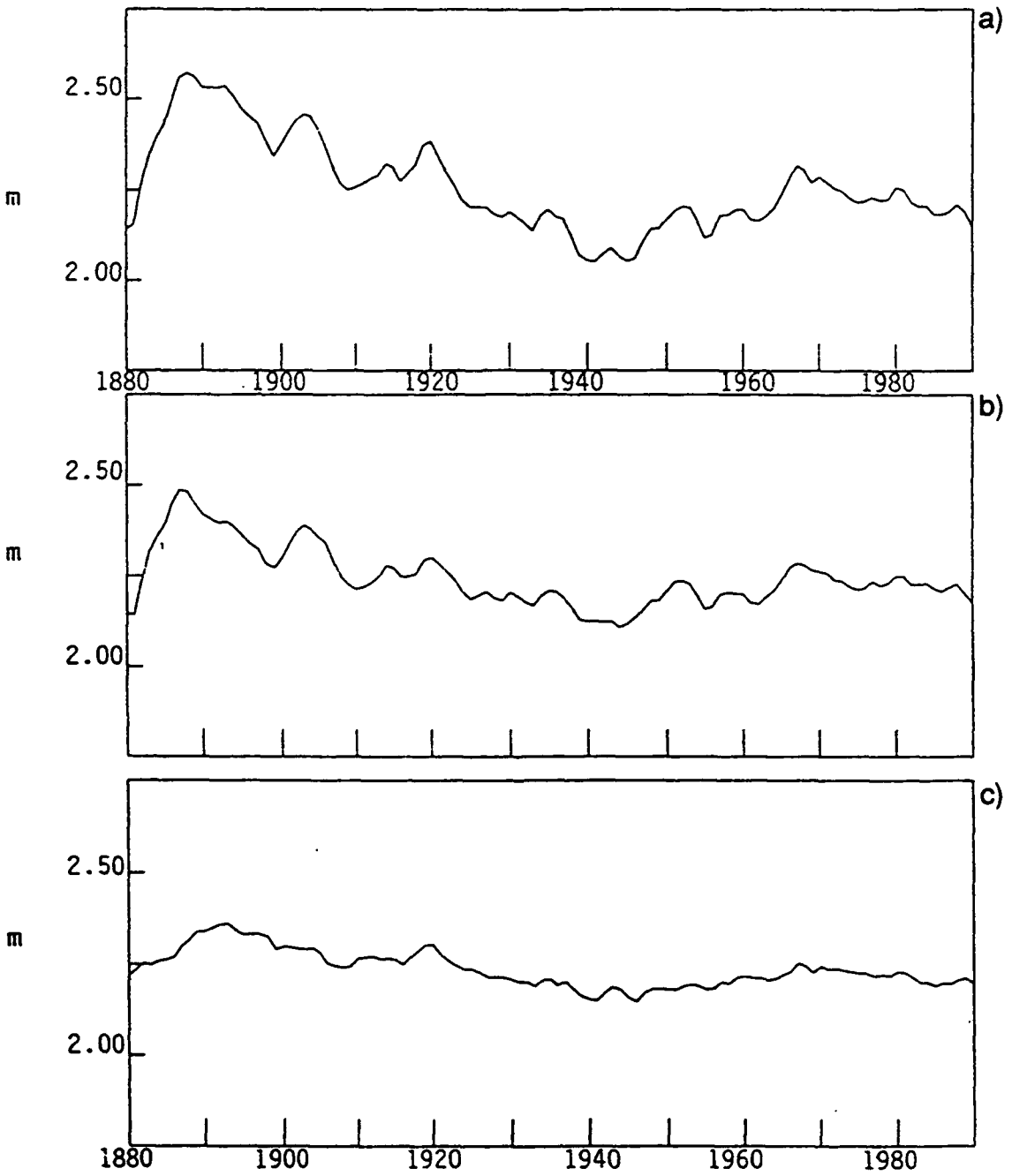

Figure 2. (a) Simulated ice thickness corresponding to Fig. 1a; (b) simulated ice thickness when winter temperature anomalies are set to zero; and (c) simulated ice thickness when summer temperature anomalies are set to zero.

C-III

Arctic Radiation Forcing Fields for Dynamic-Thermodynamic Sea Ice Models

J. Key, A. J. Schweiger, and J. A. Maslanik

Cooperative Institute for Research in Environmental Sciences

University of Colorado, Boulder

Even though radiative fluxes are among the most important controlling factors of sea ice thickness, they are treated very simply in most sea ice models. Downwelling shortwave and longwave fluxes are generally parameterized in terms of cloud fraction, which is specified for each month but with no spatial variability. This simplicity has been a matter of necessity given the few Arctic radiation measurements available and, until recently, no cloud climatology with sufficient information from which to estimate the radiative fluxes.

However, the International Satellite Cloud Climatology Project (ISCCP) (Rossow et al., 1985) cloud product can be used to produce a data set of upwelling and downwelling shortwave and longwave radiative fluxes for use in sea ice models. The data set currently spans the period mid-1983 through the end of 1989 with two additional years of data being processed every year. Both daily and monthly products are available. Spatial resolution is approximately 280 km. Cloud parameters reported include cloud amount, cloud top pressure and temperature, cloud type, and cloud optical thickness (at 0.6 μm). Surface information includes temperature and reflectance (again at 0.6 μm). Temperatures at 15 mbars, 500 mbars, and the tropopause are given, as are precipitable water and ozone abundance.

Since this is a satellite-based climatology, and since it utilizes only one visible and one thermal channel, no information on the geometric thickness of clouds or their microphysical properties (e.g., droplet radii and density) is given. Furthermore, little is known about the surface type or about atmospheric aerosols. Therefore certain assumptions must be made in modeling the transfer of radiation through the system. For example, we model the reflectance of snow using different grain radii at different times of the year. The mixture proportions of snow on ice, bare ice, open water, and melt ponds in summer are chosen to match the observed visible albedo, which is then used to estimate the albedo in 23 other wavelength bands. Standard subarctic aerosol and gaseous absorber amounts and distributions are employed. Cloud geometrical

thickness is chosen to be consistent with the observed visible optical depth for a variety of cloud microphysical models. A two-stream radiative transfer model is used for the flux calculations.

Preliminary results are shown in Figs. 1 and 2. Figure 1 gives monthly mean downwelling shortwave and longwave fluxes for the 1983-1986 period over the Arctic Basin north of 75° latitude. Figure 2 gives an example of the spatial distribution of radiative fluxes during July (mean). These fluxes compare reasonably well with those of Curry and Ebert (1991), which are based on surface observations of cloud amount and a prescribed level of ice crystal haze ("diamond dust"). The primary difference is that the longwave fluxes based on the ISCCP data tend to be smaller than those of Curry and Ebert. This is a result of the fact that the ISCCP product underestimates cloud amount, especially in summer (Rossow et al., 1988). This has been verified for the Arctic in a comparison of the ISCCP and NIMBUS-7 satellite-based cloud climatologies with a surface-based cloud climatology (Schweiger and Key, in press). In that study it was found that while spatial patterns were in general agreement in all cloud climatologies, the satellite-based cloud amounts are typically 10–30% lower than the surface-based, with the largest differences occurring in summer.

The type of results shown in Figs. 1 and 2 could be used directly in sea ice models. However, for time periods when ISCCP data have not been converted to radiative fluxes, the fluxes must be calculated from the cloud product. This would probably increase the processing time in most sea ice models to unacceptable levels. Therefore, parameterizations of radiative fluxes based on cloud fraction alone, similar to those currently used but incorporating temporal and spatial dependencies, are currently under investigation.

References

Curry, J. A., and E. E. Ebert, 1991. Annual cycle of radiation fluxes over the Arctic Ocean: Sensitivity to cloud optical properties, *Int. J. Climatology* .

Rossow, W. B., L. C. Gardner, P. Lu, and A. Walker, 1988. International Satellite Cloud Climatology Project (ISCCP) documentation of cloud data, World Climate Research Programme, WMO/TD-No. 266.

Rossow, W. B., F. Mosher, E. Kinsella, A. Arking, M. Desbois, E. Harrison, P. Missis, E. Ruprecht, G. Seze, C. Simmer, and E. Smith, 1985. ISCCP cloud algorithm intercomparison, *J. Climate Appl. Meteor.*, **24**, 877–903.

Schweiger, A. J., and J. Key, in press. Arctic cloudiness: Comparison of ISCCP-C2 and NIMBUS-7 satellite-derived cloud products with a surface-based cloud climatology. *J. Climate.*

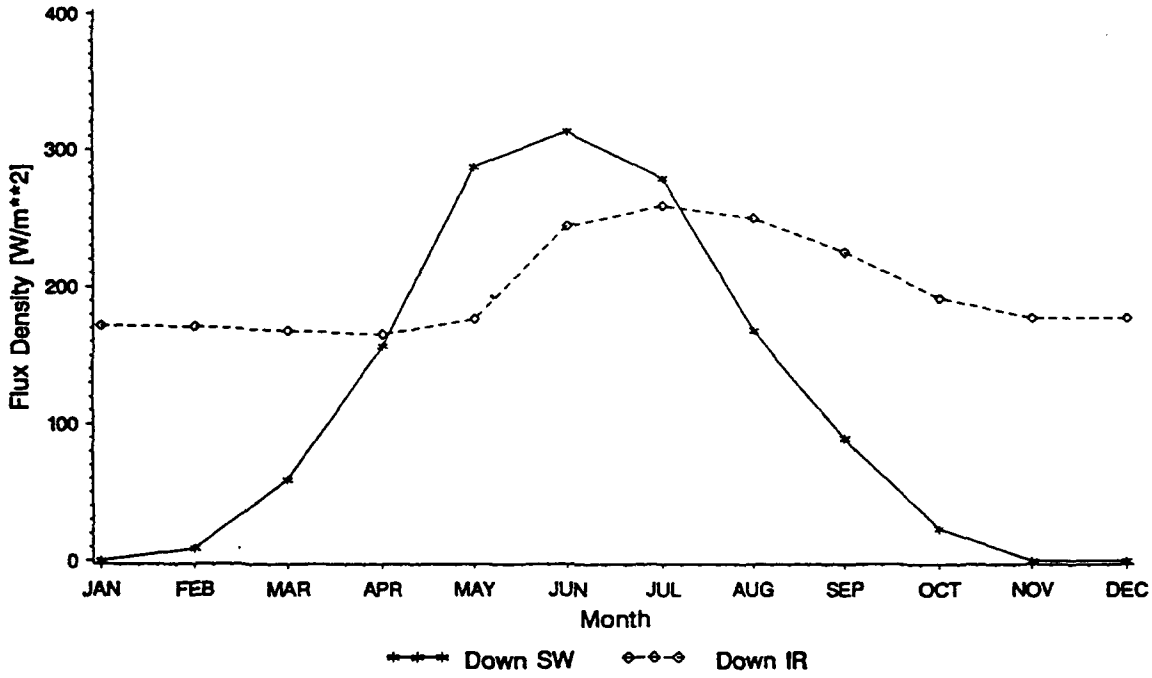

Figure 1. Surface radiation in the Arctic north of 75°. Monthly average downwelling shortwave and longwave radiative fluxes estimated using the ISCCP-C2 cloud product over the period 1983–1986.

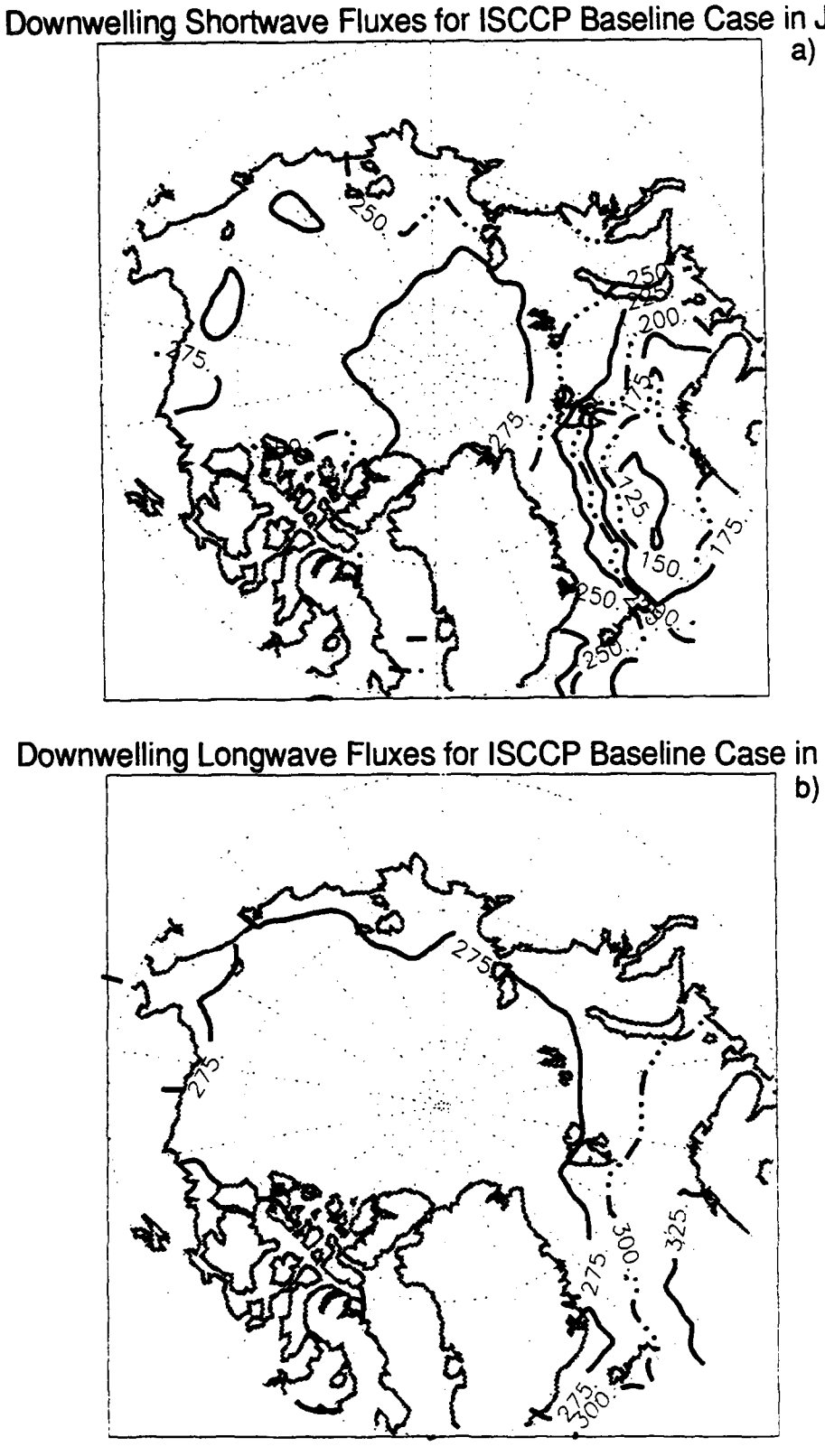

Figure 2. Downwelling shortwave and longwave radiation (W m^{-2}) over the Arctic Basin for July (mean): (a) shortwave downwelling fluxes calculated from ISCCP-C2 in July; (b) longwave downwelling fluxes calculated from ISCCP-C2 in July.

C-IV

Model Simulation of Changes in Arctic Sea Ice, 1960–1989

John E. Walsh
University of Illinois, Urbana

An intriguing recent finding based on submarine data is the apparent decrease of ice thickness between 1976 and 1987 in the region east of northern Greenland (Wadhams, 1990). Although Wadhams's submarine data were from slightly different tracks and from different calendar months (October 1976 and May 1987), the data indicated a thinning equivalent to a loss of 15% of the ice volume over an area of 300,000 km^2. In view of concern about possible climate change, a key issue is how representative these ice anomalies are. Do the differences represent interannual fluctuations or are they indicative of a more systematic trend? The same question arises with regard to the decrease of Arctic extent during 1978–1987 as reported by Gloersen and Campbell (1991).

In an attempt to place the ice anomalies of these periods into a temporal perspective, we have simulated the Arctic ice cover of 1960–1989 using a dynamic-thermodynamic sea ice model. The model is a modified version of Hibler's (1979) two-level dynamic formulation and Parkinson and Washington's (1979) thermodynamic formulation. The model includes the concentrations of two ice types: first-year and multiyear. The model is forced by daily wind fields and by monthly temperatures interpolated to daily values. The ocean dynamic topography and hence the ocean currents are prescribed and temporally invariant. There is no horizontal heat transport by the ocean currents. The model was run for 1960–1989 with a daily timestep and a spatial resolution of 110 km.

Figure 1a is a time series of the total ice mass in the entire model domain. A relative minimum of ice mass during the mid-1960s is followed by a recovery to the model's "climatological normal" by 1970, but there is no indication of a trend of ice mass through the final two decades. Plots of the spatial distribution of simulated ice thickness (and the corresponding anomalies) show that the model-derived anomalies are positive in October 1976 and nearly zero in May 1987. In this respect the anomalies are consistent with the findings of Wadhams (1990). However, the model-derived anomalies of these two years are not representative of a systematic trend in the model results. In the Fram Strait area, the model-derived thickness anomalies of 1976 and 1987 were preceded and followed by anomalies of the opposite sign.

The time series of ice coverage (Fig. 1b) contains a small negative trend. Specifically, the simulated wintertime maxima decrease by approximately 5% from the mid-1970s to the mid-1980s. This decrease is consistent with that obtained by Gloersen and Campbell (1991) from satellite passive microwave imagery for 1978–1987. It should be noted, however, that the interannual fluctuations in the model results and those in observational data are correlated at only 0.4–0.8 in most geographical sectors. These correlations are based on gridded analyses of sea ice coverage, which may also contain errors and biases that degrade the correlations.

References

Gloersen and Campbell, 1991. *Nature*, **352**, 33–36.

Hibler, 1979. *J. Phys. Oceanogr.*, **9**, 815–846.

Parkinson and Washington, 1979. *J. Geophys. Res.*, **84**, 3121–3137.

Wadhams, 1990. *Nature*, **345**, 795–797.

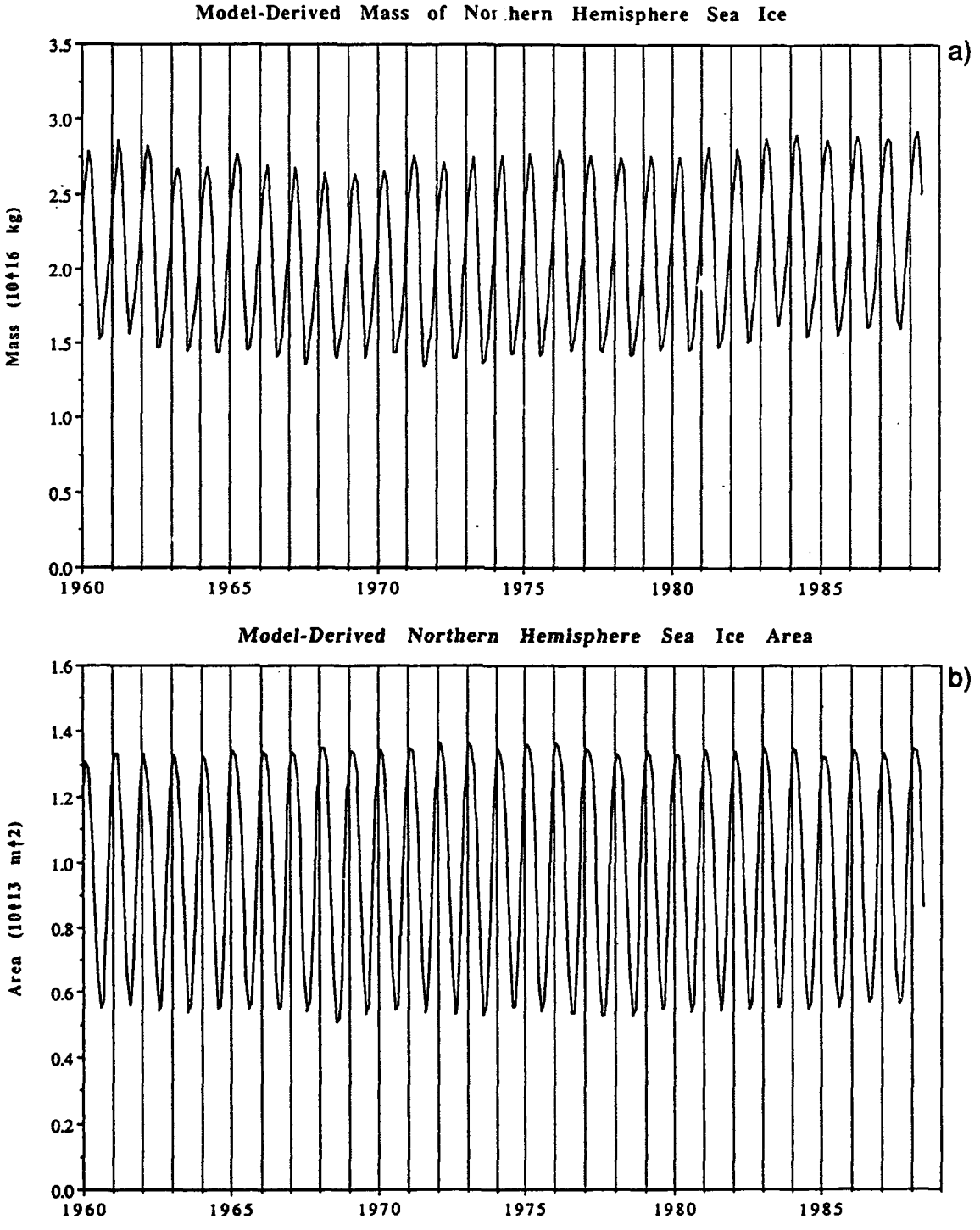

Figure 1. Time series of (a) total mass of sea ice and (b) total ice-covered area in the model domain.

APPENDIX D
Bibliography

Ackley, S. F., W. D. Hibler III, F. K. Kugzruk, A. Kovacs, and W. F. Weeks, 1976. Thickness and roughness variations of Arctic multiyear sea ice, CRREL Report 76-18, U.S. Army Cold Regions Research and Engineering Laboratory, Hanover, NH, 25 pp.

Bourke, R., and C. Garrett, 1987. Sea ice thickness distribution in the Arctic Ocean, *Cold Reg. Sci. and Technol.*, **13**, 259–280.

Bourke, R. H., and A. S. McLaren, 1992. Contour mapping of Arctic Basin ice draft and roughness parameters, *J. Geophys. Res.*, in press.

Bourke, R. H., and R. G. Paquette, 1989. Estimating the thickness of sea ice, *J. Geophys. Res.*, **94**, 919-923.

Burns, B. A., D. J. Cavalieri, M. R. Keller, W. J. Campbell, T. C. Grenfell, G. A. Maykut, and P. Gloersen, 1987. Multisensor comparison of ice concentration estimates in the marginal ice zone, *J. Geophys. Res.*, **92**, 6843-6856.

Cavalieri, D. J., P. Gloersen, and W. J. Campbell, 1984. Determination of sea ice parameters with the Nimbus 7 SMMR, *J. Geophys. Res.*, **89**, 5355-5369.

Colony, R., and A. Thorndike, 1985. Sea ice motion as a drunkard's walk, *J. Geophys. Res.*, **90**, 965–974.

Comiso, J. C., 1983. Sea ice microwave emissivities from satellite passive microwave and infrared observations, *J. Geophys. Res.*, **88**, 7686–7704.

Comiso, J. C., 1990. Arctic multiyear ice classification and summer ice cover using passive microwave satellite data, *J. Geophys. Res.*, **95**, 13,411–13,422, 13,593–13,597 (color plates).

Comiso, J. C., P. Wadhams, W. B. Krabill, R. N. Swift, J. P. Crawford, and W. B. Tucker III, 1991. Top/bottom multi-sensor remote sensing of Arctic sea ice, *J. Geophys. Res.*, **96**, 2693–2709.

Eicken, H., and M. A. Lange, 1989. Sea-ice thickness data: the many vs. the few, *Geophys. Res. Lett.*, **16**, 495–498.

Farmer, L. D., and D. T. Eppler, 1985. A method for determining sea ice type and inferred ice thickness distributions from aerial photographs, *Proceedings of the Arctic Oceanography Conference and Workshop*, Naval Ocean Research and Development Activity, Stennis Space Center, Mississippi, 205–213.

Flato, G. M., and W. D. Hibler III, 1990. A cavitating fluid sea ice model, in *Sea Ice Properties and Processes*, Proceedings of the W. F. Weeks Sea Ice Symposium, eds. S. F. Ackley and W. F. Weeks, CRREL Monograph 90-1, 239–242.

Fleming, G. H., and A. J. Semtner Jr., 1991. A numerical study of interannual ocean forcing on arctic ice, *J. Geophys. Res.*, **96**, 4589–4603.

Gloersen, P., and W. J. Campbell, 1991. Recent variations in Arctic and Antarctic sea ice covers, *Nature*, **352**, 33–36.

Gloersen P., W. Nordberg, T. J. Schmugge, and T. T. Wilheit, 1973. Microwave signatures of first-year and multiyear ice, *J. Geophys. Res.*, **78**, 3564–3572.

Gloersen, P., R. Ramseier, W. J. Campbell, P. M. Kuhn, and W. J. Webster Jr., 1975. Ice thickness distribution as inferred from infrared and microwave remote sensing during the Bering Sea Experiment, in *Proceedings of the Final Symposium on the Results of the Joint Soviet-American Expedition*, eds. K. Ya. Kondratyev, Yu. I. Rabinovich, and W. Nordberg, Gidrometeoizdat, Leningrad, pp. 282–293. (Republished as *USSR/USA Bering Sea Experiment*, by A. A. Balkema, Rotterdam, 307 pp., 1982.)

Gloersen, P., W. J. Campbell, D. J. Cavalieri, J. C. Comiso, C. L. Parkinson, and H. J. Zwally, 1992. *Arctic and Antarctic Sea Ice, 1978–1987: Satellite Passive Microwave Observations and Analysis*, NASA SP511, National Aeronautics and Space Administration, Washington, D.C.

Govoni, J. W., and W. B. Tucker III, 1990. An update on portable hot-water sea ice drilling, *Cold Reg. Sci. and Technol.*, **16**, 175–178.

Hibler, W. D. III, 1979. A dynamic thermodynamic sea ice model, *J. Phys. Oceanogr.*, **9**, 815–846.

Holt, B., J. Crawford, and F. Carsey, 1990. Characteristics of sea ice during the Arctic winter using multifrequency aircraft radar imagery. In *Sea Ice Properties and Processes* (eds. S. F. Ackley and W. F. Weeks), Monograph 90-1, U.S. Army Cold Regions Res. & Engng. Lab., Hanover, NH, 224 (abstract).

Ketchum, R. D., 1971. Airborne laser profiling of the Arctic pack ice, *Remote Sensing Environ.*, **2**, 41–52.

Koerner, R. M., 1973. The mass balance of the sea ice of the Arctic Ocean, *J. Glaciol.*, **12**, 173–185.

Kovacs, A., 1983. Characteristics of multiyear pressure ridges, In *Proceedings of the 7th International Conference on Port and Ocean Engineering Under Arctic Conditions* (POAC-83), Helsinki, **3**, 173–182.

Kovacs, A., and R. M. Morey, 1987. Estimating sea ice thickness from radar sounding time-of-flight data, In *Proceedings of the 9th International Conference on Port and Ocean Engineering Under Arctic Conditions* (POAC-87), eds. W. M. Sackinger and M. O. Jeffries, Univ. Alaska, Fairbanks, 1, 121–136.

Kovacs, A., N. C. Nalleau, and J. S. Holladay, 1987. Airborne electromagnetic sounding of sea ice thickness and sub-ice bathymetry, CRREL Report 87–23.

Krabill, W. B., R. N. Swift, and W. B. Tucker III, 1990. Recent measurements of sea ice topography in the Eastern Arctic. In *Sea Ice Properties and Processes*, eds. S. F. Ackley and W. F. Weeks, U.S. Army Cold Regions Res. & Engng. Lab., Hanover, NH, Monograph 90-1, 132–136.

Kwok, R., E. Rignot, B. Holt, and R. Onstott, 1992. Identification of sea ice types in spaceborne synthetic aperture radar data, *J. Geophys. Res.*, **97**, 2391–2402.

Lange, M. A., and H. Eicken, 1991. The sea ice thickness distribution in the northwestern Weddell Sea, *J. Geophys. Res.*, **96**, 4821–4837.

Lange, M. A., P. Schlosser, S. F. Ackley, P. Wadhams, and G. S. Dieckmann, 1990. ^{18}O concentrations in the sea ice of the Weddell Sea, Antarctica, *J. Glaciol.*, **36**, 315–323.

Leppäranta, M., and T. Thompson, 1989. BEPERS-88 sea ice remote sensing with synthetic aperture radar in the Baltic Sea, *Eos, Trans. Am. Geophys. U.*, **70**, 698–699, 708–709.

LeSchack, L. A., W. D. Hibler III, and F. H. Morse, 1971. Automatic processing of Arctic pack ice data obtained by means of submarine sonar and other remote sensing techniques, in *Propagation Limitations in Remote Sensing*, J. B. Lomax, ed., AGARD Conference Proceedings No. 90, NATO Advisory Group for Aerospace Research and Development.

Lindsay, R., and D. A. Rothrock, 1992. The calculation of surface temperature and albedo of Arctic sea ice from AVHRR. Presented at the Int'l Glac. Soc. Symp. on Remote Sensing of Snow and Ice, Boulder, May 1992. To appear in *Ann. Glaciol.*

Livingstone, C. E., 1989. Combined active/passive microwave classification of sea ice. *Proc. IGARSS-89*, **1**, 376–380.

Lowry, R. T., and P. Wadhams, 1979. On the statistical distribution of pressure ridges in sea ice, *J. Geophys. Res.*, **84**, 2487–2494.

Maykut, G. A., and N. Untersteiner, 1971. Some results from a time-dependent thermodynamic model of Arctic sea ice, *J. Geophys Res.*, **76**, 1550–1575.

McLaren, A. S., 1989. The under-ice thickness distribution of the Arctic Basin as recorded in 1958 and 1970, *J. Geophys. Res.*, **94**, 4971–4983.

McLaren, A. S., R. G. Barry, and R. H. Bourke, 1990. Could arctic ice be thinning? *Nature*, **345**, 762.

Menashi, J., C. Swift, K. St. Germain, J.C. Comiso, and A. Lohanick, submitted. Passive microwave measurement of sea ice thickness, *J. Geophys. Res.*

Moritz, R. E., 1991. Sampling the temporal variability of sea ice draft distribution, (abstract, Eos Supplement, Fall AGU meeting, 237–238 (ms in preparation).

Onstott, R. G., T. C. Grenfell, C. Matzler, C.A. Luther, and E. A. Svendsen, 1987. Evolution of microwave sea ice signatures during early summer and midsummer in the marginal ice zone, *J. Geophys. Res.*, **92**, 6825–6835.

Overland, J. E., and P. S. Guest, 1991. The Arctic snow and air temperature budget over sea ice during winter, *J. Geophys. Res.*, **96**, 4651–4662.

Parkinson, C. L., J. C. Comiso, H. J. Zwally, D. J. Cavalieri, P. Gloersen, and W. J. Campbell, 1987. Arctic sea ice 1973-1976 from satellite passive microwave observations, NASA Spec. Publ. 489.

Piacsek, S., R. Allard, and A. Warn-Varnas, 1991. Studies of the arctic ice cover and upper ocean with a coupled ice-ocean model, *J. Geophys. Res.*, **96**, 4631–4650.

Ramseier, R. O., P. Gloersen, W. J. Campbell, and T. C. Chang, 1975. Mesoscale description for the principal Bering Sea Experiment, in *Proceedings of the Final Symposium on the Results of the Joint Soviet-American Expedition*, Leningrad, May 12–17, 1974, eds. K. Ya. Kondratyev, Yu. I. Rabinovich, and W. Nordberg, Gidrometeoizdat, Leningrad, 234–269. (Republished as *USSR/USA Bering Sea Experiment* by A. A. Balkema, Rotterdam, 307 pp., 1982.)

Rothrock, D. A., and D. R. Thomas, 1990. An Arctic Ocean ice balance with assimilated satellite and buoy data. *Proc. Int. Symp. on Assim. of Obs. in Met. and Oceanog.*, Clermont-Ferrand, France, 1-13 July, 1990, 461-466.

Steffen, K., 1986. Atlas of the sea ice types, deformation processes, and openings in the ice, Zurcher Geographische Schriften Heft 20, Geographisches Institut, Eidgenossische Technische Hochschule, Zurich, 55 pp.

Svendsen, E., K. Kloster, B. Farrelly, O. M. Johannessen, J. A. Johannessen, W. J. Campbell, P. Gloersen, D. J. Cavalieri, and C. Matzler, 1983. Norwegian remote sensing experiment: evaluation of the Nimbus 7 scanning multichannel microwave radiometer for sea ice research, *J. Geophys. Res.*, **88**, 2781–2791.

Swift, C. T., L. S. Fedor, and R. O. Ramseier, 1985. An algorithm to measure sea ice concentration with microwave radiometers, J. *Geophys. Res.*, **90**, 1087–1099.

Thomas, D. R., submitted. Global pure type signatures for passive microwave sea ice algorithms, *J. Geophys. Res.*

Thomas, D. R., and D. A. Rothrock, submitted. The Arctic Ocean ice balance: A Kalman smoother estimate, *J. Geophys. Res.*

Thomas, D. R., and D. A. Rothrock, 1989. Blending sequential scanning multichannel microwave radiometer and buoy data into a sea ice model, *J. Geophys. Res.*, **94**, 10,907–10,920.

Thorndike, A. S., 1992. A toy model linking atmospheric thermal radiation and sea ice growth, *J. Geophys. Res.*, **97**, 9401–9410.

Thorndike, A. S., in press. Estimates of sea ice thickness distribution using observations and theory, *J. Geophys. Res.*

Thorndike, A. S., D. A. Rothrock, G. A. Maykut, and R. Colony, 1975. The thickness distribution of sea ice, *J. Geophys. Res.*, **80**, 4501–4513.

Tooma, S. G., R. A. Mannella, J. P. Hollinger, and R. D. Ketchum Jr., 1975. Comparison of sea-ice type identification between airborne dual-frequency passive microwave radiometry and standard laser/infrared techniques, *J. Glaciol.*, **15**, 225–239.

Tucker, W. B. III, W. F. Weeks, and M. Frank, 1979. Sea ice ridging over the Alaskan continental shelf, *J. Geophys. Res.*, **84**, 4885–4897.

Wadhams, P., 1980. A comparison of sonar and laser profiles along corresponding tracks in the Arctic Ocean, In *Sea Ice Processes and Models* (ed. R. S. Pritchard), Univ. Washington Press, Seattle, 283–299.

Wadhams, P., 1981. Sea-ice topography of the Arctic Ocean in the region 70°W to 25°E, *Philos. Trans. R. Soc. London, Ser. A*, **302** (1464), 45–85.

Wadhams, P., 1984. Arctic sea ice morphology and its measurement. In *Arctic Technology and Policy* (I. Dyer and C. Chryssostomidis, Eds.), Washington, DC, Hemisphere Publishing Corporation, 179-195.

Wadhams, P., 1990. Evidence for thinning of the Arctic ice cover north of Greenland, *Nature*, **345**, 795–797.

Wadhams, P., 1992. Sea ice thickness distribution in the Greenland Sea and Eurasian Basin, May 1987, *J. Geophys. Res.*, **97**, 5331–5348.

Wadhams, P., and R. T. Lowry, 1977. A joint topside-bottomside remote sensing experiment on Arctic sea ice, *Proc. 4th Canadian Symp. on Remote Sensing*, Quebec, 16-18 May 1977, Canadian Remote Sensing Soc., 407–423.

Wadhams, P., M. A. Lange, and S. F. Ackley, 1987. The ice thickness distribution across the Atlantic sector of the Antarctic Ocean in midwinter, *J. Geophys. Res.*, **92**, 14,535–14,552.

Wadhams, P., J. C. Comiso, J. Crawford, G. Jackson, W. Krabill, R. Kutz, C. B. Sear, R. Swift, W. B. Tucker, and N. R. Davis, 1991. Concurrent remote sensing of Arctic sea ice from submarine and aircraft, *Int. J. Remote Sensing*, **12**, 1829–1840.

Wadhams, P., W. Tucker, W. Krabill, R. Swift, J. Comiso, and N. Davis, in press. The relationship between sea ice freeboard and draft in the Arctic Basin, and implications for ice thickness monitoring, *J. Geophys. Res.*

Walsh, J. E., and H. J. Zwally, 1990. Multiyear sea ice in the Arctic: Model- and satellite-derived, *J. Geophys. Res.*, **95**, 11,613–11,628.

Weeks, W. F., S. F. Ackley, and J. Govoni, 1989. Sea ice ridging in the Ross Sea, Antarctica, as compared with sites in the Arctic, *J. Geophys. Res.*, **94**, 4984–4988.

Weeks, W. F., A. Kovacs, and W. D. Hibler III, 1971. Pressure ridge characteristics in the Arctic coastal environment, In *Proc. 1st Intl. Conf. Port & Engg. under Arctic Conditions*, ed. by S. S. Wetteland and P. Bruun), Tech. Univ. Norway, Trondheim, 152–183.

Wensnahan, M. R., T. C. Grenfell, G. A. Maykut, and D. Winebrenner, 1991. Microwave emission from thin saline ice: Field observations and their implications for remote sensing, *Eos*, **72**, 259.

Wilheit, T. T., W. Nordberg, J. Blinn, W. Campbell, and A. Edgerton, 1972. Aircraft measurements of microwave emission from Arctic sea ice, *Remote Sensing Environ.*, **2**, 129–139.

Winebrenner, D., and D. Farmer, in preparation. On the L-band polarimetric SAR response to ice thickness in new and thin sea ice types, to be submitted to *J. Geophys. Res.*

WMO, 1970. WMO sea ice nomenclature, Secretariat of the World Meteorological Organization, Geneva, Switzerland, 147 pp.